Central region study for a moderate energy cyclotron

DOI:
10.6100/IR22645

Document status and date:
Published: 01/01/1981

Document Version:
Publisher's PDF, also known as Version of Record (includes final page, issue and volume numbers)

CENTRAL REGION STUDY FOR A MODERATE ENERGY CYCLOTRON

J.I.M. BOTMAN

CENTRAL REGION STUDY FOR A MODERATE ENERGY CYCLOTRON

DISSERTATIE DRUKKERIJ
wibro
HELMOND
TELEFOON 04920-23981

CENTRAL REGION STUDY FOR A MODERATE ENERGY CYCLOTRON

PROEFSCHRIFT

TER VERKRIJGING VAN DE GRAAD VAN DOCTOR IN DE TECHNISCHE WETENSCHAPPEN AAN DE TECHNISCHE HOGESCHOOL EINDHOVEN, OP GEZAG VAN DE RECTOR MAGNIFICUS, PROF. IR. J. ERKELENS, VOOR EEN COMMISSIE AANGEWEZEN DOOR HET COLLEGE VAN DEKANEN IN HET OPENBAAR TE VERDEDIGEN OP DINSDAG 15 SEPTEMBER 1981 TE 16.00 UUR

DOOR

JOHANNES IGNATIUS MARIA BOTMAN

GEBOREN TE HAARLEMMERLIEDE

DIT PROEFSCHRIFT IS GOEDGEKEURD
DOOR DE PROMOTOREN

Prof.dr.ir. H.L. Hagedoorn

en

Prof.dr. N.F. Verster

Aan mijn ouders
Aan Thérèse-Anne

CONTENTS

CHAPTER 1

INTRODUCTION

A scope of the present study is given in the first section of this chapter. In section 1.2 a brief review of data concerning the Eindhoven cyclotron is presented. In this thesis the emphasis is put on cyclotron central region research. An introductory discussion on this subject will be given in the last section.

1.1 Scope of the present study

Since the first physical realization (in 1959) of the Azimuthally Varying Field (AVF) principle of Thomas for the design of cyclotrons, nearly all cyclotrons built have a modulated field. In the last decades this principle has even evolved to the idea of separate sector cyclotrons. Separate sector cyclotrons accelerate an already pre-accelerated ion beam. Hence, the ion production is performed at an other stage.

In conventional AVF cyclotrons, of which an increasing amount of beam time is devoted to applications in the direction of medical, chemical and engineering purposes, either an internal ion source is used, or an external ion source (for instance employing axial injection) where the energy of the incoming particles is low with respect to the acceleration voltage. This implies that especially the first revolutions of the ion beam occur in the innermost part of the cyclotron centre, and a great influence is exerted on the accelerated beam by the geometrical structure of the acceleration system.

This thesis gives account of a cyclotron central region study that has been performed at the Eindhoven University of Technology. The study was mainly devoted to the Eindhoven AVF cyclotron, but also central regions of other cyclotrons have been investigated.

The aim of a central region study is in general to obtain a good centering of the ion beam, a good beam quality, a proper high frequency phase of central particles and a large beam current. The HF phase of an accelerated particle is the phase angle of this particle with respect to the top voltage of the applied accelerating HF voltage on the dee at the moment of a gap crossing; a negative HF phase means that the particle is accelerated on the decreasing side of the HF voltage.

To obtain a large beam current a proper design of the central region of the cyclotron is of importance. The electric and magnetic field configuration in the cyclotron centre have to be determined and trajectory calculations have to be carried out. The computed cyclotron acceptance has to be large. Changes in the central region geometry and hence in the electric field configuration may lead to an increased cyclotron acceptance and to more beam current than in an old geometry. Beam diagnostic equipment is necessary to measure the properties of the ion beam. As a result experimental knowledge on the beam parameters is acquired, for instance on the emittance and on the energy and HF phase of the particles. A disturbing influence on the cyclotron acceptance can be caused by a deviation in the position of the magnetic median plane with respect to the symmetry plane of the cyclotron magnet. Then corrections are needed. If all parameters in the cyclotron centre are known the properties of the ion beam that is transmitted through selecting diaphragms positioned at the first turns can be predicted.

In chapter 2 we describe the present status of the beam diagnostic equipment of the Eindhoven cyclotron and of the beam guiding system, extensions of its use, and experiments performed with it.

In chapter 3 several effects on the accelerated ion beam by parameter changes in the central region of the cyclotron are described.

A first subject in this respect is the adaptation of the geometry of the dee-dummy dee structure for the Eindhoven cyclotron, in such a way that a considerable increase in beam current is obtained. Also notes on median plane effects in the cyclotron centre are given.
A misalignment of the median plane of the cyclotron magnet tends to decrease the axial acceptance. This can be corrected by proper means. As an application in this chapter we finally give a brief description of the effect on the accelerated beam of the median plane injector

that is used at the Eindhoven cyclotron laboratory for the injection of polarised protons.

The effects of parameter changes in the central region of the cyclotron have to be measured either within the cyclotron itself, or in the beam guiding system, after beam extraction.

First it is important to determine the ion source emittance. A method for the measurement of the axial and radial phase space area within the cyclotron employing axial and radial slits respectively is described in chapter 4.

Once the ion source emittance is known one may predict the behaviour of a beam selected from a specific area in the radial or axial phase space. In chapter 5 we describe experiments with a beam selected in the centre of the cyclotron by means of diaphragms so that single turn extraction was obtained. The relative energy spread of the extracted beam was well below 10^{-3}.

For the measurement of beam properties several diagnostic means are available, as was mentioned before. The construction and use of diagnostic equipment was the subject of extensive studies at our cyclotron laboratory.

With the present study we end a project started in 1969 by Schutte (Schutte 73) called : "The Automatic Control of the Eindhoven AVF Cyclotron". This project was continued by Van Heusden (Van Heusden 76) and was financially supported by the FOM Foundation in the Netherlands from 1975 to 1979. Within this project diagnostic beam monitoring equipment in connection with automatic cyclotron control has been developed. Besides the research on beam diagnostic means other cyclotron studies were carried out at our laboratory, e.g. studies related to theoretical research on beam dynamics (Schulte 78). The emphasis of the present research was not on beam diagnostics, but the equipment was used thoroughly as measuring equipment, and additions have been contributed to it.

In the Addendum a diagnostic system not contained in chapter 2 is described, namely a computer controlled optimization system of the extraction efficiency. The extraction efficiency is defined as the ratio of the intensities of the external and internal beam current. The extraction efficiency is dependent on several cyclotron parameters e.g. of the setting of the current through the outermost concentric correction coils and of the harmonic coils. Improvements of the original control system are given. For the control an on-line least squares parameter estimation method was applied.

1.2 The Eindhoven AVF cyclotron

The Eindhoven cyclotron is the prototype Philips AVF cyclotron. It was constructed in 1963 as a constant orbit variable energy cyclotron for the acceleration of light ions. The proton energies are up to 30 MeV.

The performance of the cyclotron has been described extensively in early publications (Verster 62a, Verster 63); for more recent descriptions we refer to the theses of Schutte and Van Heusden (Schutte 73, Van Heusden 76). Figures 1.1 and 1.2 and table 1.1 give some main information about this cyclotron.

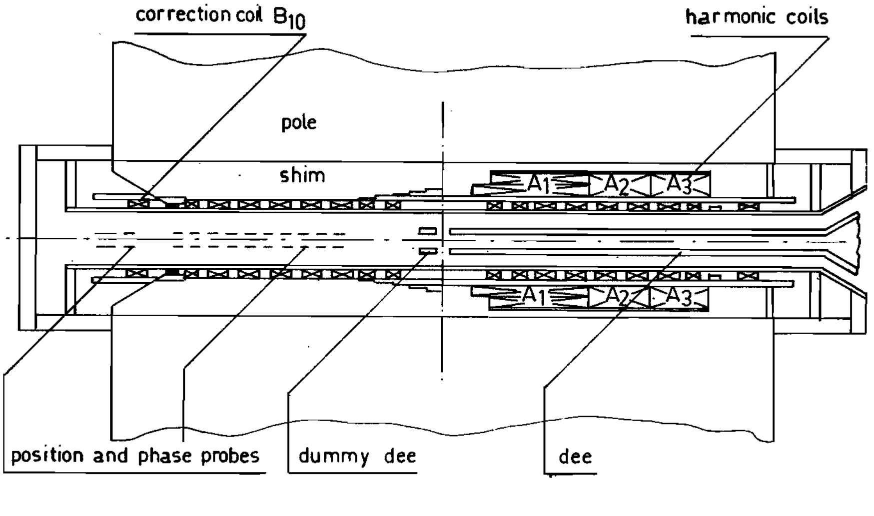

Figure 1.1 Axial cross-section of the Eindhoven AVF cyclotron.

The cyclotron has been used for several subjects :

- nuclear physics using polarised protons (Melssen 78, Polane 81, Wassenaar 81);
- PIXE analysis (Kivits 80);
- microbeam development for PIXE analysis (Prins 81);
- isotope production (Van den Bosch 79) : the following isotopes are routinely produced : ^{123}I, ^{52}Fe, ^{81}Rb (with the $^{81}Rb/^{81m}Kr$-generator), ^{87}Y (with the $^{87}Y/^{87m}Sr$-generator);
- atomic physics (Baghuis 74, Coolen 76);
- cyclotron research (Botman 80b, Corsten 80, Kruis 80).

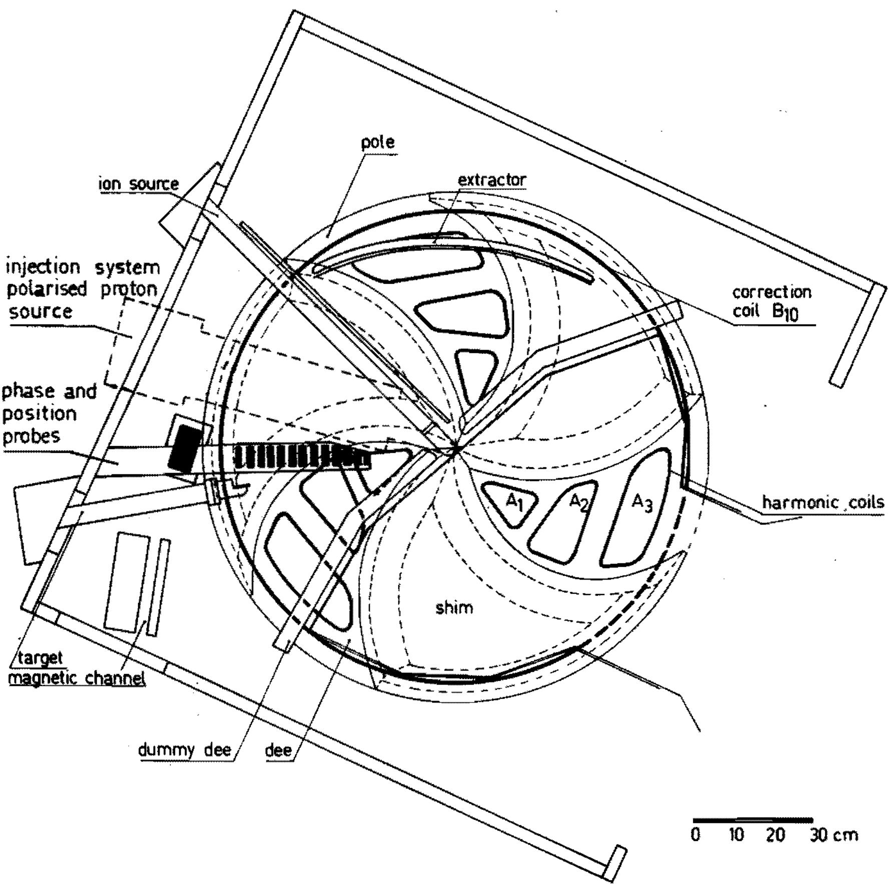

Figure 1.2 Horizontal cross-section of the Eindhoven AVF cyclotron. The z-direction, perpendicular to the median plane, is often refered to as the axial or vertical direction.

Table 1.1 Main data and properties of the Eindhoven cyclotron.

ion source	Livingston type $I_{filament} \leq 300$ A; $I_{arc,max} = 2$ A $V_{arc,max} = 500$ V
180° bevelled dee	$V_{dee,max} = 50$ kV; stabilized 1 : 10^4 $f_{HF} = 5 - 23$ MHz; stabilized 1 : 10^5
main magnetic field	pole diameter = 1.30 m threefold symmetry - spiral ridge min. gap = 150 mm, $B_{max} = 2.0$ T max. gap = 300 mm, $B_{min} = 1.2$ T max. mean magn. induction $\langle B_{max}\rangle = 1.55$ T stabilized 1 : 10^5
10 pairs of concentric correction coils B_i	$B_{max} = 24$ mT
3 pairs of harmonic coils A_{ij} 1)	$B_{max} = 2.5$ mT
electrostatic extractor	$r_{extr} = 0.534$ m, $\langle r\rangle = 0.52$ m $V_{extr,max} = 60$ kV over 4 mm max. extraction efficiency $\varepsilon_{max} = 85\%$
magnetic channel	length = 250 mm max. magnetic gradient 6 T/m
proton energy	$E_p = 1.5$ to 29.6 MeV
energy of other particles	$E_x = Z^2/A.E_p$
energy spread	$(\Delta E/E)_{fwhm} = 0.3\%$
quality	$q_{hor} < 18$ mm-mrad for 20 MeV protons $q_{vert} < 12$ mm-mrad for 20 MeV protons
energy spread of analysed beam	$(\Delta E/E)_{fwhm} = 0.07\%$ for slit widths $\Delta x_{entrance} = 1.0$ mm, $\Delta x_{exit} = 1.2$ mm

1) The inner harmonic coils A_{1j} are excited by independent excitation of A_{11} and A_{12} ($I_{A13} = -I_{A11} - I_{A12}$); the outer coils by excitation of A_{31} and A_{32}. Presently the middle harmonic coils are not used.

1.3 Radial and axial stability

After leaving the central region of the cyclotron, which can be regarded for the Eindhoven cyclotron as having a radial extent of about 10 cm, the motion of the particle can be described accurately using a general orbit theory (Hagedoorn 62, Schulte 78). Particles oscillate around a central spiralised orbit. The radial and axial oscillation frequencies ν_r and ν_z are mainly governed by the magnetic field focusing properties (in case of a rotational symmetric magnetic field given by the equations of Kerst and Serber (Kerst 41)).

In the centre of the Eindhoven cyclotron the azimuthal variation of the magnetic field (flutter) is negligible, and the radial variation may also be neglected. Then the magnetic vertical focusing is equal to zero. In this region electric focusing becomes important.

In a uniform acceleration gap the electric field between the dee and the dummy dee exerts a lense action on the ions. In case the particle has gained energy after crossing the gap, this focusing can be seen as a combination of several effects :

- alternating focusing : first the particle is pulled to the median plane, then it is pushed from it;
- acceleration focusing : due to the acceleration the particle is for a shorter time in the defocusing area;
- phase focusing : in contrast to the two previously mentioned effects which are also present for static electric lenses, phase focusing is purely a result of the time variation of the electric field, i.e. a result of the variation of the field strength during the gap crossing of the particle.

The electric vertical focusing strength rapidly decreases with the number of the revolution. The first formulas on the focusing action of a dee gap were given by Rose (Rose 38) and Wilson (Wilson 38). Kramer et al. and Hazewindus and Van Nieuwland have derived formulas based on a lense description of the accelerating field (Kramer 63, Hazewindus 67).

A typical picture of the vertical focusing in the Eindhoven cyclotron is shown in figure 1.3. It represents ν_z^2, being a good measure of the vertical focusing strength (Cohen 59), as a function of the radius. The plot is given for a proton energy at extraction radius of 7 MeV. Then the main magnetic induction in the cyclotron centre is 0.667 T, corresponding to a particle revolution frequency of 11.299 MHz. The electric focusing strength is HF phase dependent; it is given for particles having a HF phase of -30^o at the first half revolution in the dee. At a radius of approximately 8 cm there is an area of minimal axial focusing, giving rise to maximal vertical beam width.

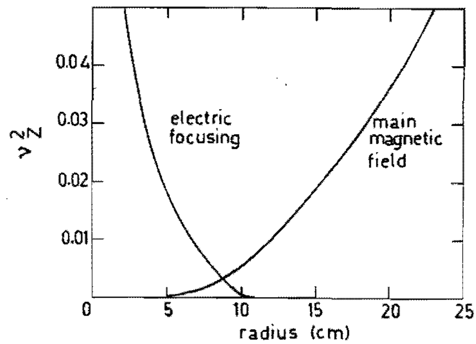

Figure 1.3 Axial focusing strength for the Eindhoven cyclotron. The figure is given for a main magnetic induction in the cyclotron centre of 0.667 T, corresponding to a revolution frequency of 11.299 MHz. The final proton energy is then 7 MeV. The electric focusing strength is given for particles having a HF phase of -30^o at the first revolution in the dee.

In practice, the shape of the electrodes in the centre of the cyclotron will be complicated. Then a precise calculation based on an electric field map of the acceleration gap is necessary.

1.4 Central region research

As was pointed out in the previous section a complete electric field map of the interior of the cyclotron is necessary for a proper calculation of the particle trajectory. This is done by obtaining the electric field components in a static field configuration; a time dependent factor then has to be added.

In the region of the ion source and the puller the dee gap is both non-uniform and asymmetric. The electric field components in the median plane have strong gradients in this region resulting in asymmetrically curved equipotential lines in the median plane.

Dutto (Dutto 75) and Gordon (Gordon 80) have given a theoretical approach for the relation between the focal strength of the electric lenses in the dee gap and the inhomogeneity of the electric field in the median plane. The radial field components in the cyclotron centre give rise to a momentary change in the revolution frequency and to a change in the oscillation frequencies.

To obtain the electric field map for a cyclotron centre three methods are in use. First there is the electrolytic tank method. Numerous cyclotron centres have been designed based on electrolytic tank measurements. At first two dimensional measurements in the median plane have been reported (Blosser 63, Kramer 63, Reiser 68). Later the method was extended to three dimensional measurements. This method has recently been used for the design of the MSU superconducting cyclotron (Liukkonen 79). In the electrolytic tank the electrostatic potential is measured and the electric field components are determined by differentiation.

A second method that becomes more and more important is a numerical field calculation using relaxation techniques. A recent description of such a numerical program has been given by Kost (RELAX 3D, Kost 80). Boundary conditions have to be given by the user in a mesh of points. For a complex cyclotron centre this may require a considerable amount of memory space in the computer.

A third method that has been reported is the magnetic analogue method (Van Nieuwland 68, Hazewindus 74). In a three dimensional magnetized iron model of the cyclotron centre the magnetic field components are measured by three Hall probes. Thus the electric field between the acceleration electrodes is simulated by a magnetic field in the model. The method is based on the fact that the electric field in the cyclotron and the magnetic field in the model obey the same differential equations and that they have the same boundary conditions. In the magnetic analogue method the field components are determined directly, while in an electrolytic tank measurement one obtains voltages which require differentiation to get the field components.

An advantage of the magnetic analogue method is that it is very directly related to reality.

The magnetic analogue method has been used extensively for studies of the central region of the 72 MeV SIN injector cyclotron which had to be operated in a first and third harmonic mode (Hazewindus 75, Van Nieuwland 77) and for the design of the interior of a Philips compact isochronous cyclotron (Van Nieuwland 72).

In our laboratory this method is used for a study on the cyclotron centre of the Eindhoven cyclotron (Borneman 77). Furthermore a model was constructed for the cyclotron of the Free University of Amsterdam, which is rather similar to the Eindhoven cyclotron. Next a model was constructed for the cyclotron of the KVI Groningen. In this particular case a central region has to be designed capable of accelerating particles in first or third harmonic mode with an internal ion source or by axial injection (Van Asselt 79).

The design of the central region of the Eindhoven cyclotron was originally based on studies of electrolytic tank measurements of centre models (Kramer 63). In this design of the central region the original idea of Smith (Smith 60) has been incorporated. The particles have an increased path length on the first half revolution. Then they are accelerated on the decreasing side of the HF dee voltage after one half turn. This improves the axial focusing. For this reason the angle between the ion source puller-system and the acceleration gap is about 20^{o}.

In chapter 3 results of measurements in a magnetic analogue model of the Eindhoven cyclotron will be presented.

CHAPTER 2

DIAGNOSTIC EQUIPMENT

This chapter gives a survey of the diagnostic equipment of the cyclotron and the beam guiding system. Special attention is given to some new developments. These regard energy measurements using a time of flight method and the reproducibility of vibrating beam scanners in the beam guiding system. Special features of a recently installed ion source allow better control of the positioning and allow measurements of radial and axial beam emittances in the central region of the cyclotron by remote-controlled movable diaphragms.

2.1 Introduction

In this chapter we describe the diagnostic equipment of the cyclotron with emphasis on some new developments. The ion beam of the AVF cyclotron is pulsed with a repetition rate equal to the frequency of the accelerating field. The phase of the centre of charge within a beam pulse with respect to the applied HF field is determined by the isochronism of the cyclotron magnetic field. In section 2.2 the phase measurements of the ion beam on several radii within the cyclotron, developed by Van Heusden is shortly described.

Phase probes in the beam guiding system allow a time of flight measurement to determine the energy of the extracted beam. The energy measurements are described in section 2.3 together with a comparison with energy measurements using other methods.

The duty cycle of the cyclotron, defined as the ratio of the time duration of the beam pulse and the repetition time of the HF field, is approximately 10% for the Eindhoven machine. This means that the phase width of the ion beam pulse is about 40°. The measuring system for the determination of the time structure of the external beam is described in section 2.4.

In the beam guiding system vibrating scanners are operating, by which the horizontal and vertical beam width and position can be measured. In the past variations in amplitude and symmetry of the vibration with respect to the optical axis of the scanners caused an inadmissable inaccuracy in the results. Therefore, an amplitude and symmetry control system was designed. The scanner system is described in section 2.5.

For many experiments with the ion beam a stable performance of the cyclotron operation is essential. High stability criteria are imposed on the main magnetic field, on the dee voltage amplitude and dee frequency and on power supplies for correction coils. At present we have a dee frequency stability better than 10^{-5} and a magnetic field stability of 10^{-5}. The dee voltage stabilization is essentially achieved by two main changes (Aerssens 80) : a thyristor feedback system for the high voltage rectifier is used and the filament of the oscillator is fed with DC current. The stability is presently better than 10^{-4}. The increase of the dee voltage stability, which results from the DC supply of the oscillator filament, can be nicely observed in single turn experiments (chapter 5). The single turn effect disappears when an AC current is used.

The data handling system for the diagnostic- and control-equipment of the cyclotron consists of a PDP 11 computer and CAMAC modules. Figure 2.1 shows the set-up of the system. Two PDP 11 computers have access to the system crate and two CAMAC branches originate from it.

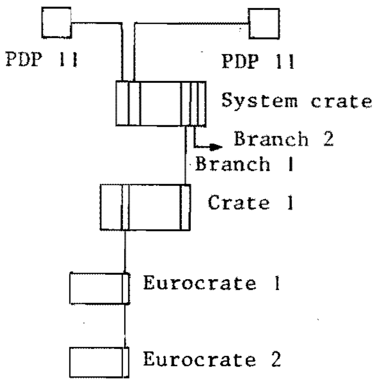

Figure 2.1 Set-up of the CAMAC data handling system for the cyclotron control and beam diagnostics.

Peripheral equipment like plotter, printer, and video display is common for both computers. The cyclotron branch consists of a CAMAC crate, extended with two home-made so-called Euro-crates (Van Nijmweegen 80).

The CAMAC crate contains among others modules for the phase measuring and control equipment (section 2.2), for the extraction efficiency optimization equipment (described in the Addendum), for the computer control of the magnetic analogue measuring machine (see chapter 3), and for the positioning of the ion source and diaphragms in the cyclotron centre.

All important cyclotron setting parameters can be computer controlled with the use of stepmotor controlled potentiometers, via a stepmotor control unit in the CAMAC crate. They are used for the phase control and for the extraction efficiency optimization.

In the Particle Physics Group of the Physics Department a modular computer-to-experiment interface system was developed, with similarity to the CAMAC system (Van Nijmweegen 80). This system is employed as an extension of the CAMAC system. We use it for applications where low cost Eurobus modules like scalers, preset scalers, and I/O registers are available. The addressing of a module in an Euro-crate is performed via a special CAMAC module : the CAMAC-Eurobus-converter. Two Eurobus crates are present : one for beam scanner signal detection (section 2.5) and one for pulse formation for the extraction optimization system (Addendum).

For reasons of reproducible adjustments a new ion source was installed in 1979 at the Eindhoven cyclotron [1)].

The ion source is a Livingston type source (Livingston 54, Kramers 63) for production of light ions (protons, deuterons, alpha particles, etc.). Maintenance, such as the renewal of the filament after several days of operation, demands an easy access to the ion source; this means facilities for simple removal of the source from the vacuum chamber.

---

1) The ion source is constructed (among others) by P. Magendans and A. Platje, by the mechanical workshop of the Physics Department (besides H. Habraken and H. Heller we mention J. van Asten and G.M. Weijers) and by the EUT Central Technical Division.

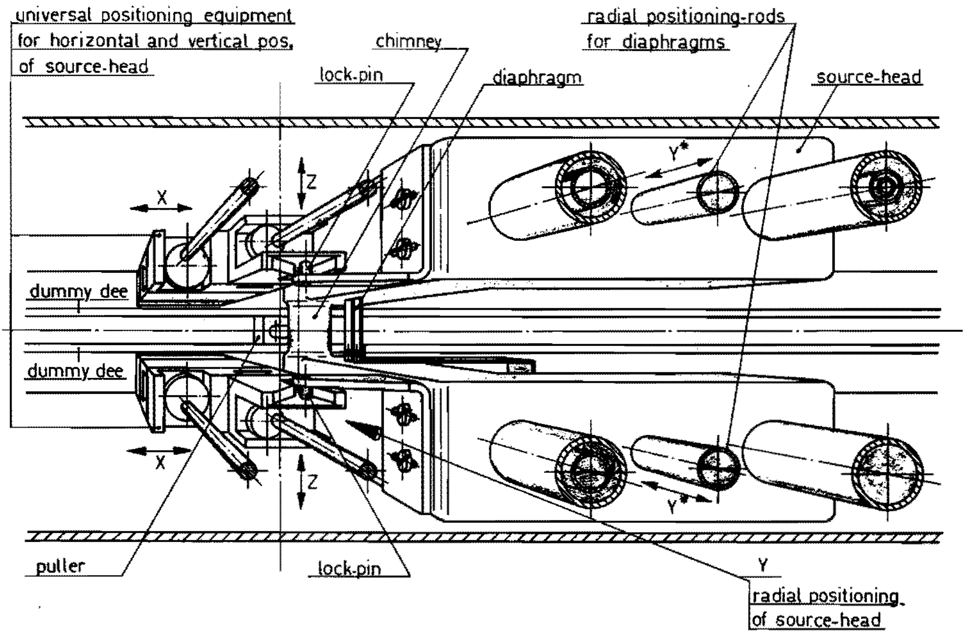

Figure 2.2 The head of the ion source.

The design of the chimney and of the power supply unit for the gas discharge were improved. The ion source can be operated in DC or pulsed mode (msec pulsing). The head of the ion source was made of one piece of copper, through which channels for supply of gas, cooling water and electric current were constructed. It is a suitable place to install diaphragms, current probes and deflection plates. On the new ion source two remote controlled diaphragm movements are available : radially over several centimeters or azimuthally over about 10^{o}. Three electric connections are present, which can be used for instance for beam current measurements in the centre of the cyclotron. One of these is a 200 Ω transmission line, to which a 50 to 200 Ω pulse transformer is connected, allowing beam pulsing in the nanosecond region.

An essential feature of the new ion source is that it can be positioned in a reproducible way in three directions : radially, vertically and along the dee gap. This positioning, the adjustment of the diaphragms, and also the movement of the source into or out of the vacuum chamber is performed completely by remote control. The initial conditions in the cyclotron centre, which are of essential importance for the rest of the acceleration process, can thus be fixed reproducibly.

A drawing of the present ion source is given in figure 2.2.

2.2 Phase measuring system

The phase information of the internal beam is obtained from eight pairs of capacitive pick-up probes; each pair consists of plates lying above and below the median plane respectively (Feldmann 66, Schutte 73). The phase probe signals are correlated with a frequency-doubled dee-signal. At first, sampling-techniques were applied to transform the signals to lower frequency ($\sim$ 1 kHz), to be able to perform the correlation (Schutte 73). Later high frequency double balanced mixers became available. Thus the correlation can be performed using the HF signals directly. A system based on HF mixers, which works for every dee frequency, was designed and built by Van Heusden (Van Heusden 79). Besides some HF amplifiers for amplification of the pick-up probe signals, the system consists of passive electronic components like power splitters and combiners, double balanced mixers, sharp filters, attenuator-switches, etc. After some years of operational experience the HF mixer system has turned out to be useful and reliable. Minimum measurable beam currents are of the order of 10 nA. The accuracy of the phase measurement is better than 0.5^{o} for a current of 50 nA. This method is also used for the Jülich cyclotron (Bräutigam 79), for HMI Berlin (Schulte 78) and will be built for NAC (Schneider 80).

The probe signals are selected with a high frequency multiplexer, near the probes and are transported to the control room via one cable. Some extra channels of the multiplexer can be used for phase pick-up probes directly after the extractor and in the beam guiding system. They serve for energy measurement and position determination. This is described in section 2.3.

2.3 Phase probes in the beam guiding system

At two locations in the beam guiding system capacitive pick-up probes are placed. They consist of shielded half cylinders with a length of 13 cm. The inner cylinder has a diameter of 4 cm, whereas the diameter of the vacuum chamber is 4.5 cm. In front of the probes carbon diaphragms of 3.5 cm diameter are installed, so that no beam can hit the probe. The signals from the two electrodes in a probe are added or subtracted by power combiners, and are amplified directly near the probes (figure 2.3). The probes are used for energy measurements and for horizontal position determination, i.e. position determination in the horizontal plane and perpendicular to the direction of propagation of the beam. The distance between the two probes in the beam guiding system is 12.7 m.

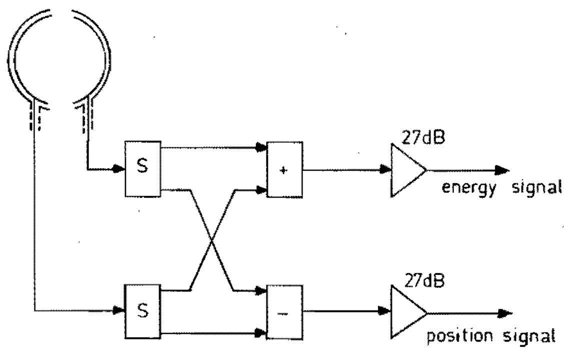

Figure 2.3 External phase probe used for energy and position determination.

2.3.1 Position determination

The amplitude and the phase of the subtraction signal of an external phase probe provides information on the beam position. Figure 2.4 shows a measurement with this probe, together with a beam position and width determination by a beam scanner (*BC3*, see figure 2.7) located 30 cm from the phase probe. A bending magnet was used to vary the beam position. Generally for the phase probe position determination an accuracy of 0.5 mm is achieved, even for 10 nA beams (see page 24). When the beam position changes sign with respect to the ion optical axis (see figure 2.5) a zero transition of the "in phase" signal occurs. The 180^{o} phase jump provides a very sensitive position indication (even better than the amplitude of the subtraction signal) and may be used for fast monitoring or optimization of the transport of the external beam.

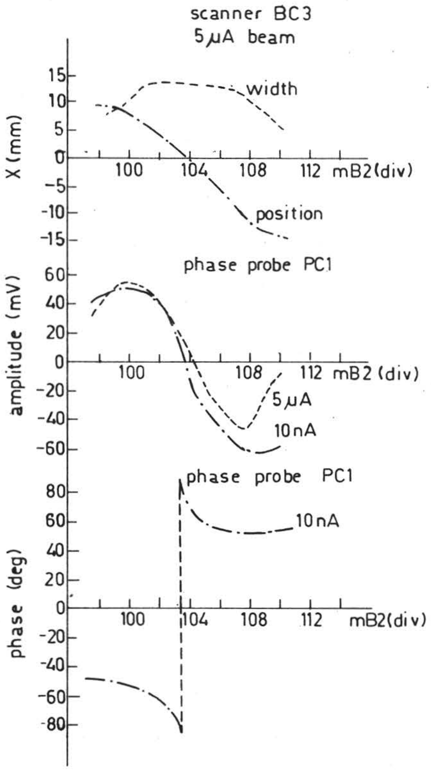

Figure 2.4
Position determination with phase probe PC1 and with beam scanner BC3. Correction magnet mB2 was used to sweep the beam (see figure 2.7 for a lay-out of the first part of the beam guiding system). For the 10 nA beam the phase probe signal was amplified by an extra factor.

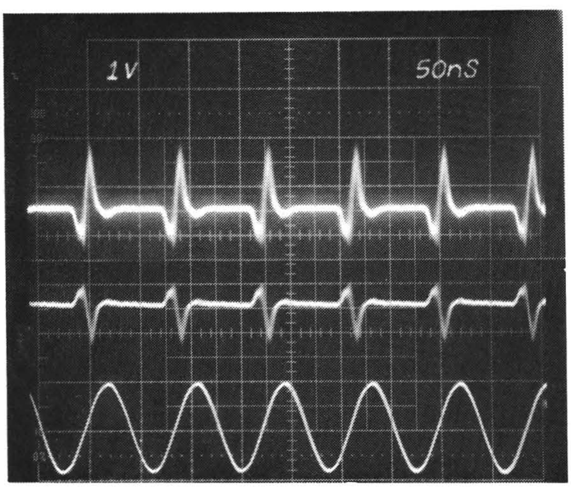

position + 1 mm

position - 1 mm

dee voltage

Figure 2.5 Phase probe signal on probe PC1 together with the dee voltage. A 180° phase jump occurs for a beam changing position with respect to the optical axis. The beam current was 1 µA. Proton energy 7 MeV; $f_{dee} = 11.299$ *MHz.*

2.3.2 Energy determination with phase probes

The two phase pick-up probes in the beam guiding system allow an accurate and absolute measurement of the energy of the extracted beam. The energy is evaluated from a Time Of Flight (TOF) measurement. The energy E relates to the relative speed $\beta = v/c$, where v and c are the speeds of the particle and of light respectively, as follows

$$E = E_o \left(\frac{1}{(1-\beta^2)^{\frac{1}{2}}} - 1 \right) \tag{2.1}$$

in which E_o represents the particle rest energy, 938 MeV for protons. The speed v of the particle is obtained from the phase difference $\Delta\phi$ in the beam signals on the two probes, the angular frequency ω of the voltage on the accelerating electrodes, and the distance d between the probes :

$$v = \frac{\omega \; d}{(\Delta\phi + 2\pi k)} \tag{2.2}$$

where k is an integer. In our case $k = 4$ since the distance between the probes (12.7 m) is about 4 times the distance the particle travels in the cyclotron at the last complete turn (extraction radius ≈ 0.5 m). This implies that four beam pulses are propagating between the phase probes at a time.

The phase of the beam at the two capacitive pick-up probes with respect to the phase of the accelerating voltage is measured with the equipment described in section 2.2. The two probes are connected to the probe channel multiplexer via coaxial cables of equal delay time. The energy is displayed by the PDP 11 computer as the mean value of ten measurements, together with the standard deviation.

Special care must be taken that the voltage level of unwanted signals on the phase probes is small with respect to that of the beam pick-up signal. This is mainly achieved by a proper shielding of the probes. The beam signals are amplified immediately near the probes by 27 dB amplifiers. Presently for a 7 MeV proton beam (dee frequency 11.3 MHz) the voltage level of the disturbance signal is about 60 µV, whereas the beam signal level is 180 µV for a 100 nA beam current. The disturbance signal (measured at zero beam current) is vectorially subtracted by the computer from the beam signal.

The energy determination method shows that the energy can be measured with an absolute accuracy better than 10^{-3} and with a relative accuracy better than 10^{-4}.

The TOF method provides a measurement of the mean value of the inverse of the velocities of the particles. Several effects may influence the inverse velocity distribution. Changes of this distribution due to the energy spread of the beam, i.e. $\Delta E/E \simeq 3 \cdot 10^{-3}$ (FWHM) (Schutte 73), or due to path length differences (i.e. in the analysing magnets) are negligible. The time structure can change considerably if a part of the beam is cut away by an improper setting of beam guiding system parameters. A loss of beam of 10% may give rise to an apparent relative energy change of 10^{-3}.

2.3.3 Energy measurements

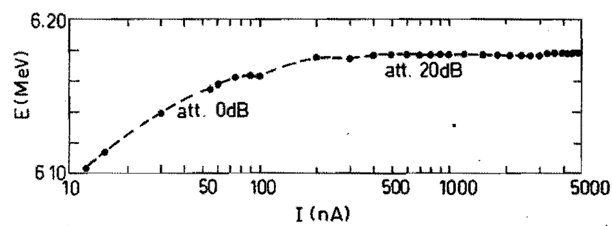

Figure 2.6 *Energy determination with phase probes PB1 and PC1. For lower currents the influence of the disturbance signal increases giving rise to less accurate energy determinations. The nominal cyclotron setting was 6 MeV protons; dee frequency 10.437 MHz. The attenuation of the phase probe signals for larger beam currents is required for a proper adaptation of the voltage level of these signals to the correlators.*

As an example of the performance of the energy measurements figure 2.6 shows a plot of the external energy versus beam current for a 6 MeV proton beam (phase width $\sim 40^\circ$). The deviation at the low current side is due to disturbance signals with an amplitude of the order of the amplitude of the beam signal.

The time stability of the energy determination was found to be better than 10^{-3} for a beam of 40° phase width. The stability increases by a factor of 10 or more if a well defined beam (e.g. through the use of slits in the cyclotron centre) with a small phase width ($\sim 5^{\circ}$) is produced. In chapter 5 phase and energy measurements in this situation are presented.

Degrader foils are used for a check of the double achromaticity of the beam guiding system (cf. section 2.3.4). The stopping power can be evaluated with equations given by Zaidens (Zaidens 74).

We measured the stopping power of polyethylene foils for a 7 MeV proton beam by performing a difference measurement : an energy determination without or with a foil in the beam guiding system in front of the external phase probes. For a 1.4 mg/cm^2 foil we measured ΔE = 80 ± 5 keV, whereas the calculated value is ΔE = 83.9 keV. For a formvar foil of estimated thickness 0.2 mg/cm^2 we found ΔE = 14 ± 2 keV.

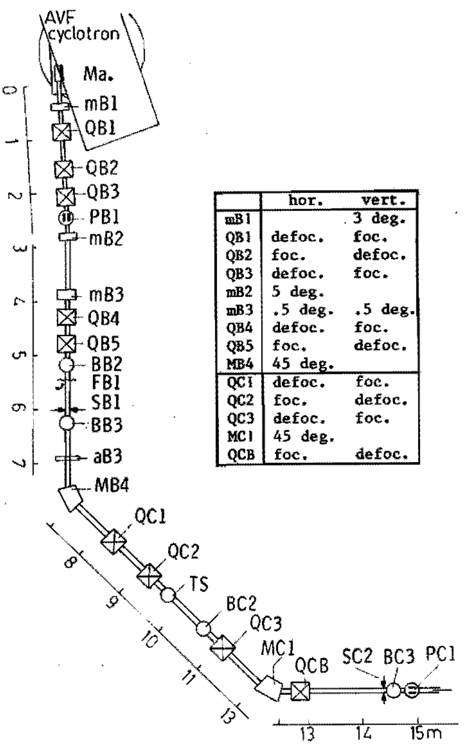

	hor.	vert.
mB1		.3 deg.
QB1	defoc.	foc.
QB2	foc.	defoc.
QB3	defoc.	foc.
mB2	5 deg.	
mB3	.5 deg.	.5 deg.
QB4	defoc.	foc.
QB5	foc.	defoc.
MB4	45 deg.	
QC1	defoc.	foc.
QC2	foc.	defoc.
QC3	defoc.	foc.
MC1	45 deg.	
QCB	foc.	defoc.

a	current measurement
B	beam scanner
F	foil
m	correcting magnet
M	bending magnet
Ma.	magnetic channel
P	phase pick-up probe
Q	quadrupole lens
S	slit
TS	time structure

Figure 2.7 Lay-out of the first part of the beam guiding system.

For several cyclotron settings the time of flight energy measurement method employing the two phase probes in the beam guiding system was compared with two different energy determinations, namely with a nuclear physics cross-over measurement (Smythe 64, Bardin 64), and a numerical evaluation using the field data of the cyclotron magnet. For the numerical calculation the precise shape of the fringe field and the exact position of the extractor have to be taken into account. For a specific proton cyclotron setting a maximum deviation of 1.5% was obtained for the three different energy determinations.

2.3.4 Dispersive or double achromatic mode of the beam guiding system

Figure 2.7 shows a part of the beam guiding system that is relevant to the experiments described in this thesis. The quadrupoles *QC1*, *QC2* and *QC3* can be set in such a way that either a dispersive, or a double achromatic mode of operation is obtained (Schutte 73, Sandvik 73). In the dispersive mode the beam through slit *SB1* is focused on slit *SC2*, where an analyzed beam is obtained, with an energy definition of $3 \cdot 10^{-4}$ for 2% of the total beam current.

To verify whether the dispersive or double achromatic setting is correct, we use a foil (*FB1*) that lowers the energy of the beam by about 0.8% [1]. By a specially placed quadrupole *QCB* the focus of the beam can be put either on slit *SC2* or on beam scanner *BC3*. Figures 2.8a and 2.8b show the beam spot on *BC3* for both cases with and without the foil. The energy degradation in the foil was measured with the external phase probes (section 2.3), and also calculated (Zaidens 74). The broadening of the beam spot is due to energy and angle straggling in the foil. The width and position of the beam agrees with data from a beam transport optimization program (BGS, Van Genderen 79). In the dispersive mode the dispersion is 0.18 mm/keV.

---

1) *In this case we used a polyethylene foil of 1 mg/cm^2. For a 7 MeV proton beam the energy loss is ΔE = 60 keV, the energy straggling is η = 15 keV, the angle straggling is $\theta_{1/e}$ = 4.5 mrad.*

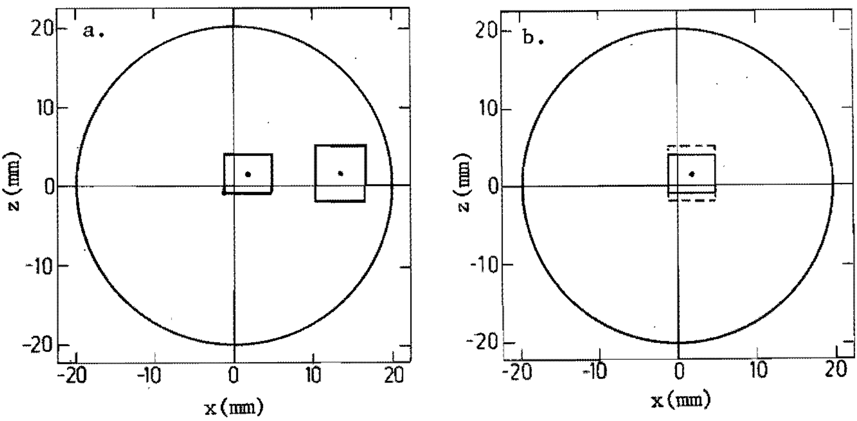

Figure 2.8 *Position of the beam spot at beam scanner station BC3 in the dispersive mode (a) and in the double achromatic mode (b) with and without the use of foil FB1. The proton energy is 7 MeV. The energy degradation due to the foil is 60 keV. The dispersion is 0.18 mm/keV.*

2.4 Time structure measurement of the beam pulse

A standard nuclear physics multichannel time analyser method is used to measure the time structure of the external cyclotron beam (Rethmeier 69, Johnson 69, Van Heusden 76). A small fraction of the proton beam is scattered by a polyethylene foil towards a solid state detector. If necessary a degrader foil in front of the detector can be used to lower the energy of the incoming protons. A block scheme of the time structure system is given in figure 2.9.

The detector signal is fed into a Constant Fraction Discriminator (CFD) via a pre-amplifier. This discriminator converts the incoming

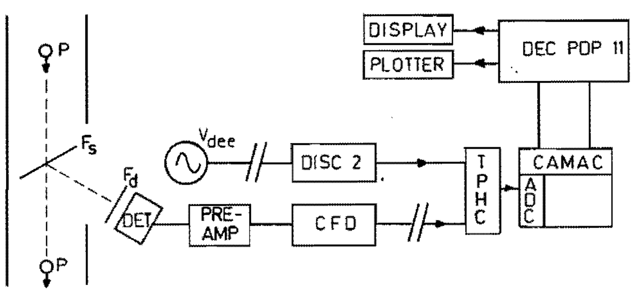

Figure 2.9 *Block scheme of the time structure equipment.*

voltage pulse into a standard logical NIM pulse, and compensates for height and risetime differences in incoming pulses, in such a manner that the time difference between the beginning of an incoming pulse and the standard NIM pulse is constant. The standard logical pulse of the CFD is used as start signal for a Time to Pulse Height Converter (TPHC). A pulse, obtained for each positive slope zero crossing of the dee voltage, is used as a stop signal for the TPHC. The output of the TPHC is either directly fed into a multi-channel analyser or into a nuclear ADC in CAMAC for further computer handling. The obtained spectrum gives the time structure of the external beam.

With this set up a pulse width resolution of 250 ps was measured, which means for 7 MeV protons (dee-frequency 11.3 MHz) a phase width resolution of 1^{o}. Under normal operation conditions the phase width of the cyclotron beam is measured to be about 40^{o}. In case slits are used in the central region of the cyclotron the phase width can be decreased to about 6^{o} (chapter 4 and chapter 5).

2.5 Beam scanners

Scanner units are placed at ten locations in the beam guiding system to measure the position and width of the external beam (Schutte 73, Van Heusden 76). Each unit consists of two vibrating scanners (Danfysik) : iron wires of 0.5 mm that sweep through the beam, one for horizontal and one for vertical detection. The scanners are driven simultaneously by a sine generator with a frequency of about 12 Hz. The amplitude of the scanner oscillation is about 2 cm.

In the past it turned out that the movement of the scanner wire was not sufficiently stable : variations in amplitude and symmetry of the oscillation (e.g. due to friction) caused an inaccuracy of measurements. Therefore an amplitude and symmetry control system was designed to compensate for these variations. Essential in this control system is the use of a so-called dummy-beam [1)]. A metal plate with a well determined width is mounted on the scanner arm, but outside the beam area. It incercepts the infrared light of an optical detector

---

1) The control system is designed by A. Kemper of our group.

(slotted optical limit switch) consisting of a LED and a phototransistor. Two times in a period the metal plate intercepts the light of the LED, causing current pulses in the phototransistor.

The width of these current pulses and the time interval between them are measures of the oscillation amplitude and of the deviation from the optical axis. Deviations are compensated by changing the amplitude and the DC level of the scanner vibration steering voltage. This control loop takes about 1 minute to stabilize. Figure 2.10 shows a picture of a beam scanner unit, consisting of a horizontal and a vertical scanner, and assembled with the dummy-beam electronics.

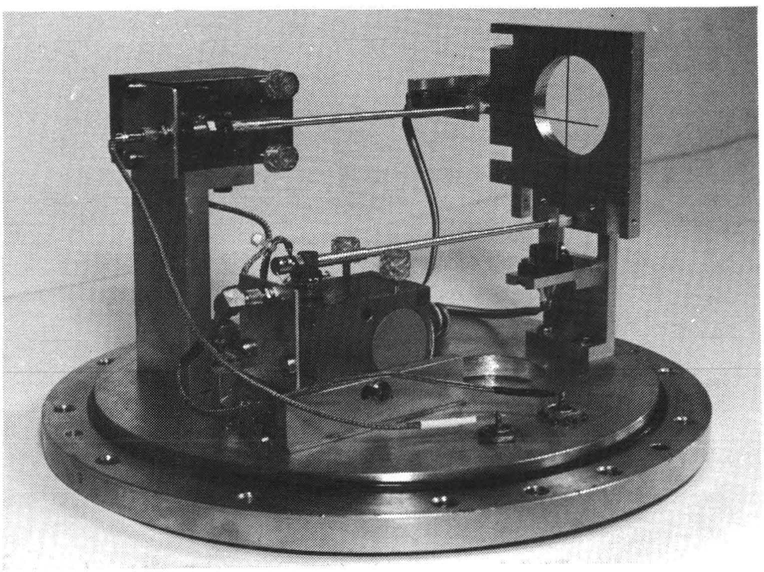

Figure 2.10 *Beam scanners for horizontal and vertical width and position detection. On the scanner arms metal plates are mounted that intercept the infrared light of an optical detector. With the induced current pulses the scanner arm movement is stabilized.*

The computer handling is performed via Eurobus modules and CAMAC. The PDP 11 computer evaluates the formulas for the vertical as well as the horizontal width and position of the beam and sends the results to a terminal, a video-display or a plotter. An on-line view on the video display may be given of the beam envelope at several stations along the beam guiding system, which makes the equipment very helpful for optimization of the beam transport.

With our scanner system it is possible to determine the beam width and position with an accuracy of 0.1 mm for a minimal beam current of 1 nA. Finally, the current signal of a vibrating wire can be observed directly on a scope, and may show spatial structure in the beam. If, for example, the scanner is located behind the analysing part of the beam guiding system, this indicates energy differences in the ion beam (see chapter 5).

CHAPTER 3

INVESTIGATIONS ON THE ION BEAM IN THE CENTRAL REGION

In this chapter we describe investigations on the ion beam in the cyclotron central region employing the magnetic analogue technique. The central region parameters essentially fix the properties of the accelerated beam. With the magnetic analogue method the shape of the electric field in the cyclotron centre is determined. Calculations based on the obtained field map provide the theoretical knowledge on the beam properties, in particular for a beam transmitted through selecting diaphragms positioned on the first few turns.

Investigations of several electrode configurations and associated numerical calculations have led to a new puller design. The beam current output increased by at least a factor three.

The median plane of the main magnetic field of the cyclotron does not coincide with the midplane of the cyclotron magnet at small radii. This tends to decrease the axial acceptance of the cyclotron for the injected beam. We will discuss this together with related phenomena and point out methods to correct the deviations.

As an application we finally consider the effect of the median plane trochoidal injector for polarized protons on the axial behaviour of the accelerated ion beam.

3.1 Introduction

For a caluclation of the particle trajectories in the centre of the cyclotron the precise shape of the magnetic and especially of the electric field is required. For the equations of motion either a constant magnetic field or a field containing the azimuthal and radial variations obtained from field measurements can be used. The electric field shape is acquired from measurements in a magnetic analogue model of the electrode configuration (Van Nieuwland 68, Hazewindus 74).

The particle beam is represented as an ensemble of points in the six dimensional phase space with the generalized particle coordinates and momenta as axes (Banford 66). In our case the influence of the transverse motion on the longitudinal motion is neglected. As we neglect the spread in the starting velocity from the ion source, we get a collection of trajectories characterized by the starting HF phase and the starting geometrical conditions. The transverse motion is then solved seperately for each value of the HF phase. The two transverse motions can often be considered to be uncoupled. Then Liouville's theorem implies the constance of the beam areas in the separate two-dimensional transverse phase spaces, the radial r, p_r phase space and the axial z, p_z phase space. Here r and z are the radial and axial distance from the trajectory of a central particle which is defined for each starting phase, while p_r and p_z are the radial and axial momenta respectively.

The beam quality is defined as the area the beam possesses in phase space. Generally a "good" beam quality is required, which means a "small" phase space area. In chapter 4 radial and axial beam quality measurements in the central region are presented. This chapter deals with calculations on particle trajectories in the centre of the cyclotron which provide model figures for the occupied beam area in phase space. The actual calculations are carried out in x, y, z-coordinates which are transformed to r, p_r- and z, p_z-values at certain inspection positions.

We split the motion in two parts viz. the trajectory from the plasma surface of the ion source to a point in the puller where the electric field strength vanishes (first dee transition of the particle) and the rest of the trajectory. For the first part we estimate trajectories (for each starting phase) neglecting velocity spread at the plasma boundary. As a result we get zero emittance distributions in the transverse phase planes at the transition points. We take as initial conditions for the actual calculations suitably chosen phase grids around these data. Moreover the calculation of the first trajectory gives the energy of the particle.

3.2 The magnetic analogue method

A static magnetic field is generated between the dee and the dummy dee in a three dimensional iron model of the electrode configuration in the cyclotron centre. The method is based on the similarity of magnetic fields and electric fields. The three magnetic field components are measured with Hall probes.

A measuring machine, constructed at the Philips Research Laboratories (cf. figure 3.1), takes care of the positioning of the Hall probes. In one complete field measurement a grid of at least 4000 points has to be scanned. The machine is controlled by a PDP 11/03 computer via CAMAC. The Hall voltages are measured by a dual slope ADC in CAMAC and the data are stored on floppy-disk. Figure 3.2 shows a block diagram of the measuring system.

In figure 3.3 a lay-out is given of the centre configuration of the Eindhoven cyclotron. The acceleration gap has a width of 20 mm, the aperture of the dee and the dummy dee is 25 mm and the aperture of the puller is 6 mm. The analogue model of the EUT cyclotron is a 2.5 times enlarged model. A pair of exciting coils of each maximal 500 ampere-turns is used to obtain a maximum field in the acceleration gap of about 200 gauss. Figure 3.4 shows a part of the analogue model. We define the x- and y-coordinates as cartesian coordinates lying in

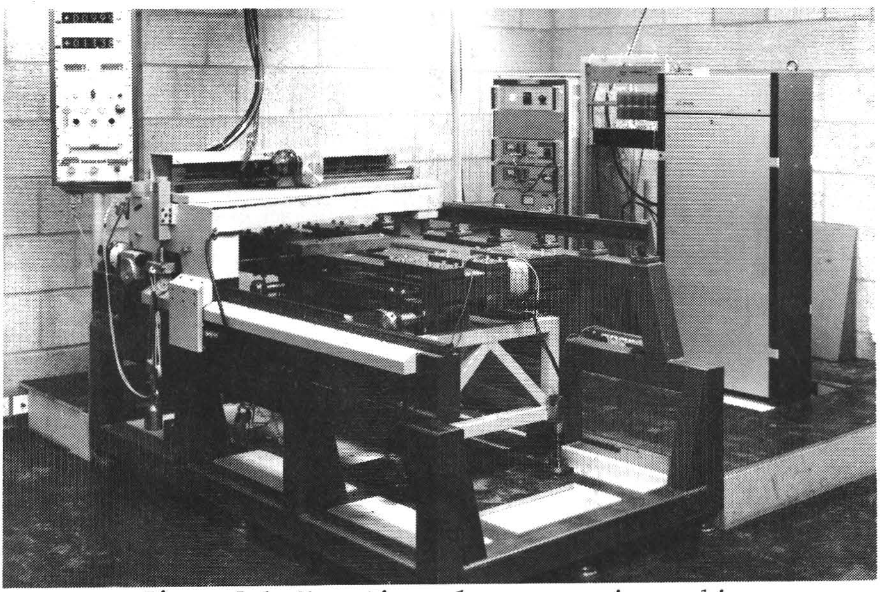

Figure 3.1 Magnetic analogue measuring machine.

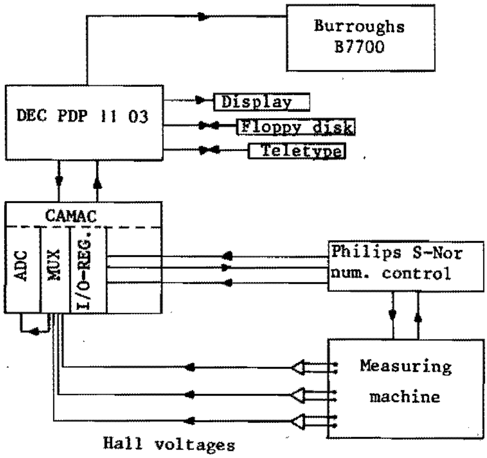

Figure 3.2
Block diagram of the computer-controlled measuring system.

the median plane, x along the dee gap. The z-coordinate is perpendicular to this plane. The B_x and B_y Hall probes lie in the median plane. Because of symmetry the vertical field component B_z is equal to zero in the median plane and is up to third order linear in z above the median plane :

$$B_z(x,y,z) = z\left(\frac{\partial B_z}{\partial z}\right)_{z=0} + \frac{z^3}{6}\left(\frac{\partial^3 B_z}{\partial z^3}\right)_{z=0} + O(z^5) \qquad (3.1)$$

The linear approximation is taken, which holds for paraxial trajectories. Therefore the vertical field component is measured by two Hall probes at fixed heights z_o and $-z_o$ with respect to the median plane. An extensive discussion of alignment tolerances of Hall plates and other experimental aspects is given by Hazewindus (Hazewindus 74).

3.3 Equations of motion

The data obtained from the magnetic analogue measurements are sent to the Burroughs B7700 computer of the EUT Computing Centre for further analysis. Numerical calculations are performed based on the electric field map. Information on the radial and axial particle motion is obtained. The equations of motion are integrated by an ALGOL 60 program called ORBIT/CALCULATION (Borneman 77).

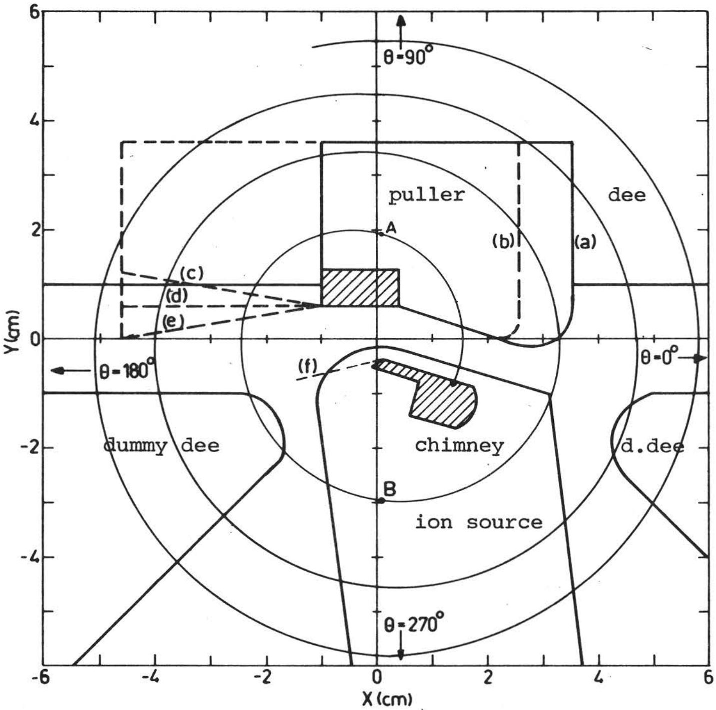

Figure 3.3 *Lay-out of the central region of the Eindhoven AVF cyclotron. The shaded areas (of the chimney and of the puller) represent intersections of the median plane. The orbit for particles starting with a CP phase of -30^o in the puller (point A) is drawn. The dashed lines show new central region geometries that have been investigated (cf. section 3.5) : (b) is the reduced puller on the right-hand side, (c), (d) and (e) are extensions of the puller at the lefthand side, (f) is a sheet constructed at the chimney to capture spurious beam. The puller shape with the full lines ("old puller" (a)) is the original design.*

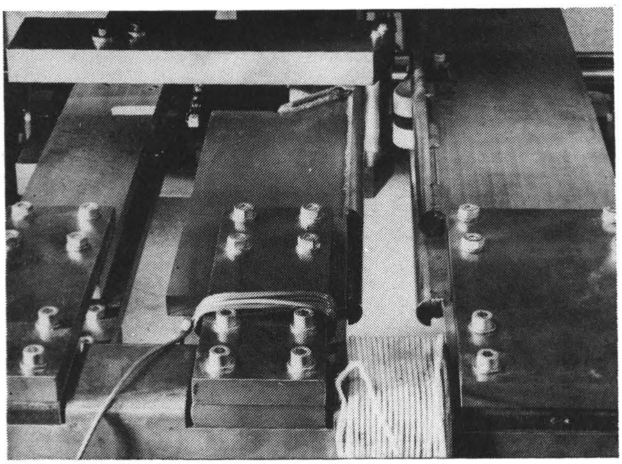

Figure 3.4
A part of the centre model of the Eindhoven cyclotron.

The magnetic field $\vec{B}$ is reduced by B_{iso} which is defined by $B_{iso} = m_o\omega/\Omega e$, where ω is the angular dee frequency, where m_o and e are the particles rest mass and charge respectively and where the integer Ω gives the ratio of the HF frequency applied on the dee and the revolution frequency of the ions [1)], the time t is reduced to τ by $\Omega\tau = \omega t$, while the amplitude of the dee voltage V_{dee} is contained in a parameter R defined by $R = (2m_o\ V_{dee}/e\ B^2_{iso})^{\frac{1}{2}}$. Then the equations of motion for a particle of mass m and charge e in the field $\vec{B}$ are expressed in the independent variable τ (Van Nieuwland 77) :

$$\ddot{x} = \frac{m_o}{m}\ [\tfrac{1}{2}\ R^2\ F_x(x,y,0)\cos\Omega(\tau+\tau_o) + \frac{B_z}{B_{iso}}\ \dot{y}]$$

$$\ddot{y} = \frac{m_o}{m}\ [\tfrac{1}{2}\ R^2\ F_y(x,y,0)\cos\Omega(\tau+\tau_o) - \frac{B_z}{B_{iso}}\ \dot{x}]$$

$$\begin{aligned}\ddot{z} = \frac{m_o}{m}\ [\tfrac{1}{2}\ R^2\ \frac{z}{z_o}\ F_z(x,y,z_o)\cos\Omega(\tau+\tau_o) &+ \\ + \frac{z}{B_{iso}}\left(\frac{\partial B_z}{\partial\theta}\right)_{z=0}\frac{x\dot{x} + y\dot{y}}{x^2 + y^2} - \frac{z}{B_{iso}}\left(\frac{\partial B_z}{\partial r}\right)_{z=0}&\frac{x\dot{y} - \dot{x}y}{(x^2+y^2)^{\frac{1}{2}}}]\end{aligned} \tag{3.2}$$

In these equations the differentiation is with respect to τ. The functions F_x, F_y and F_z are electric field components divided by V_{dee} obtained from the analogue measurements.

In the centre of the cyclotron the relativistic mass increase is negligible. In this region the azimuthal and radial field variations $\partial B_z/\partial\theta$ and $\partial B_z/\partial r$ are also small. For particle trajectory calculations up to larger radii, or for field bumbs in the centre of the cyclotron, they can be taken into account.

The parameter R equals the radius of an orbit of a particle with mass m_o and energy eV_{dee} in a magnetic field of induction B_{iso}. For the constant orbit cyclotron operation the acceleration voltage V_{dee}

---

1) *The integer $\Omega \neq 1$ in the case of higher harmonic acceleration. In this thesis only calculations are presented for first harmonic acceleration.*

is adapted to the magnetic field such that R is constant for all final energies and for all ion types.

The equations (3.2) are integrated numerically by a fourth order Runge-Kutte procedure with a fixed step increment. We have taken a step increment of 1°.

The starting parameters for the radial motion are the horizontal position coordinates $x(0)$ and $y(0)$, the velocities $\acute{x}(0)$ and $\acute{y}(0)$ and the starting phase $\tau(0)$. The differential equation for the vertical particle motion is linear. A general solution is obtained as a linear combination of the solutions for two independent starting conditions : $z(0) = 1$, $\acute{z}(0) = 0$ and $z(0) = 0$, $\acute{z}(0) = 1$.

The computer code delivers the following output as a function of the azimuth :

- the x and y coordinates (expressed in cm) of the particle and the horizontal velocity components $\acute{x}$ and $\acute{y}$ (expressed in cm).
- the momentary coordinates of the orbit centre, defined by

$$\begin{aligned} x_c &= x + \acute{y} \\ y_c &= y - \acute{x} \end{aligned} \qquad (3.3)$$

- the energy and the phase of the particle.
- the vertical motion (z and $\acute{z}$) for two particles with independent starting conditions.
- the momentary electric field vector in cartesian coordinates encountered by the particle (components in kV/cm).
- the $\vec{E}$ vector in radial, tangential and vertical coordinates with respect to the trajectory (components in kV/cm).

The phase of the particle is often given by the High Frequency phase (HF phase), which is expressed by the time difference between the moment of dee-gap crossing of the particle and the moment of the top voltage on the dee. Also the computer code gives as output the so-called Central Position phase (CP phase, Schulte 79), to take into account the fact that the orbit centre may be different from the cyclotron centre. Defining the circle motion of the particle as the horizontal particle motion minus the orbit centre motion, the CP phase is defined as the HF phase of the circle motion. The CP phase and the energy are canonically conjugate variables in a Hamiltonian description. The energy gain per turn is determined by the CP phase (Schulte 79).

3.4 Examples of calculations

We shall present now several general results of the numerical calculations. They are based on the electric field map of the Eindhoven cyclotron.

In figure 3.3 the beam pattern is shown for particles starting with a CP phase of -30° under the puller (see figure 3.3, point A). The ion beam passes the puller directly after extraction from the ion source and again at the third dee gap crossing.

The behaviour of a grid of points in the radial phase plane is given in figure 3.5. The particles started with a CP phase of -30°; the phase plane has been calculated for eight successive revolutions at an azimuth of 270°. The coordinates $(r, p_r/eB_{iso})$ both with the dimension of a length, are canonically conjugate coordinates.

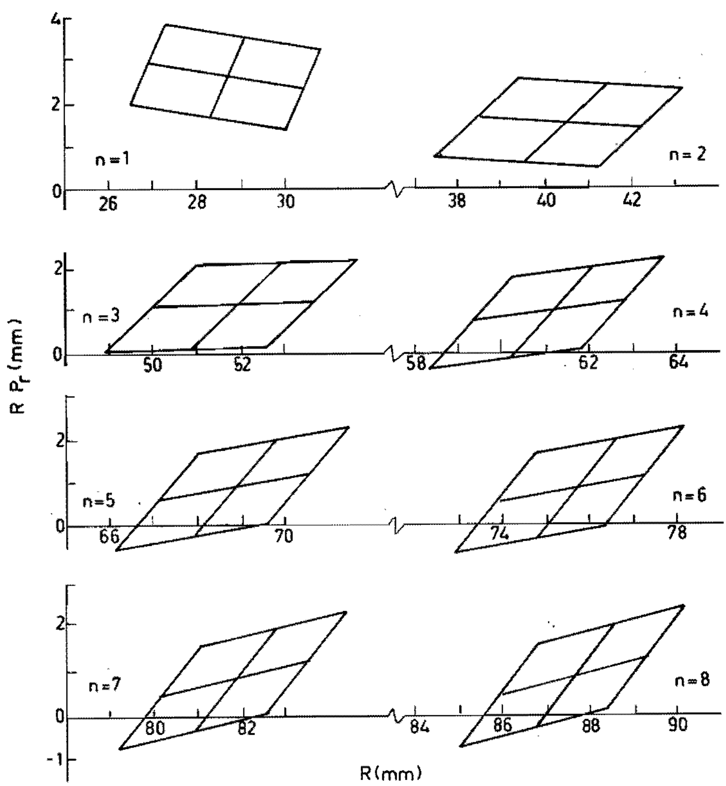

Figure 3.5 Behaviour of a grid of points in the radial phase space for ϕ_{CP} = − 30°, given for eight successive revolutions at an azimuth of 270°. The rotation of the grid is due to radial electric field components.

This phase plane grid was evaluated for a field map with the large puller opposed to the ion source (see figure 3.3 full line). This puller was in use until 1979. With this puller the centre geometry has shown a bad axial focusing (cf. section 3.5). In homogeneous magnetic fields without electric fields there will be no rotation of the phase plane. The rotation observed in figure 3.5 however must be ascribed to radial electric field components affecting the revolution frequency and the radial oscillation frequency.
In section 3.5 the relation between the electric field components and the axial focusing properties is examined closer.

The energy gain per gap crossing of a particle can be expressed by the gapfactor G defined as the ratio of the actual energy gain and the energy gain in a static electric field with potential difference V_{dee}. For optimum acceleration values of G larger than 0.9 can be found. In figure 3.6 G is shown for the first and the second dee gap crossing as a function of the starting phase with respect to the

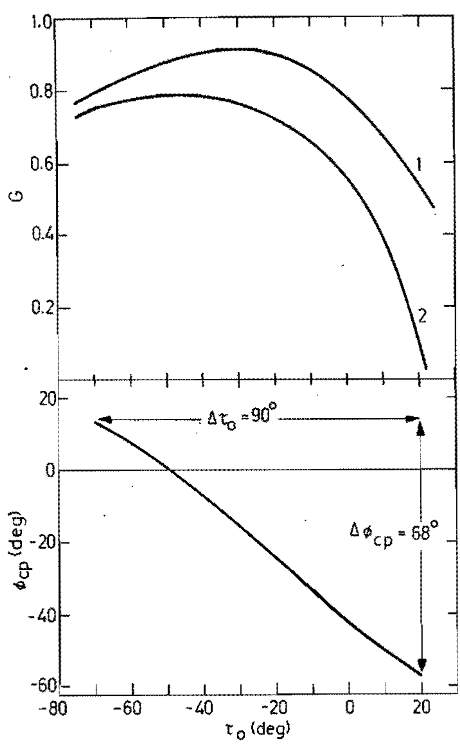

Figure 3.6
Gap factor for the first and the second dee gap crossing and CP phase after the first gap crossing as a function of the starting phase at the ion source.

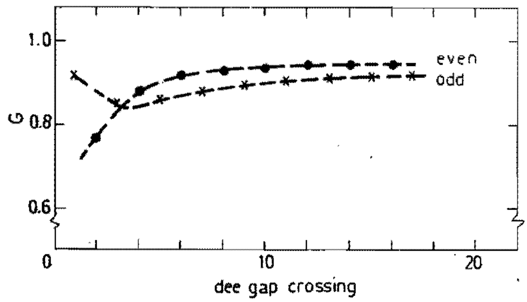

Figure 3.7
Gap factor for even and odd gap crossings for $\phi_{CP} = -30^o$.

moment of peak voltage of the HF field at the ion source. This figure gives also the CP phase in the puller for these particles. From this picture it is clear that for maximum energy gain an initial phase of about -30^o is needed. For the second gap G is much smaller because of the acceleration on the decreasing side of the dee voltage due to the increased path length of the ions at the first half turn. Figure 3.7 shows G for the successive gap crossings for the particle with CP phase of -30^o in the puller. For the different geometries of the central region that have been investigated these figures hardly change.

The orbit centre positions at the first and at the seventh revolution are given in figure 3.8 for several CP starting phases. The coherent oscillation amplitude increases from about 1 mm at the

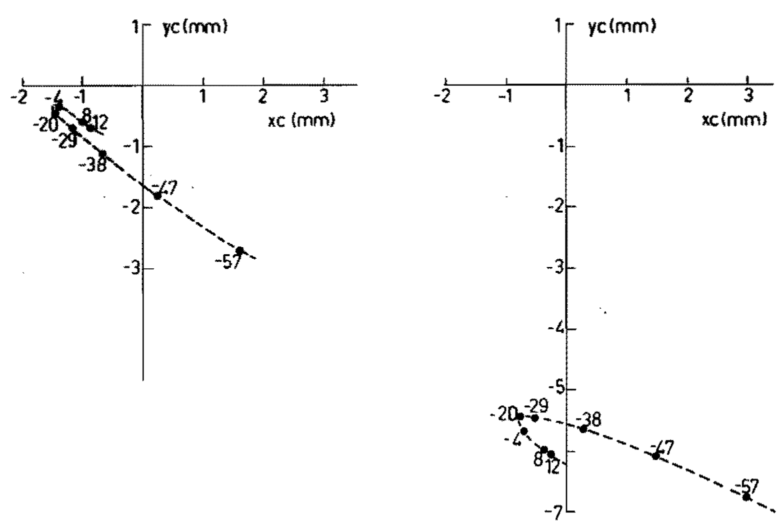

Figure 3.8 Orbit centre positions at the first and at the seventh revolution for several CP phases.

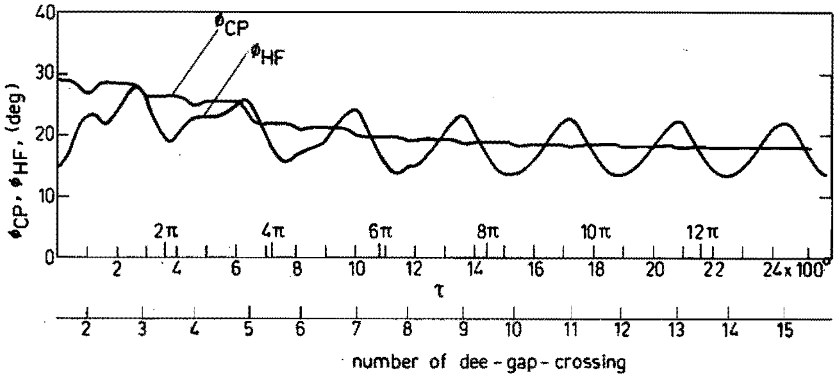

Figure 3.9 Behaviour of CP phase and of HF phase for particles starting with $\phi_{CP} = -30^o$.

first revolution to about 6 mm at the seventh revolution, due to radial electric field components. It can be corrected by a first harmonic magnetic field component in the centre of the cyclotron. The coherent oscillation amplitude is responsible for the phenomenon of HF phase mixing. It results in an enlarged apparent phase space area at larger radii (Blosser 69, Linz 75).

Figure 3.9 shows the behaviour of the CP phase and of the HF phase for particles started in the puller with a CP phase of -30^o. The HF phase oscillates around the CP phase due to a small off-centering of the orbit. For increasing turn number the CP phase decreases due to radial electric field components causing changes in the revolution frequency.

In first harmonic mode of acceleration a phase compression exists of about 15% after the first dee gap crossing and of about 10% for the successive eight revolutions. See figure 3.6 and figure 3.10.

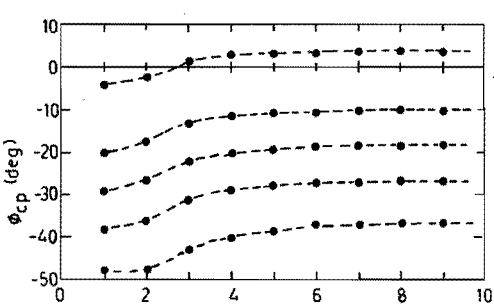

Figure 3.10
CP phase versus turn number for several phases at the first turn at azimuth $\theta = 90^o$.

3.5 Improvements of the central region of the Eindhoven cyclotron [1)]

3.5.1 Introduction

In this section we discuss investigations of several different geometries of the cyclotron central region. These geometries are given in figure 3.3. In the first paragraphs we restrict ourselves to the effect of a shortening of the puller on the righthand side. At the lefthand side of the puller some extensions have been added to it to influence the acceleration phase of the particles at the second and fourth turn in order to improve the axial focusing. The effects of these puller extensions will be discussed in section 3.5.4. As figure 3.3 shows the beam crosses the puller for the second time at the third dee gap transition. The puller is drawn with full lines ("old" puller). The dashed lines give alterations in the geometry ("new" geometries).

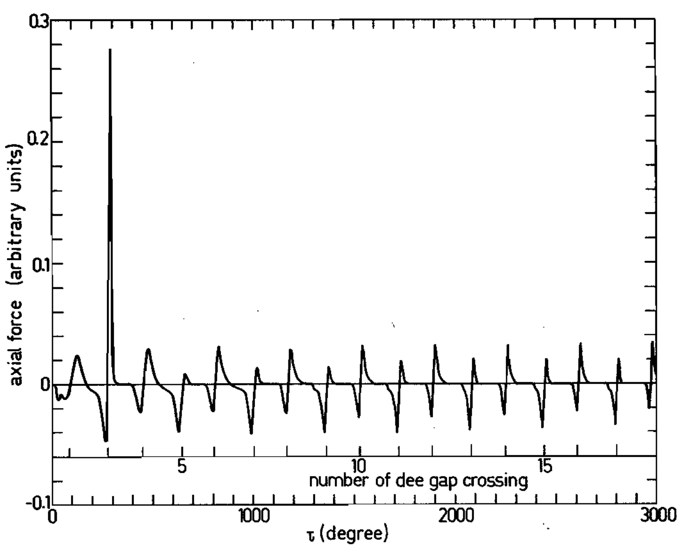

Figure 3.11 Axial force on particles with starting phase -30° for the old puller geometry. Positive means defocusing.

---

1) *The contents of this section has been published previously in Nuclear Instruments and Methods (Botman 80a).*

At the third dee gap crossing a large axial defocusing force is exerted on the particles in the case of the old puller. A picture of the vertical force exerted on particles started in the puller with a CP phase of -30^{o} and positioned +2.4 mm above the median plane is given in figure 3.11. In this picture a negative sign means focusing. The same effect occurs for particles of different CP phases (in our cyclotron the phase width of the accelerated beam is approximately 40^{o}).

3.5.2 Axial focusing

The axial field strength E_z is essential for axial focusing. For a symmetric dee gap crossing the following relation holds :

$$I = \int_{-\infty}^{\infty} E_z(z_o)\mathrm{d}y = 0 \qquad (3.4)$$

Here, the integration is carried out over a line perpendicular to the dee gap, and at a fixed height z_o above the median plane. The influence of space charge is neglected. In the neighbourhood of the ion source and the puller the symmetry is broken, and there are transverse field components such that $I > 0$. This deviation from zero gives rise to extra defocusing forces. For this effect the relation between the field component E_x in the median plane and the coordinate x is of importance. The following expression holds for the integral I for a non-symmetric dee-dummy dee crossing :

$$I = -z_o \int_{-\infty}^{\infty} \left(\frac{\partial E_x}{\partial x}\right)_{z=0} \mathrm{d}y \qquad (3.5)$$

The integral I gives an impression of the perturbation of the axial focusing for a dee-dummy dee crossing.

Now it is observed that the strong defocusing effect at the third dee gap crossing, which was shown in figure 3.11, results from the fact that $I > 0$. This is equivalent to strong negative values of $\partial E_x/\partial x$ along the path of integration. In figure 3.12 the field components as a function of y near this gap transit are shown.

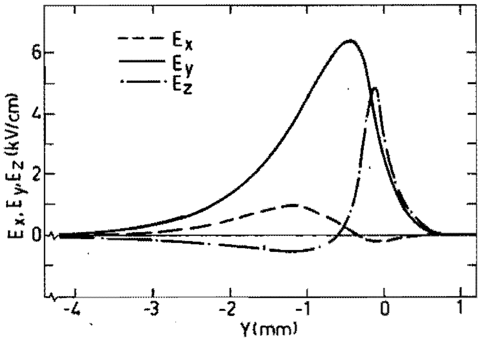

Figure 3.12
Electric field components for $x = 2.8$ cm for the old puller geometry.

3.5.3 The results of two different geometries

We compare the field lines and the results of the numerical calculations for the old puller shape and the new one, which is less extended at the righthand side. Note, that the ion beam passes the new puller only directly after extraction out of the ion source.

Figure 3.13 gives some plots of the field components E_x, E_y and E_z as a function of the y-coordinate for both the old and the new puller geometry. For the old puller geometry the field components are given for $x = 2.4$ cm up to $x = 3.6$ cm and for the new geometry for $x = 2.4$ cm up to $x = 3.0$ cm. The figures show clearly that for these regions the integral $I > 0$, and a strong defocusing force results. It is seen that in these regions $\partial E_x/\partial x \leq 0$ for all values of y. Figure 3.14 contains some plots of field components at the righthand side of the new puller geometry for the region of $x = 3.2$ cm up to $x = 4.2$ cm. In this figure it is seen that $\partial E_x/\partial_x < 0$ for $y < -0.8$ cm and $\partial E_x/\partial x > 0$ for $y > -0.8$ cm. Moreover

$$\int_{-\infty}^{\infty} \frac{\partial E_x}{\partial x}\, dy > 0$$

resulting in a net focusing action. This can also be concluded from figure 3.14c : $I < 0$. The field components for the old puller geometry at the righthand side of $x = 3.6$ cm behave in a similar fashion as in figure 3.14.

The measurements thus show that there is a defocusing ($I > 0$) and a focusing region ($I \leq 0$) at the righthand side of both the new and old puller. The defocusing region extends for the old puller

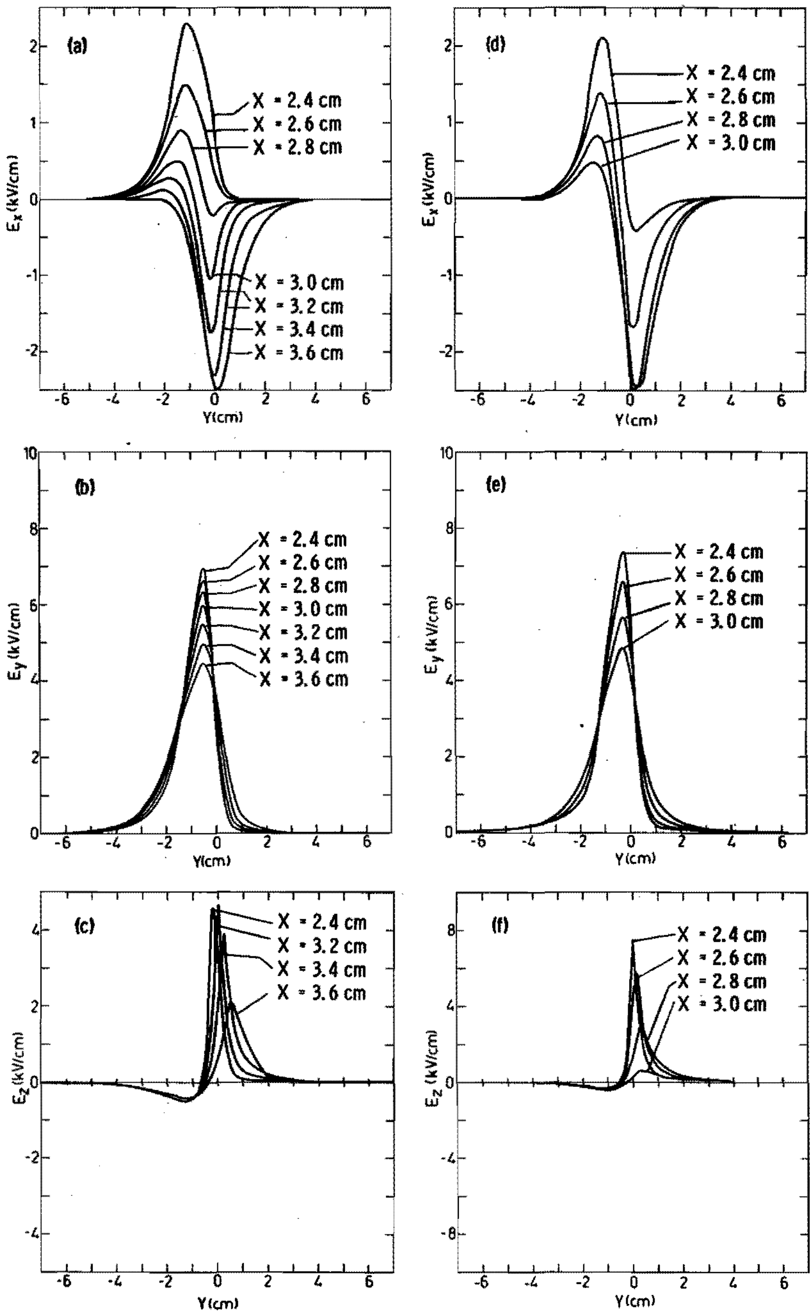

Figure 3.13 Electrical field components in the defocusing region for both the old (figures a, b, c) and the new puller geometry (figures d, e, f).

geometry up to x = 3.6 cm and for the new one up to x = 3.0 cm. The ion beam crosses the dee gap at the third dee transit at approximately x = 3.3 cm. From the observations made above it can now be seen that the particles experience a completely different axial force in the two situations. There is a large improvement of the vertical focusing for the new puller geometry. We also show the different effect of the two cases in plots of the transverse component E_x versus x for some values of the coordinate y (figure 3.15). Once again it is clear that for the old geometry the beam goes through the defocusing region ($\partial E_x/\partial x > 0$), and that for the new puller-shape the beam goes through the focusing region ($\partial E_x/\partial x > 0$) at the third dee gap crossing.

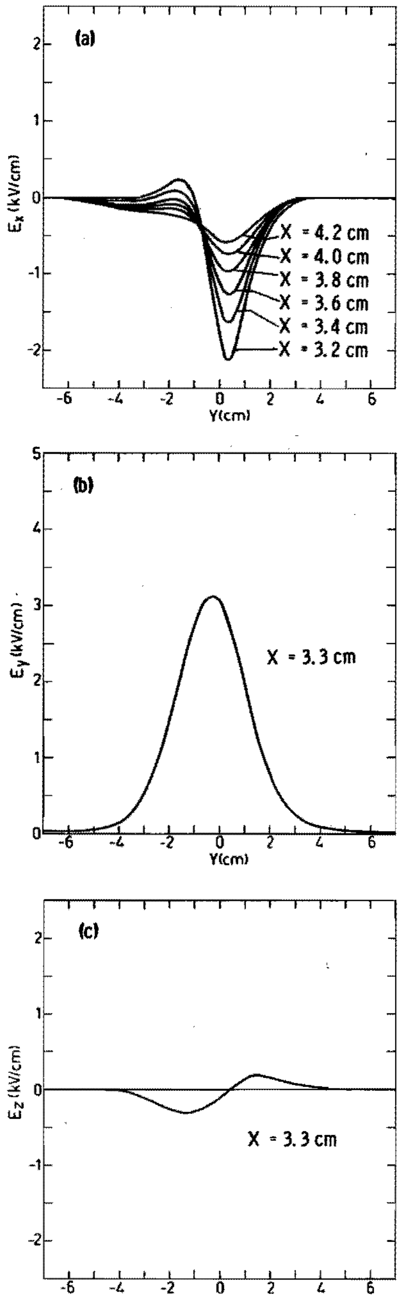

Figure 3.14
Electrical field components in the focusing region of the new puller geometry.

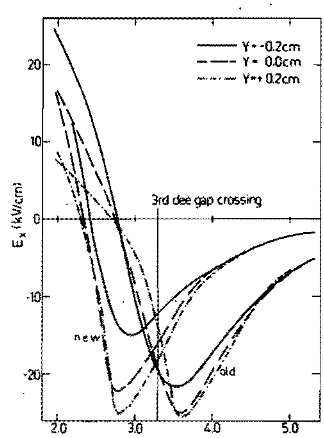

Figure 3.15
E_x versus x for the old and the new puller geometry.

Orbit calculations with the computer program ORBIT/CALCULATION, employing the new puller field map reveal quite a different axial force on particles off the median plane (figure 3.16), with respect to the axial force with the old puller situation. This picture has to be compared with the one in figure 3.11. The huge defocusing force at the third dee gap transit has completely disappeared.

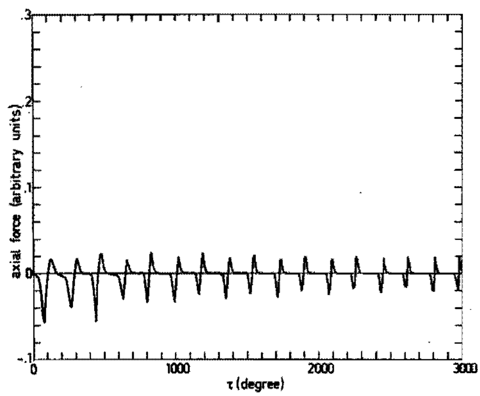

Figure 3.16 Axial force on particles with starting phase -30° for the new puller geometry. Compare this with figure 3.11.

Another way to illustrate the better beam behaviour using the adapted puller is to look at the axial oscillations of the particles. Since the axial field is taken to be linear as a function of the height z, a linear differential equation results for the axial motion (see eqs. (3.2)).

The complete solution for this differential equation can therefore be found by solving the equation for two independent initial conditions (we take them to be $(z,z') = (1,0)$ and $(z,z') = (0,1)$, where the prime means differentiation with respect to the azimuth).

Our computer program ORBIT/CALCULATION calculates these solutions numerically, and the result is given in figure 3.17 for both the old puller shape and the new one. The amplitude of the axial oscillations at the first few turns in the cyclotron has drastically diminished for the new puller shape.

First tests in the cyclotron with the new puller have shown an increase in beam current of at least a factor three with respect to the old situation.

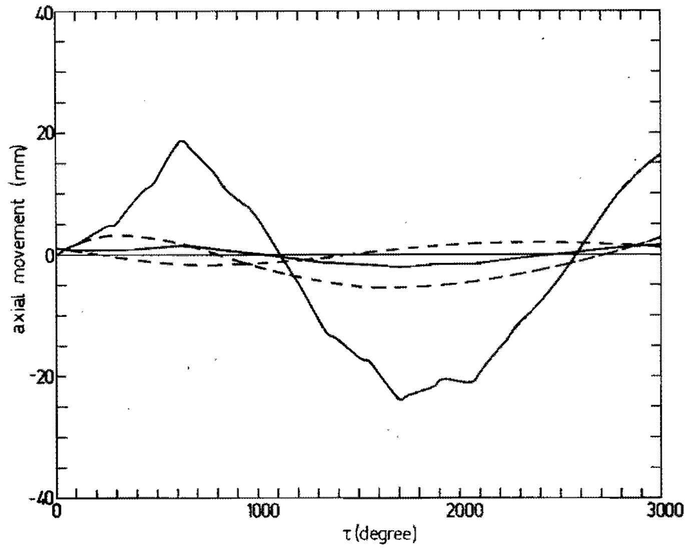

Figure 3.17 Axial movement of particles with starting phase -30^o. The full lines give the result for the old puller, the dashed lines for the new puller.

3.5.4 Further improvements

The improvement of the vertical focusing at the third dee gap crossing by an adaptation of the field shape of the accelerating field was the base for some further numerical calculations to examine the influence of extensions that have been constructed at the lefthand side of the puller. In figure 3.3 these extensions are drawn by dashed lines ((c), (d) and (e)).

These extensions cause a variation in the $\vec{E}$-field behaviour such that

$$\int \partial E_x / \partial x \ \partial y > 0$$

resulting in an extra focusing action at the second and the fourth dee gap crossing. The precise shape of these extensions also have some favourable effect on the HF phases of the particles that cross them. Furthermore the influence of a copper sheet at the lefthand side of the ion source chimney (denoted in figure 3.3 by (f)) was examined. Such a sheet is used for instance in the cyclotron fo the Free University in Amsterdam to capture spurious beam.

A good way to observe the overall effect of the different puller-ion-source modifications is to look at the axial acceptance of the central region. Axial boundaries at several azimuthal positions are transformed back to point A in the puller (figure 3.3). Figure 3.18 shows these axial acceptances. It is noted that an appreciable increase of the acceptance area is found. The puller with the largest extensions gives the largest acceptance. An enlarged puller at the lefthand side has not yet been tested experimentally in the cyclotron.

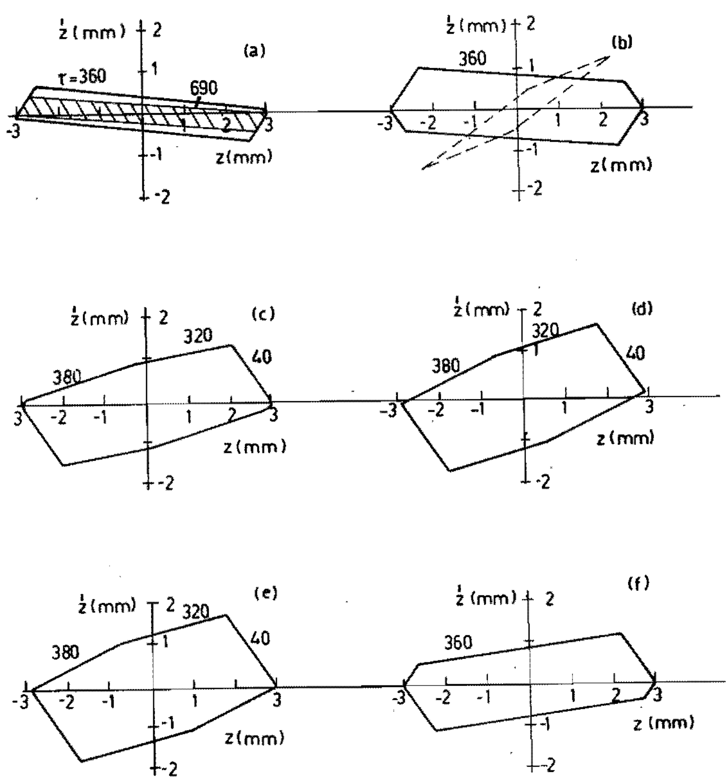

Figure 3.18 *Axial cyclotron acceptance at azimuth 90° at the first revolution for the old central region geometry (a), and for alterations of the centre geometry with the puller reduced at the righthand side ((b) up to (f)) : (b) new puller without extensions at lefthand side, (c) small extensions, (d) straight extensions, (e) large extensions, (f) sheet beside the source. The time moments where axial boundaries occur are indicated. In figure (b) ("new puller") the axial ion source emittance, based on visual observations, is drawn by dashed lines. In figure (a) the acceptance is given by the shaded area. The main boundary occurs at the third gap crossing (τ = 690°).*

In figure 3.18 (b) the ion source emittance is also given by dashed lines. The ion source axial emittance is estimated using two observations :

1. the height of the beam in front of the ion source has been determined photographically (Krämer 63);
2. the height of the beam at point B (figure 3.3) has been determined by the dimensions of the hole burned in a thin paper foil placed radially over several centimeters at the azimuth of B. In chapter 4 the phase space area occupied by the beam, measured at the second revolution, is given.

Presently, the "small" puller is used in the cyclotron. For this puller figure 3.19 shows the motion of a grid of points in the radial phase space for particles started with a CP phase of -30° in the puller. The figure has to be compared with the one of figure 3.5. There is no notable rotation of the grid ($\nu_r - 1 \approx 0$). The increase of ν_z^2 goes together with a decrease of ν_r^2, as explained for example by the formula of Dutto which relates these quantities (Dutto 75).

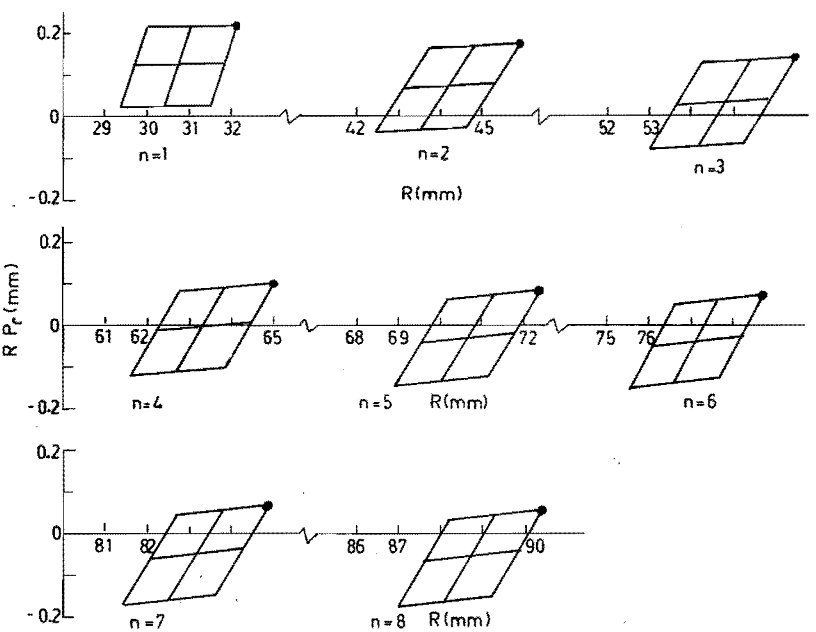

Figure 3.19 Behaviour of a grid of points in the radial phase plane for a CP phase of -30^{o} for the new puller geometry. Compare this with figure 3.5.

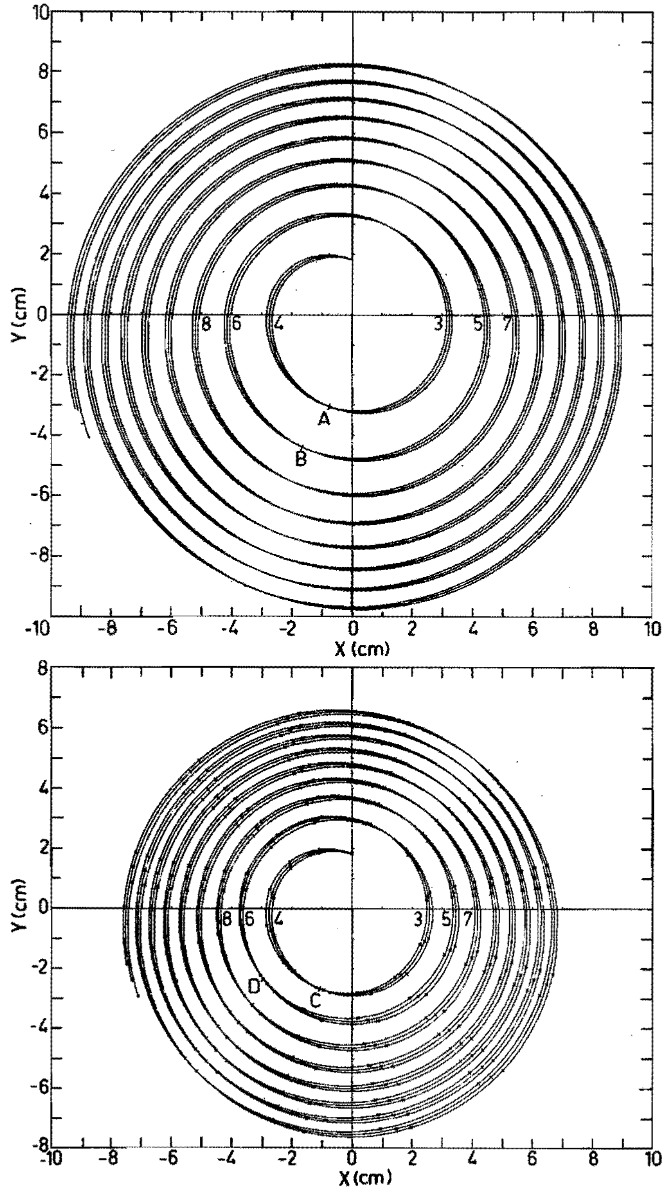

Figure 3.20 *Radial particle motion for particles with starting phase -30^o for the new puller geometry. Two cases are shown : (a) normal dee voltage. Then the third gap crossing occurs in the axially focusing region ($\partial E_x/\partial x > 0$); (b) decreased dee voltage in such a way that the third gap crossing occurs at the edge of the puller (axially defocusing region, $\partial E_x/\partial x < 0$). In this case the ν_r^2 is increased : compare the azimuthal length AB in figure (a) with CD of figure (b).*

Finally we note that the new puller enhances again the large axial defocusing force at the third dee gap crossing when the dee voltage is decreased such that this crossing occurs at the edge of the puller. In this case the value of $\nu_r - 1$ becomes larger. The effect is illustrated in figure 3.20.

3.5.5 Conclusion

The axial focusing in the central region of a cyclotron is very sensitive to small changes of the electric field shape.

In particular we showed that when the transverse electric field component can be made to be constant or to increase with radius an appreciable improvement of the axial focusing occurs.

Changes in ν_z affect the radial oscillation frequency ν_r. However, since $\nu_r^2 \simeq 1$ and $\nu_z^2 < 0.1$ these changes have only a small influence on the motion in radial phase space.

The new adapted puller has been tested experimentally and is permanently installed now in the cyclotron and yields at least three times more beam current.

3.6 Median plane effects in the Eindhoven AVF cyclotron [1)]

3.6.1 Introduction

In many experiments on the beam behaviour in the centre of the cyclotron it turned out that the ion beam does not move in the plane of symmetry of the cyclotron magnet. The difference in vertical position of the orbit on two successive revolutions can amount to several millimeters.

Examinations to explain these deviations and possibly to correct them, were undertaken. They are based on the magnetic field data (Verster 62b) and on the three dimensional electric field maps of the

1) *This section has been published in the proceedings of the 1981 Particle Accelerator Conference (Botman 81a).*

electrode system in the central region. The magnetic and electric field data are used in the numerical particle trajectory program. The cyclotron has ten pairs of circular correction coils, B_1 to B_{10}. Of these the inner two pairs (with 8 turns and with diameter of 10 cm and 15 cm respectively) can be excited asymmetrically. The vertical distance of these coils is about 13 cm.

The effect of an asymmetric excitation of the inner circular correction coils is described. With this it is possible to alter the position of the magnetic median plane and thereby change the area of the axial acceptance of the cyclotron.

A deflection voltage on axial deflection plates in the centre of the cyclotron can shift the axial cyclotron acceptance, so as to properly match the ion source emittance. In combination with the asymmetric excitation of inner circular correction coils this parameter provides a good means to optimize the beam current in the centre of the cyclotron.

Finally, numerical calculations show that there is only a small effect on the ion beam of an accelerating gap which has an inclined dee with respect to the dummy dee.

Floating wire experiments performed in the Eindhoven cyclotron have shown that the median plane of the main magnetic field differs from the midplane of the cyclotron magnet at small radii. In figure 3.21 this deviation above the midplane is plotted versus radius.

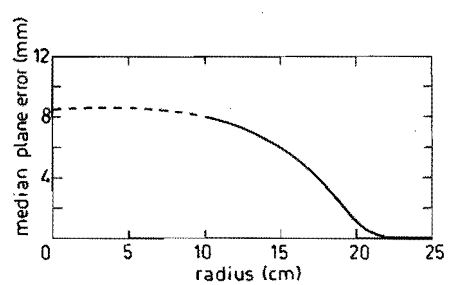

Figure 3.21 Deviation of the main magnetic field median plane from the midplane of the cyclotron magnet. The dashed part represents an extrapolation towards the centre.

Asymmetric excitation of correction coils changes the vertical position of the magnetic median plane. For equal excitation of upper and lower coils the coil symmetry plane coincides with the midplane between the poles; for excitation of only the upper coils such a symmetry plane coincides with the lower pole face. We define the magnetic median plane as that plane with horizontal magnetic field strength equal to zero. An estimation of the vertical position z of the magnetic median plane of asymmetrically excited coils with respect to the midplane of the cyclotron can now be given :

$$z \approx -\tfrac{1}{2}h \, \frac{I_u - I_\ell}{I_u + I_\ell} \tag{3.6}$$

In this formula I_ℓ represents the current through the lower coil, whereas I_u represents the current through the upper coil. The quantity h is the distance between upper and lower coils. Typical values for the inner circular correction coils of our cyclotron are :
I_u = 90 Amp, I_ℓ = 50 Amp. With these currents the median plane of coils B_1 can be approximately lowered by 20 mm.

3.6.2 The effective median plane

In ideal magnetic and electric fields in the cyclotron the axial particle motion is described by the differential equation :

$$z'' + \nu^2_{z,el}\, z + \nu^2_{z,magn}\, z = 0 \tag{3.7}$$

where the differentiation is with respect to the azimuth and where $\nu^2_{z,el}$ and $\nu^2_{z,magn}$ represent the electric focusing of the dee gap and of the magnetic field respectively. The values of $\nu^2_{z,el}$ are strongly phase dependent. However, we present in the following only calculations carried out for particles with a CP phase of -30° in the puller after the first dee gap crossing.

In the presence of a median plane error $z_o(r)$ of the main magnetic field (figure 3.21) an inhomogeneous differential equation results for the axial motion :

$$z'' + \nu^2_{z,el}\, z + \nu^2_{z,magn}\, (z - z_o(r)) = 0 \tag{3.8}$$

When the inner circular correction coils B_1 and B_2 are excited an extra axial focusing term must be added. The focusing strengths calculated from the cyclotron field data (Verster 62b) are given in figure 3.22, together with ν_z^2 for the main magnetic field.

The differential equation for the vertical motion in the cyclotron in the presence of asymmetric excitation of coils B_1 and B_2 has the form :

$$z'' + \nu^2_{z,total}\, z = \nu^2_{z,magn}\, z_o + \nu^2_{z,B_1}\, z_{B_1} + \nu^2_{z,B_2}\, z_{B_2} \qquad (3.9)$$

Asymmetric currents are supplied to coils B_1 and B_2 such that their median planes lie at height z_{B_1} and z_{B_2} respectively. In this equation ν^2_{z,B_1} and ν^2_{z,B_2} are the focusing strengths of coil B_1 and B_2, and $\nu^2_{z,total}$ is the sum of the separate focusing strengths :

$$\nu^2_{z,total} = \nu^2_{z,el} + \nu^2_{z,magn} + \nu^2_{z,B_1} + \nu^2_{z,B_2} \qquad (3.10)$$

The effective median plane error is now given by

$$\Delta z = \frac{\nu^2_{z,magn}}{\nu^2_{z,total}}\, z_o + \frac{\nu^2_{z,B_1}}{\nu^2_{z,total}}\, z_{B_1} + \frac{\nu^2_{z,B_2}}{\nu^2_{z,total}}\, z_{B_2} \qquad (3.11)$$

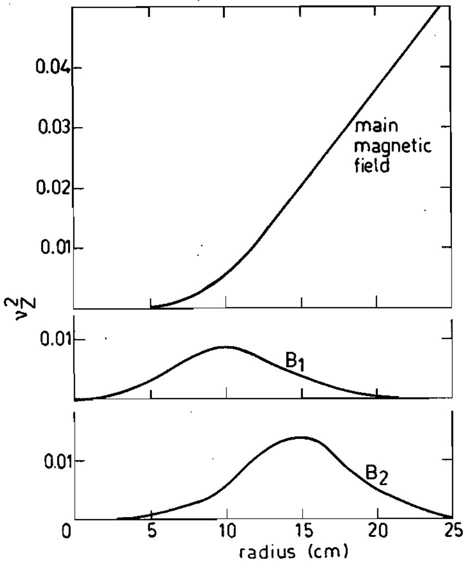

Figure 3.22
ν_z^2 versus radius for the main magnetic field, for B_1 and for B_2.

The several terms in this equation are given in figures 3.23a and 3.23b. By a proper asymmetric excitation of B_1 and B_2 the median plane heights z_{B_1} and z_{B_2} can be chosen such that Δz is as small as possible. In figure 3.23c this situation is given, for z_{B_1} = 6 mm and z_{B_2} = 5 mm. One must remark that the effective median plane is phase dependent because the electric focusing is phase dependent.

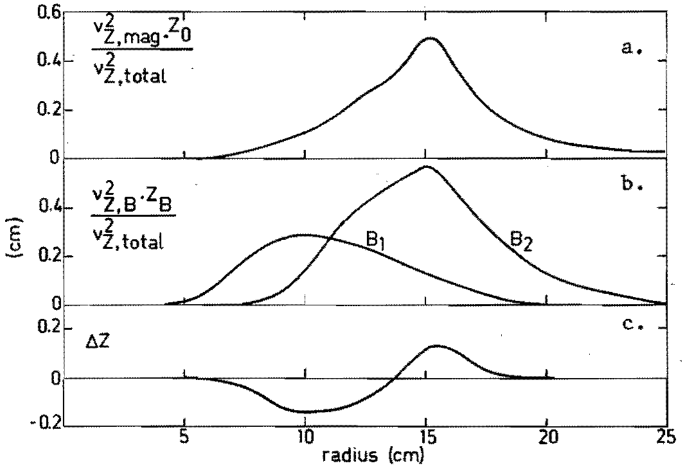

Figure 3.23 The effective median plane error. In (b) the value of z_B belongs to maximum values of I_a and I_s.

3.6.3 Axial acceptance

The axial particle motion is taken linear in z. Therefore the transformation of an axial phase space point from one azimuthal position to another one is given by a 2 × 2 matrix. Physical boundaries by which the beam is intercepted (for instance the dee aperture) are transformed back to a position in the puller at azimuth 90° after the first dee gap crossing, and yield the axial cyclotron acceptance (see point A in figure 3.3). We will show two cases :

a. The axial cyclotron acceptance using the conventional ion source. For this case the vertical opening of the cyclotron is 20 mm.
b. The axial acceptance of the cyclotron using the trochoidal injector system (Beurtey 67) (see also section 3.4). This system is used at the cyclotron for injection of polarized protons of 5 keV initial energy. In this case the vertical opening of the cyclotron is 8 mm.

For the above mentioned cases the oscillation amplitudes may not be larger than 10 mm and 4 mm respectively. When median plane errors are present, they have to be even smaller.

In figure 3.24 and figure 3.25 the axial cyclotron acceptances are drawn. They are given for the case with no median plane error, for the case with a median plane error present due to the main magnetic field, and in the case after correction by asymmetric excitation of coils B_1 and B_2. It is seen that the axial acceptance diminishes substantially, or even vanishes for the situation of 8 mm vertical opening, due to the deviation of the main magnetic field median plane with the cyclotron magnet midplane. A proper asymmetric excitation of correction coils B_1 and B_2 can largely restore the axial acceptance.

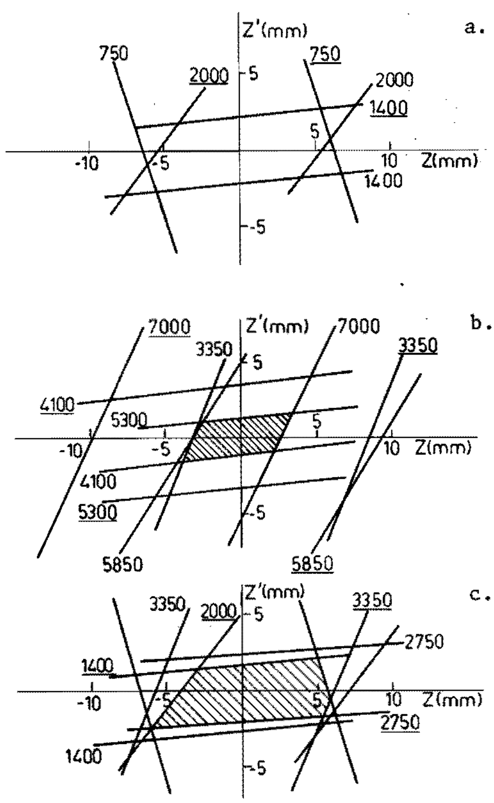

Figure 3.24 Axial acceptance for a verticle opening of 20 mm, without a median plane error (a), with a median plane error of the main magnetic field (b) and for correction by asymmetric excitation of B_1 and B_2 (c). Only those lines limiting the axial acceptance are drawn.

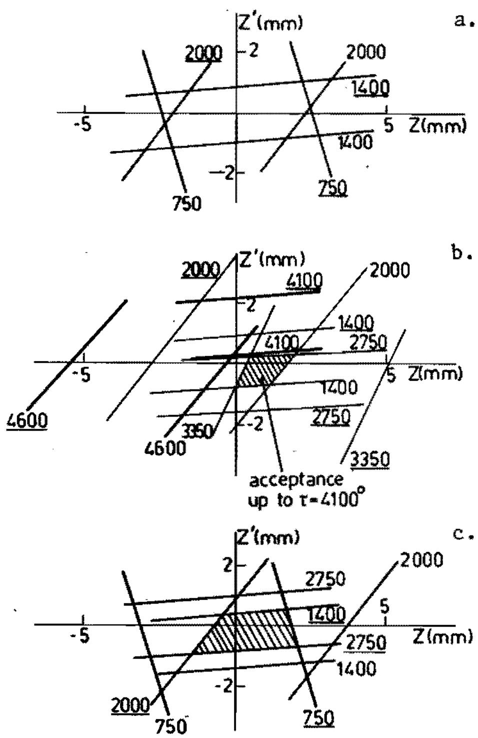

Figure 3.25
Same as figure 3.24, except for a vertical opening of 8 mm, which occurs in case of use of the trochoidal median plane injector.
In b. the shaded area gives the acceptance up to $\tau = 4100^o$.

3.6.4 Axial deflection

Electric fields, especially between ion source and puller, can have a certain angle with respect to the symmetry plane of the cyclotron magnet due to a small inclination of the chimney or due to a wrong axial position of the ion source. Because of these fields axial oscillations can be induced. In the cyclotron electric deflection plates are positioned at the second turn. For a proton beam of 50 keV (final energy 7 MeV) a DC voltage of approximately 300 V has to be applied to get maximum internal beam current (and maximum extraction efficiency).

The effect of a deflection voltage at a certain azimuthal position is a shift of the ion beam emittance along the z'-axis in the axial phase space at that azimuth, or conversely a shift of the cyclotron acceptance in the opposite direction. The magnitude of the shift can easily be calculated in terms of the particle energy, deflection voltage and azimuthal extent of the deflection plates. The shift of the cyclotron acceptance has been transformed back to the azimuth of 90^{o} in the puller (cf. figure 3.26). At this azimuth we have also indicated the shift of the ion source emittance when the vertical position is lowered, and when the chimney is inclined with respect to the magnetic field lines. An inclination of the chimney of several mrad can easily occur. The figure shows that such an inclination can be corrected for by the deflecting voltage.

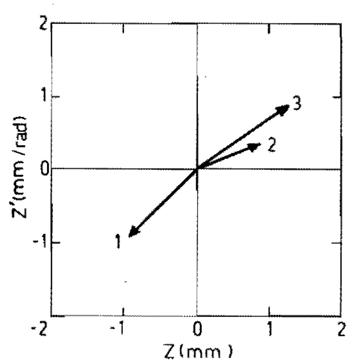

Figure 3.26
Shift of axial acceptance at a deflection voltage of 400 V (1) and shift of ion beam emittance for axial mispositioning of 0.5 mm (2) and for vertical inclination of 40 mrad (3) of the ion source.

Experimental data of the internal beam current versus deflection voltage, and versus asymmetric excitation of B_1 are given in figure 3.27. In this situation we have placed an axial slit with an opening of 3 mm and a radial extent of 8 cm in the centre of the cyclotron, to make the median plane effects more pronounced. It shows that both the deflection voltage and the asymmetric excitation have to be present to get any beam current.

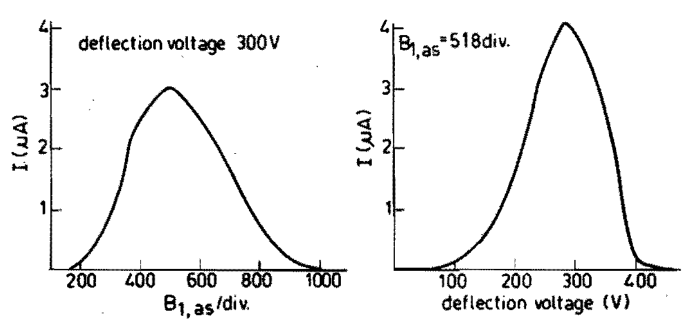

Figure 3.27 Internal beam current through a 3 mm axial slit, radial extent 8 cm, as a function of deflection voltage and of asymmetric excitation of coil B_1.

3.6.5 A tilt of the accelerating field outside the first gap crossing

Exact positioning of the dee with respect to the dummy dee is a tedious task. Misalignments of a few millimeters can easily occur. A vertical misalignment of the dee with respect to the dummy dee at a particular dee gap crossing can be described by a rotation of the electric field around the centre point in the dee gap at that crossing. Then to the weak vertical electric field components a portion of the strong accelerating field component is added.

An overall vertical displacement of the dee with respect to the dummy dee seems to yield a negligible effect since the vertical displacement of the dee on the one crossing is roughly compensated at the next crossing. However, for a vertical inclination of the dee along the dee gap with respect to the dummy dee the vertical displacements at the successive turns are additive.

We have investigated these effects numerically by applying a position dependent rotation to the electric fields encountered by the particles. As said the numerical trajectory calculation program uses a three dimensional electric field map measured for the cyclotron centre. The results of these numerical evaluations will be mentioned briefly :

- an overall vertical displacement of the dee with respect to the dummy dee gives a negligible vertical displacement of the trajectories. A vertical beam displacement of about 0.2 mm was calculated for an overall dee displacement of 2 mm.
- vertical height displacements of the particles of the order of 1.5 mm per turn in the cyclotron centre could only be reached for a large dee inclination of 40 mrad with respect to the dummy dee.

3.6.6 Conclusion

Asymmetric excitation of the inner correction coils increases the axial acceptance of the cyclotron if the main magnetic median plane does not coincide with the midplane of the cyclotron magnet.

A deflection voltage in the centre of the cyclotron can shift the axial acceptance, so as to properly match a wrong position of the ion source emittance in phase space.

3.7 The effect of the trochoidal median plane injector on the accelerated particles in the cyclotron

3.7.1 Introduction

The nuclear physics group of EUT has a polarised ion source facility at its disposal for production of 5 keV polarised protons (Van der Heide 72). The polarized protons are injected radially in the centre of the cyclotron with a trochoidal median plane injector (Beurtey 67). The ordinary ion source is removed when the injector is used for the transport of polarized protons. This device consists of a system of electrodes on which a DC voltage is applied, to compensate the deflecting forces of the magnetic field. Figure 3.28 shows a schematic cross section of the injector at a distance of 4 cm from the cyclotron centre. It is constructed in such a way that particles already accelerated can cross the injector transversely. The motion of these particles will be affected by the electrostatic field of the injector.

An estimation of the effects on the accelerated motion will be presented in this section. It is based on numerical calculations in which field data for the injector measured in a simplified analogue model are inserted (Kruip 80).

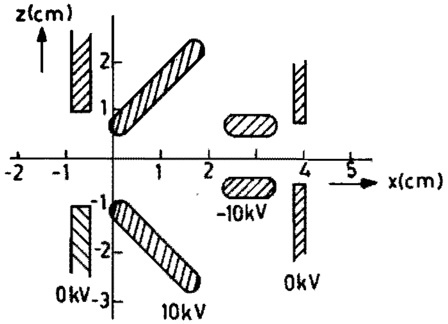

Figure 3.28 Schematic cross-section of the trochoidal median plane injector. Polarized protons with an initial energy of 5 keV are guided towards the centre of the cyclotron. The electric force due to the voltages on the electrodes compensates the Lorentz force of the cyclotron magnetic field on the injected protons. Particles accelerated in the cyclotron cross the injector from negative to positive x-values.

3.7.2 Field measurements and numerical calculations

A five times enlarged iron model of the injector was constructed. The model was magnetized and the magnetic field was measured with Hall probes (magnetic analogue technique).

The following simplifications were made :

- the injector lies along the y-axis (cf. figure 3.3);
- only the E_x and E_z field components are considered; they are independent of y.
- E_x is independent of the height z above the median plane;
- E_z is linear in z.

These simplifications do not have a serious influence on the effects that we want to study.

The following relations should hold for the field components :

$$\int_{-\infty}^{\infty} E_x\,(x,0)\,dx = 0$$

$$\int_{-\infty}^{\infty} E_z\,(x,z)\,dx = 0 \qquad (3.12)$$

The E_x field component was measured in the median plane and the E_z component was measured at a fixed height (9 mm) above the median plane. These field components are plotted in figure 3.29.

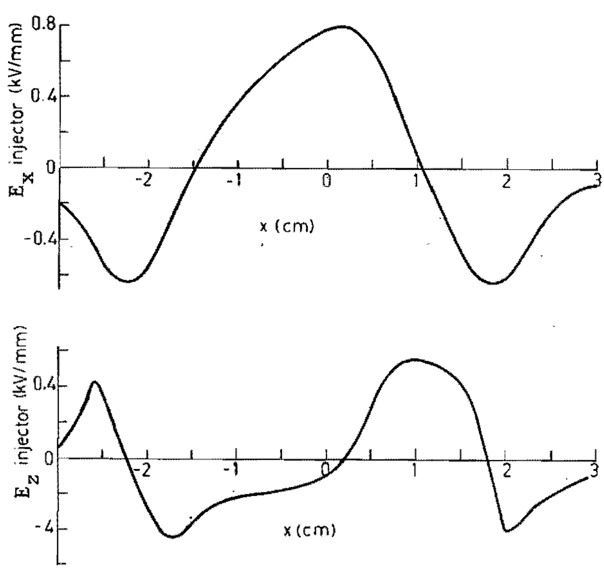

Figure 3.29
Injector field components as a function of x. E_z is measured at a height z_o = 9 mm above the median plane.

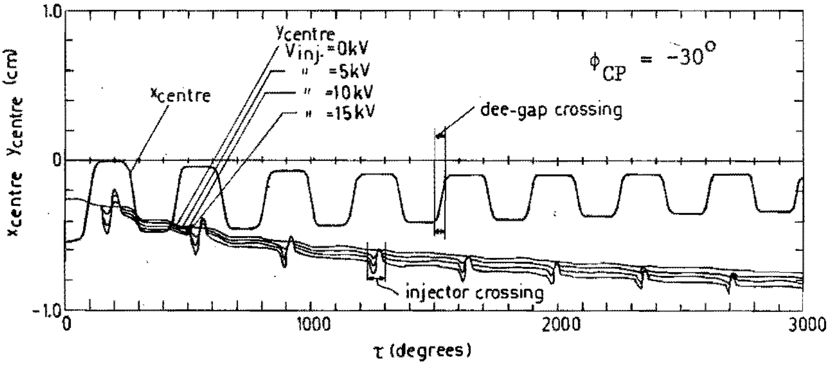

Figure 3.30 Orbit centre position for several injector voltages.

We computed a number of particle trajectories with increasing values of the injector voltage. These computations were done for a 20 MeV proton energy cyclotron setting and a 5 keV injected beam. The values of $V_{injector}$, the voltage on the electrodes, were 0, 5, 10 and 15 kVolts (10 kV is the nominal injector voltage value for the 20 MeV protons setting).

As was expected the radial particle behaviour was hardly affected by the injector, except for a slight drift of the orbit centre in the negative *y*-direction. This drift increases with increased $V_{injector}$ (cf. figure 3.30). The CP phase was not affected at all.

Axial particle trajectories are substantially influenced by the injector. Three positive lense actions are exerted on the particles as they cross the injector. As an example ν_z^2 is increased by about 60% at the third turn by these lense actions. The axial motion for particles of starting CP phase −30° is given for the four values of $V_{injector}$ (cf. figure 3.31). Only during the first revolutions in the cyclotron the particles are influenced by the injector.

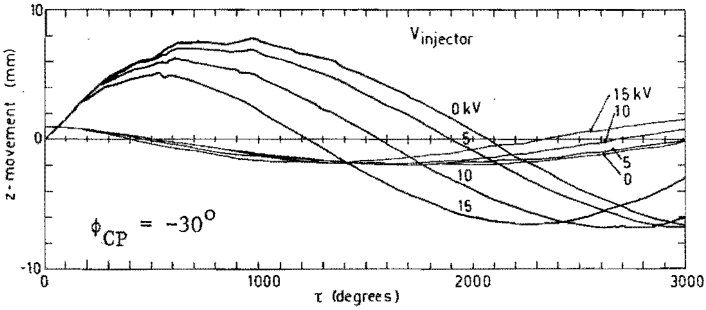

Figure 3.31 Axial particle motion for several injector voltages.

3.8 General Conclusions

The beam current output of the ion source, measured at a radius of about 10 cm, depends on the plasma conditions of the ion source and of the transmission of the ion beam through the central region. Our aim was to optimize the beam current output by improving the transmission through the central region.

For this purpose we have investigated the electric field configuration in the cyclotron centre. We have described our method to measure the electric field in the electrode system. The beam properties are calculated with the obtained fields.

An adaptation of the electrode shape has led to a beam current output that is increased by a factor of three with respect to the old shape.

Disturbing influences on the transmission can occur. We have traced several disturbing effects in our cyclotron and we have shown ways to correct them. In particular the median plane effects in the cyclotron centre were discussed.

If all parameters in the central region are set properly, the beam current transmission is optimal, and the properties of the ion beam can be predicted on the basis of numerical evaluations.

As an application of the numerical trajectory computations the focusing action of the trochoidal injector on accelerated ions has been calculated.

CHAPTER 4

BEAM PHASE SPACE AREA MEASUREMENTS IN THE CYCLOTRON CENTRE

The phase space area of the ion beam in the centre of the cyclotron is determined. The phase space area was scanned with two diaphragms. Different techniques were employed to measure the axial and the radial phase space area. With the obtained measurements the properties of a beam transmitted through selecting diaphragms can be predicted. For radial selection an HF phase-radial position relation has been found.

4.1 Introduction

The phase space area of the ion beam can be determined with the use of two diaphragms, located a certain azimuthal distance apart. The first diaphragm selects a part of the beam, the second diaphragm allows a measurement of the transverse momentum spread of the selected beam. A comparison of several phase space density measurement techniques has been given by Van Steenbergen (Van Steenbergen 67).

The axial and radial phase space areas of the ion beam in the centre of our cyclotron were measured. Diaphragms were positioned in the central region on the first few turns. The transmitted beam was intercepted by a probe at a radius of 40 cm for current measurement. For constructional and operational reasons the diaphragms were mounted on the ion source head (cf. section 2.1). We note that the distribution function in radial phase space was measured while integrating over the axial phase space and vice versa. Since in good approximation the axial and radial particle motions are uncoupled, this procedure is correct.

The axial beam phase space area was determined by sweeping the beam over two diaphragms positioned at the third and at the fourth turn, using electrostatic deflection fields, with the diaphragms apertures fixed in the median plane. The complete axial phase space can thus be scanned. This sweeping method has advantages above the use of movable slits because there is limited space for vertical movement of the diaphragms in the cyclotron centre and further because the axial acceptance of the cyclotron does not permit to measure the complete emittance of the ion source in case movable diaphragms are used.

For the determination of the radial phase space distribution functions these limitations are not present. Here movable diaphragms were used.

4.2 Axial phase space density measurements

4.2.1 Sweeping method for the axial phase space area determination

A schematic lay-out of the method is given in figure 4.1. The beam is deflected under the influence of a DC voltage on electrodes at θ_1 and at θ_3, and is sampled by the diaphragms at azimuths θ_2 and θ_4. The first pair of deflection electrodes lies on the second turn, the second pair on the third turn, both at an azimuth of 270^o. The first diaphragm is positioned at the third turn at azimuth $\theta_2 = 240^o$, the second one at the fourth turn at an azimuth $\theta_4 = 290^o$ (cf. figure

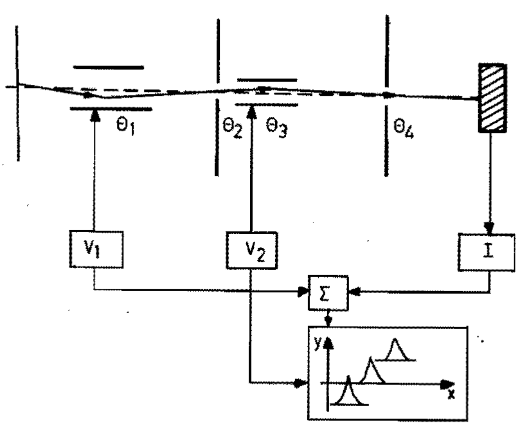

Figure 4.1 *Scheme of the axial phase space area measurement method*
deflection electrodes : $\theta_1 = 270^o$, *2nd turn*
$\theta_3 = 270^o$, *3rd turn*
diaphragms : $\theta_2 = 240^o$, *3rd turn*
$\theta_4 = 290^o$, *4th turn*

3.3). The azimuthal extent of the deflection electrodes is one radian. The distance between the electrodes is 8 mm for the first pair and 4 mm for the second pair. This distance is smaller for the second pair, because these are situated immediately after the first diaphragm. The axial aperture of the two diaphragms is 0.2 mm.

In first order the influence of deflection electrodes on the particle beam is described by a stepwise increment of the axial momentum (defined as $p_z = z' = dz/d\tau$) of the particles :

$$\Delta z' = \frac{e\ V\ \theta_{defl}}{m\ \omega^2\ d} \tag{4.1}$$

where e/m is the charge to mass ratio of the particle, ω is the (angular) revolution frequency of the particles in the cyclotron, V/d is the electric field strength between the deflection electrodes and θ_{defl} is the azimuthal extent of the deflection electrodes. In our case this means for a cyclotron setting of 7 MeV protons (f = 11.299 MHz) for the two pairs of deflection electrodes :

$$\begin{aligned} \Delta z'_1 &= \alpha\ V_1 \quad \text{with} \quad \alpha = 0.25 \cdot 10^{-2}\ mm/radV \\ \Delta z'_2 &= \beta\ V_2 \quad \text{with} \quad \beta = 0.5 \cdot 10^{-2}\ mm/radV \end{aligned} \tag{4.2}$$

Let $A = \begin{pmatrix} A_{11} & A_{12} \\ A_{21} & A_{22} \end{pmatrix}$ be the matrix relating phase space points (z, z') at azimuth θ_1 to those at azimuth θ_2, and C and D the matrices between θ_3 and θ_4, and between θ_2 and θ_4 respectively. Then the point in axial phase space at azimuth θ_1 that is imaged in the centre of both diaphragms is related to the applied voltages on the deflection electrodes in the following way :

$$\begin{aligned} \begin{vmatrix} z \\ z' \end{vmatrix} &= \begin{vmatrix} 0 & A_{12} \cdot C_{12}/D_{12} \\ -1 & -A_{11} \cdot C_{12}/D_{12} \end{vmatrix} \begin{vmatrix} \Delta z'_1 \\ \Delta z'_2 \end{vmatrix} \\ &= \begin{vmatrix} 0 & A_{12} \cdot C_{12}/D_{12} \\ -1 & -A_{11} \cdot C_{12}/D_{12} \end{vmatrix} \begin{vmatrix} \alpha & V_1 \\ \beta & V_2 \end{vmatrix} \end{aligned} \tag{4.3}$$

The matrices A, C and D depend on the HF phase. The method breaks down when the azimuthal distance $\theta_4-\theta_2$ between the diaphragms becomes a half oscillation wavelength, i.e. $D_{12} = 0$. We have selected, however, azimuthal positions for diaphragms and bending electrodes such that the axial phase space can be scanned for all HF phases of the particles. The matrices A, C and D are evaluated for several HF phases by the numerical orbit trajectory calculations based on the field map of the electrode configuration in the cyclotron centre. Table 4.1 gives the relevant matrix elements for several HF phases.

Table 4.1 Matrix elements belonging to the axial phase space density measuring system.

ψ	-20°	-29°	-38°	-47°	-56°
A_{12}	5.084	5.136	5.327	5.706	5.733
A_{11}	0.354	0.387	0.528	0.825	0.942
C_{12}/D_{12}	0.973	0.980	0.986	0.991	0.983
D_{12}	6.146	5.943	5.750	5.553	5.607

We note that :

a) $C_{12}/D_{12} \simeq 1$, which is caused by the relatively small difference in azimuthal position between the diaphragm at θ_2 and the pair of deflection electrodes at θ_3. It implies that a good description is obtained if the deflection plates at θ_3 are supposed to lie at θ_2.

b) $|A_{12}| >> |A_{11}|$, and $A_{11} \cdot C_{12}/D_{12} < 1$; this means that each point in the phase space at azimuth θ_1 can be represented by a linear combination of two vectors, having an angle difference of nearby 90° and resulting from the vectors $\begin{pmatrix}1\\0\end{pmatrix}$ and $\begin{pmatrix}0\\1\end{pmatrix}$ in the V_1, V_2-space.

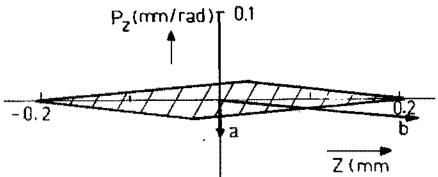

Figure 4.2
Acceptance at θ_1 of the diaphragms for particles of phase -38^{o}. Vectors a and b give the shift of this area due to applied voltages :
a: $\Delta p_{z1} = 0.04$ mm/rad for $V_1 = 16$ V.
b: $\Delta p_{z2} = 0.04$ mm/rad for $V_2 = -8$ V.

In figure 4.2 the acceptance of the diaphragms at azimuth θ_1 has been drawn for particles of starting phase -38^o. The shift of this area due to applied voltages on the two pairs of deflection electrodes is indicated.

4.2.2 Results of the axial phase space area measurements

The measurements of the axial beam phase space area are performed for a cyclotron setting belonging to a 7 MeV extracted proton beam. The dee frequency corresponding to this cyclotron setting is 11.299 MHz, and the dee voltage is 12 kV. The measurements yield the phase space density at the second turn at an azimuth of 270^o. At this position the proton energy is about 45 keV. The beam was partially transmitted through the two diaphragms and the intensity was registered at a current probe located at a radius of 40 cm. The beam current was measured as a function of the deflection voltages V_1 and V_2.
In figure 4.3 a plot is shown of these measurements in the V_1,V_2-space. The total current contained in the axial phase space was found to be 3 μA.

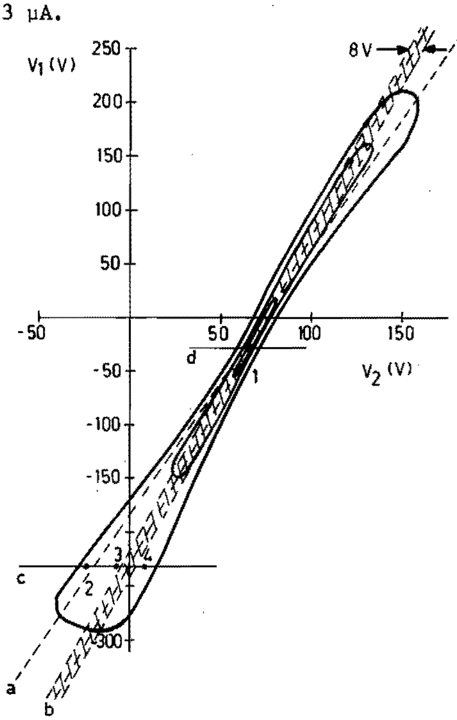

Figure 4.3
Measured $I(V_1,V_2)$ plot. Two lines (a and b) of equal phase are given. Areas of width (FWHM) ∿ 8 V in V_2 around these lines can be drawn in which the particles of one particular HF phase (± 0.5°) are situated. Such an area is indicated around line b. The HF phase difference of lines a and b is 20°. The time structures in point 1 on line d and points 2, 3 and 4 on line c are given in figure 4.5. The iso-current lines are given for 30%, 75% and 99% of the total measured beam current (3 μA).

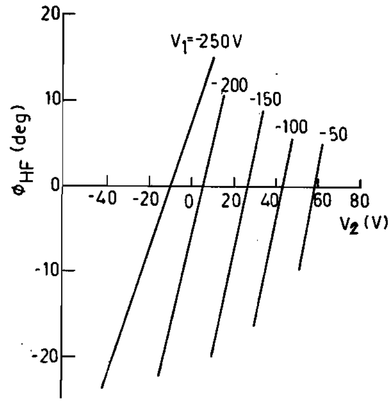

Figure 4.4
Beam phase at a radius of 30 cm as a function of deflection voltage V_2 for several voltages V_1.

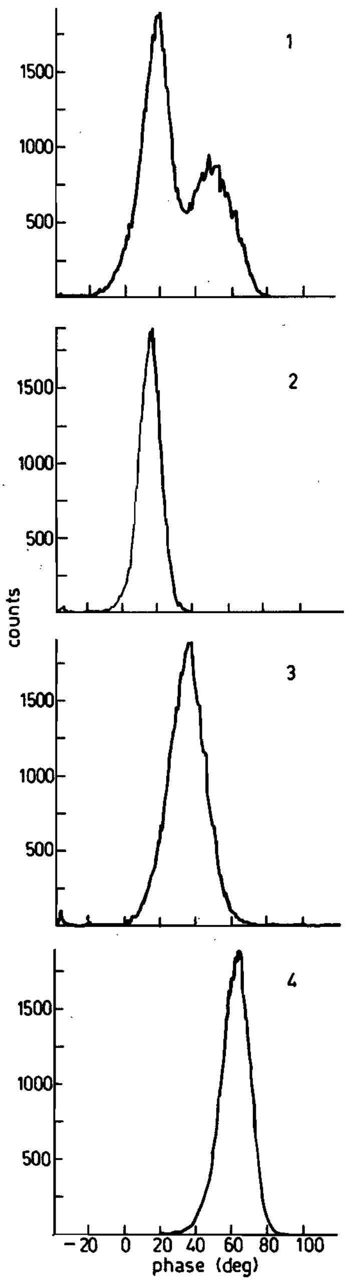

Figure 4.5
Time structure of the beam in points 1 to 4 of figure 4.3.

During these measurements the HF phase at several radii in the cyclotron was registered simultaneously using the non-intercepting phase measuring equipment described in section 2.2. Figure 4.4 shows the beam phase at the internal phase probe at radius 30 cm as a function of deflection voltage V_2 for several values of the voltage V_1. In figure 4.3 we have drawn two lines of equal HF phase (line a and line b), having a phase difference of 20^{o}.

The phase measuring equipment does not give the HF phase width of the ion beam. To check the phase behaviour of the beam, the time structure was measured with the equipment described in section 2.4 for a lot of points in the V_1,V_2-space. As an example figure 4.5 shows the time structures measured for the points 1, 2, 3 and 4 of figure 4.3. A phase width between 10^{o} and 20^{o} is found for points 2 to 4. In point 1 the phases of points 2 to 4 are all present.

To transform the $I(V_1,V_2)$ plot into a true phase space plot $I(z,\dot{z})$ at the second turn, the starting HF phases of the particles have to be known. The measured HF phases are not equal to the starting phases, but differ from these by a constant unknown amount, depending on the isochronism. Therefore, we have related starting HF phases to the measured HF phases assuming that the maximum beam current occurs for a starting phase of -30^{o}, as follows from numerical calculation. Then the transformation matrices that are calculated with the program ORBIT/CALCULATION are applied to transform the V_1,V_2-space into the phase space at the second turn. The phase measurements indicate that the contribution of particles with one particular HF phase originates from an area in the V_1,V_2-space of width ΔV_2 = 8 V (cf. figure 4.3). Figure 4.6 shows the phase space area at the second turn at azimuth 270^{o}, in which two areas of constant phase are also indicated.

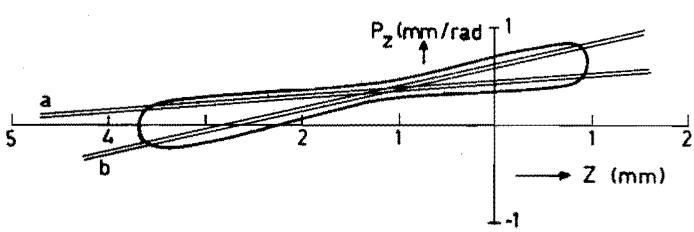

Figure 4.6 Axial phase space area at the second turn (45 keV). Areas a and b correspond to particles of HF phase -48^{o} and -28^{o} respectively.

We note the following :

1. The phase space figure is not symmetric with respect to the origin.
2. An axial height of 5 mm is measured while a height of 8 mm can be accepted by the measuring system.
3. There is a very small axial angular spread; especially for particles of one particular HF phase : 0.04 mm/rad. This means for the $\sim$ 45 keV beam an angular divergence spread of $\approx$ 1 mrad.

The first two phenomena are ascribed to misalignments of the median plane of the main magnetic field with respect to the midplane of the cyclotron magnet, and with respect to the plane of symmetry of the electric field in the acceleration gap (cf. section 3.6). These effects also account for deviations of the total beam current estimated from the phase space figure ($\sim$ 3 μA) with respect to the total internal beam current belonging to that ion source setting ($\sim$ 7 μA). By an alteration of the magnetic field median plane with an asymmetric excitation of the inner circular correction coils B_1 the phase space area figure at azimuth 270^o at the second turn is shifted along the z'-axis (see figure 4.7). By different axial positioning settings of the measuring system the complete axial phase space area can be determined. In the next section a comparison of the measured phase space area with the axial emittance based on other observations will be made. At the second turn at 270^o a total phase space area, containing all phases, of 120 mm-mrad is estimated.

4.2.3 Comparison with the emittance of the ion source

In figure 3.18 the acceptance area at an azimuth of 90^o after the first gap crossing was drawn for the "old" puller shape. The axial ion source emittance was based on two visual observations, the first one being that the axial height of the beam at the entrance of the puller is about 1 mm, the second being the observed axial height of about 18 mm at an azimuth of 270^o at the first revolution. These observations lead to a phase space area at the entrance of the puller of about 100 mm-mrad. The proton energy at this position is about 11 keV.

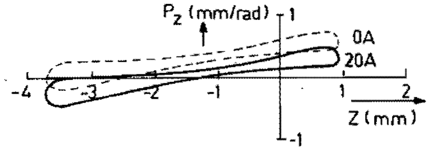

Figure 4.7 *Shift of the axial phase space area on the second turn due to an asymmetric excitation of the inner circular correction coils B_1. For an extra current of 20 Amp. in the upper coils of B_1, which lowers the magnetic field median plane, a shift of the phase space area of -0.24 mm/rad is measured; the shift is linear with this current.*

The acceptance figure shows that a large portion of the beam is cut away at the second revolution when the beam passes again the puller (time moment $\tau \simeq 360^o$, time moment $\tau = 0^o$ is at the first revolution at 90^o). The puller causes again a severe limitation of the acceptance area at the third revolution (time moment $\tau \simeq 690^o$). However, this latter limitation plays no role in the determination of the axial emittance, due to the requirement that the beam should pass the first diaphragm of the measuring system. Therefore the measured axial phase space area at the second turn at azimuth 270^o must be an image of that part of the ion source emittance that is limited by the boundaries of the puller at the time moment $\tau = 360^o$. This accepted area transformed to $\theta = 270^o$ at the second turn gives at that position an area of length $\Delta z = 13$ mm and of angular width $\Delta z' = 0.04$ mm/rad (see figure 4.8) for particles starting with a HF phase of -30^o (the transformation is phase dependent). The phase space figure at azimuth $\theta = 270^o$ at the second revolution is a rotation of the upright emittance figure at the entrance of the puller; the rotation angle is about 80^o. The rotation angle is different for particles starting with different HF phases. The rotation angle data for different HF phases show that the measured phase space at the second revolution at azimuth 270^o is consistent with the estimated ion source emittance figure at the entrance of the puller : the emittance can be regarded as the phase space belonging to a diaphragm of 1 mm at the entrance of the puller with an area of 100 mm-mrad.

The fact, that the rotation angle of the emittance figure at the puller is HF phase dependent, causing an apparantly enlarged phase space area at the second turn (see the end of section 4.2.2), is an example of the phase mixing phenomenon (cf. section 3.4).

A comparison of the ion source emittance and the cyclotron acceptance for particles of one particular phase is given in figure 4.8.

4.2.4 Consequences for axial phase selection

The measurements described in section 4.2.2 show that phase selection is obtained for particular settings of the DC voltages V_1 and V_2 on the deflection plates (see figure 4.3). The selected HF phase can be chosen freely. A beam current of 25 to 50 nA with a phase width of about 10^o can be reached for an ion source setting of 7 μA internal beam current. Figure 4.5 has shown the time structure of several selected beams.

Van Heusden has described an axial phase selection method for the Eindhoven cyclotron employing two diaphragms (Van Heusden 76). The transmission through both diaphragms should be sharply peaked around the selected phase with a low background of all possible phases arising from particles moving in the median plane. In the experiments no such background was found. The absence of this background must be ascribed to the median plane effects presented in chapter 3.

Since the ion source emittance can be seen as the image of a diaphragm of 1 mm at the entrance of the puller, one diaphragm should be sufficient to obtain phase selection. The diaphragm must be placed

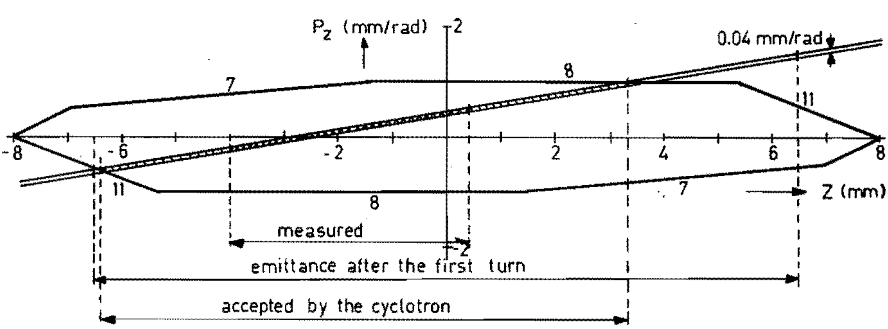

Figure 4.8 Ion source emittance and the cyclotron acceptance at the second turn at azimuth θ = 270° for particles of starting phase −38°. The number at the lines limiting the acceptance area gives the turn number at which this limitation occurs (at azimuth 270°).

at a position such that the phase space figure is rotated over 180° or 360° for one particular phase. Figures 4.9 and 4.10 show the experimental result of this method, where the dee voltage was varied for optimal imaging of the puller entrance on the diaphragm. A phase selection of about 10° was reached for a current of 100 nA.

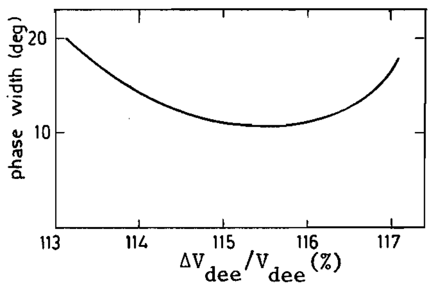

Figure 4.9
Measured phase width as a function of the dee voltage, employing one diaphragm.

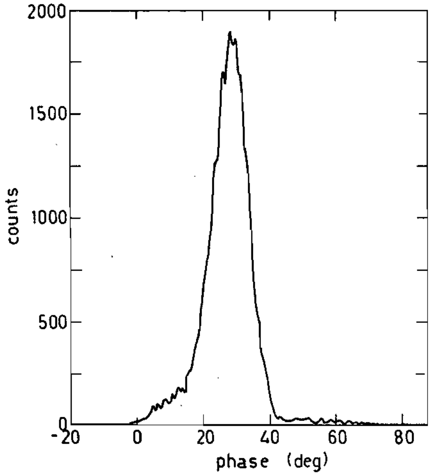

Figure 4.10
Time structure for a beam transmitted through one diaphragm. Phase width 12°.

4.3 Radial phase space density measurements

4.3.1 Introduction

For the radial phase space density measurements in the centre of the cyclotron use is made of two radially selecting diaphragms that can be moved independently via remote control. The positioning occurs with a precision better than 0.1 mm. The radial extent of the diaphragms is 12 mm, and the aperture is 0.3 mm. The diaphragms can be moved over several centimeters. Mostly they were installed such that the second up to the fifth turn could be intercepted. The azimuthal angle between the two diaphragms at the fourth turn is about 25°, corresponding to a distance of 2.6 cm. Figure 4.11 gives the positions of the diaphragms in the centre of the cyclotron, as used for the radial beam quality measurements. The radial beam quality was deter-

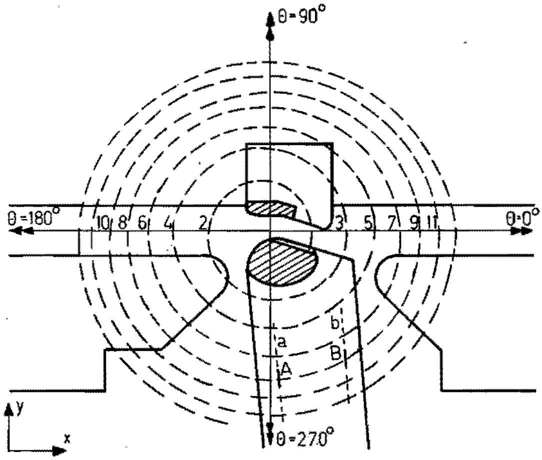

Figure 3.11 Central region of the cyclotron with diaphragms A and B for the radial phase space area measurements.

mined for several energy settings of the cyclotron, but most experiments were carried out for a 7 MeV setting for protons.

4.3.2 Radial beam quality determination

The measurement was performed by successively putting the first diaphragm (see figure 4.11, line a) at a larger radius with respect to the cyclotron centre, and by determining the width and position of the selected beam by the second diaphragm (line b). The transmitted beam was intercepted by a probe near extraction radius [1]. From the turn separations the turn numbers and the radius for maximum current in one turn are fixed. Figure 4.12 is an example of a measurement in which for each fixed position of the first diaphragm the second diaphragm was put such that the transmitted current was at maximum value (radial beam profile measurement). The phase of the selected beam is also given.

---

1) In one cyclotron shift we used a current probe located directly after the second diaphragm at a radius of 7 cm. Then a large background of spurious beam is measured. In this situation, however, the beam quality figure has the same shape as in other measurements.

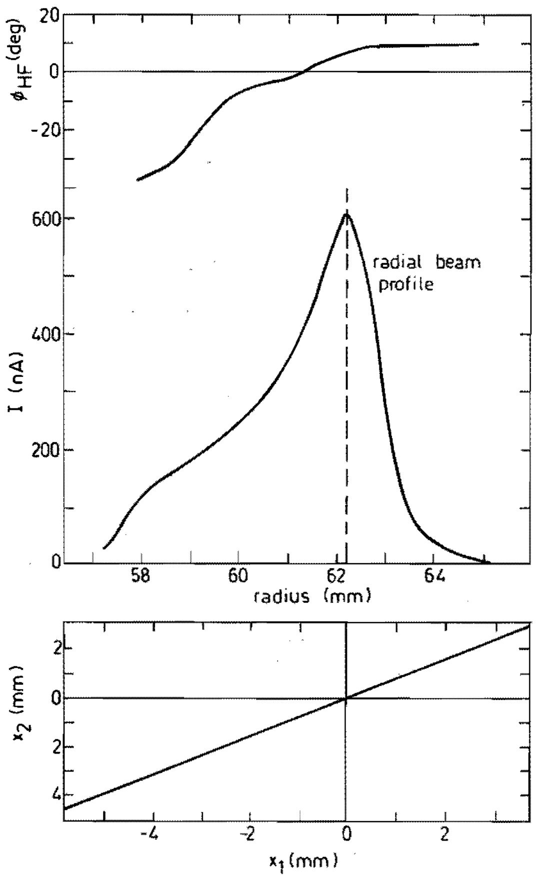

Figure 4.12
Radial beam profile at the fourth turn at an azimuth of 270°, and HF phase measured at a radius of 40 cm. For maximal transmitted current the second diaphragm position x_2 varies linearly with the first diaphragm position x_1.

It is noted that ϕ_{HF} is strongly coupled to the radial position. Generally with the use of the two diaphragms in the centre an extraction efficiency between 85% and 95% was achieved, whereas for normal operation a value of about 55% to 65% was found. This indicates that the phase width of the selected beam is small. The phase width of the selected beam was not measured directly in these experiments. However, single turn experiments employing the two radial diaphragms in the centre (cf. chapter 5) showed that the phase width was smaller than 6^o.

We denote by x_1 and x_2 the radial distance of the selected beam in the fourth turn at the azimuths of diaphragm *A* and *B* respectively, with respect to the position of maximum intensity (cf. figure 4.12). The following relation between x_1 and x_2 was found experimentally :

$$x_2 = 0.792\ x_1 \qquad (4.4)$$

This linearity implies a linear relation between the divergence $dx_1/d\theta$ and the displacement x_1.

As the magnetic induction in the central region may be taken constant, the transformation between the two azimuthal positions is given by the matrix equation (Banford 66) :

$$\begin{pmatrix} x_2 \\ x_2' \\ \Delta p/p \end{pmatrix} = \begin{pmatrix} \cos\phi & r\sin\phi & r(1-\cos\phi) \\ -1/r\sin\phi & \cos\phi & \sin\phi \\ 0 & 0 & 1 \end{pmatrix} \begin{pmatrix} x_1 \\ x_1' \\ \Delta p/p \end{pmatrix} \quad (4.5)$$

where r is the orbit radius of the fourth turn at maximum beam intensity and ϕ is the azimuthal angle between the two diaphragms. The measured quantities are the position and width of the selected beam as a function of the first diaphragm position: $x_2 = x_2(x_1)$ and $\Delta x_2 = \Delta x_2(x_1)$. They have to be transferred to the overal divergence $x_1'(x_1)$ and the spread $\Delta x_1'(x_1)$. Further the first diaphragm moves perpendicular to the dee gap and it may be expected that the orbit centres lie along the dee gap. Then a relative change in the momentum may be approximated by

$$\Delta p/p = \Delta r/r \simeq x_1/r \quad (4.6)$$

The measured relation (4.4) together with (4.5) and (4.6) yield

$$x_1' = \{-7.8 \ rad/m\} \ x_1 \quad (4.7)$$

This is equivalent to a linear change (Δs) of the orbit centre position along the dee gap as a function of x_1: $\Delta s = r \cdot x_1' = \{-7.8 \text{ rad/m}\} \cdot x_1 \cdot r$, with r = 62.4 mm. An orbit centre spread of 4 mm for the 8 mm total width of the beam (see figure 4.12) is found. On the other hand for $x_1 = 0$ (maximum intensity) a total divergence spread of 65 mrad is found, corresponding to an orbit centre spread of 4 mm.

The measured radial beam phase space area is given in figure 4.13. Table 4.2 gives the relevant data. The data correspond to the data obtained by Mallory and Blosser (Mallory 66) in an emittance measuring test facility, and are in agreement with the measured values of the radial phase space area in the beam guiding system (Schutte 73).

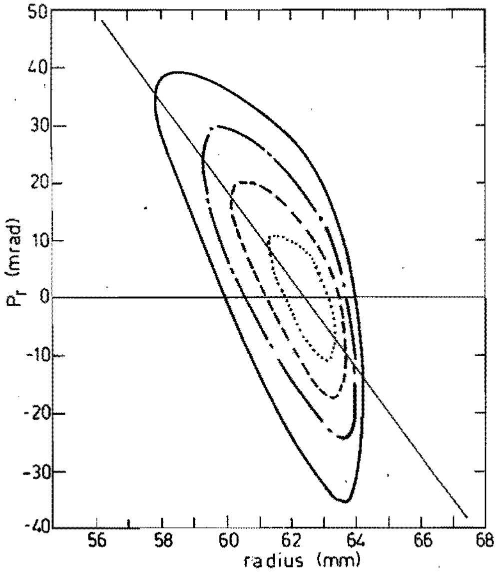

Figure 4.13 *Measured radial phase space area at the fourth turn at azimuth θ = 270°. Proton energy 100 keV. The lines are drawn for 50%, 75%, 96% and 100% of the total beam current (15 μA). The areas are 29, 80, 156 and 300 mm-mrad respectively.*

Table 4.2 *Radial emittance area at a total beam current of 15 μA.*

Fraction of total beam current	Radial Emittance Area	
	Energy 100 keV 1)	Energy 230 keV 2)
%	mm-mrad	mm-mrad
50	29	23
75	80	71
96	156	122
100	300	242

1) proton energy at extraction radius : 7 MeV.

2) proton energy at extraction radius : 20 MeV.

4.3.3 Measurements of the displacement of the beam due to a bias voltage on the dee

A negative DC bias voltage is applied on the dee to prevent multipactoring of the dee. At different operating conditions of the cyclotron the bias voltage is set at -100 V to -1000 V. The bias voltage causes the orbit centres to be shifted along the dee gap :

$$\Delta X_{centre}(n) = \sum_{k=1}^{2n} \frac{r_k}{2k} \frac{V_{bias}}{g \cdot V_{dee}} \tag{4.8}$$

where $\Delta X_{centre}(n)$ is the orbit centre displacement at the n^{th} turn and r_k is the radius after the k^{th} dee gap crossing. In eq. (4.8) g is the gap factor.

For the maximum intensity in the fourth turn a change $\Delta x'_1$ = 43.4 mrad was measured for a bias voltage change of 600 V. This corresponds to an orbit centre shift of Δs = 2.71 mm. This shift is in agreement with the number ΔX_{centre} = 2.69 mm obtained from eq. (4.8). (ΔV_{bias} = 600 V, V_{dee} = 12 kV, g = 0.9, $r_k = k^{\frac{1}{2}}R$, r_8 = 62.4 mm). For a negative bias voltage on the dee the orbit centre shift is in the negative x-direction (see figure 4.11).

4.3.4 Measurement of ν_r-1 on two successive turns

The radial phase space area has been measured on both the third and the fourth turn. A rotation between the two measurements gives directly a value of the radial oscillation frequency ν_r if these figures are given in orbit centre coordinates. A value of ν_r differing from 1 should be ascribed to the influence of the acceleration gap. As shown in chapter 3, the quantity ν_r differs slightly from 1 only for the first two turns and then remains constant and equal to 1 in the central region. The measurements show no rotation, in agreement with this expectation.

4.4 Conclusion

The axial phase space area measurements in the cyclotron centre have shown that the ion source emittance can be regarded as the image of a 1 mm axial selecting diaphragm at the entrance of the puller (energy 11 keV) with an area of 100 mm-mrad. The transformation of this area towards larger radii is very sensitive to the shape of the accelerating field and the HF phase. Due to HF phase mixing this area is enlarged to about 120 mm-mrad for the 45 keV beam at the second turn.

The measured radial phase space area for a 100 keV beam is 150 mm-mrad for 96% of the total beam current (10 μA), with an orbit centre spread of about 4 mm. These data are in agreement with the data of the externally measured cyclotron emittances (for 20 MeV the radial phase space area is between 10 and 20 mm-mrad, corresponding to an area between 141 and 282 mm-mrad at 100 keV).

CHAPTER 5

SINGLE TURN EXPERIMENTS

With two radially selecting diaphragms in the cyclotron centre a beam can be selected from the radial phase space area, as is described in chapter 4. Single turn extraction experiments have been performed with the selected beam. The single turn mode of operation is observed by changing the dee voltage with small amounts, in such a way that one can choose the turn number at the extraction radius. In this situation the effect of the inner harmonic coils could be compensated by the effect of the outer harmonic coils. Deterioration of the beam quality was observed by increasing the accelerated beam intensity. This must be ascribed to the influence of space charge in the region of the first dee gap crossing. A relative energy spread better than $0.8 \cdot 10^{-3}$ *was measured. An energy-position relation was found in the beam guiding system without using diaphragms in the cyclotron centre. At the place of the extractor this relation can be improved (i.e. the energy can be defined sharper as a function of the position) by creating a field bumb of the proper shape with circular correction coils.*

5.1 Introduction

The radial phase space density measurements in the centre of the cyclotron, described in the previous chapter, always showed a high extraction efficiency of 90% or more. Furthermore it turned out that the HF phase of the beam selected by the two diaphragms on the fourth turn is strongly related to the radial beam position within that turn. Under normal conditions (without diaphragms in the centre) the HF phase width is so large (30^o to 40^o), that there is a considerable difference in energy gain per turn for particles accelerated on the top of the dee voltage and particles beside this top, resulting in an energy and thereby radial position deviation after the nominal number of turns. Therefore the particles of the lower energy have to be accelerated over more turns than the higher energy particles before they reach the extractor. In this case (normal situation) multi turn extraction occurs. In the case of a selected beam a small HF phase width results, and the particles can be extracted in one turn (single turn mode of operation).

In this chapter the experimental evidence is given of single turn extraction. The two radially selecting diaphragms in the centre of the cyclotron were employed for phase selection. As shown in the previous chapter the HF phase of the selected beam can be chosen, as well as the intensity. With the use of diaphragms with an aperture of 0.5 mm an internal as well as an external current can be obtained of several μA. The first experiments were always carried out for a selected beam intensity of about 100 nA.

Single turn experiments with a cyclotron that is designed as a multi turn machine require a high stability of the magnetic field, the dee voltage and frequency together with a small HF phase width (Hagedoorn 69, Vader 81). The last demand (small HF phase width) is less stringent when a third harmonic frequency mixing is applied to the HF system (flat topping).

5.2 Experimental aspects

5.2.1 Introduction

To investigate the properties of the beam selected by the two diaphragms in the centre of the cyclotron the beam was extracted and guided to measuring station *BC3* (cf. figure 2.7) and behind the external phase probe *PC1*. The beam guiding system was either set in the double achromatic or in the dispersive mode.

In chapter 2 several available diagnostic means in the beam guiding system are described. We mention the foil (*FB1*) in front of the analysing system, which is used for a check of the double achromaticity or for a calibration of the dispersion; the scanners *BB2* and *BB3* by which the beam quality can be determined; scanner *BC3* necessary for the measurement of the energy spread of the beam; the phase probes *PB1* and *PC1* allowing a measurement of the energy of the beam. Furthermore small variations in the currents through the analysing magnets *MB4* and *MC1* have been used for a check of the dispersion calibration, while the small correction magnet *MB2* was used to sweep the beam over diaphragm *SB1* for a measurement of the dispersion in the beam. With the quadrupole *QCB* it is possible to focus the beam through diaphragm *SB1* on diaphragm *SC2* or on scanner *BC3* in the dispersive mode.

5.2.2 Cyclotron setting

Generally the cyclotron was set to accelerate protons up to the final energy of 7 MeV for our experiment. For this setting the dee frequency is 11.299 MHz, the main magnetic induction is 0.667 T. The dee voltage was set at a value of about 19 kV and a fine adjustment was made such that this value can be varied in steps of a few volts.

Two radially selecting diaphragms were positioned on the fourth turn. The aperture is 0.5 mm. As can be inferred from figure 4.13 a current of about 200 nA can be transmitted through the diaphragms at an ion source setting giving about 10 μA internal current without the use of diaphragms. The diaphragms were mostly positioned at the small radius side of the beam profile (cf. figure 4.12), because at this side the phase of the selected beam is most sensitive to diaphragm position changes.

5.2.3 Measurement of the beam dispersion and energy

In the dispersive mode of the beam guiding system the dispersive action was measured in several ways. The energy spread of the beam is determined by measuring the width of the beam at scanner *BC3*. Then diaphragm *SC2* is opened completely.

A foil (polyethylene) of 1.0 mg/cm^2 in front of the analysing system was used to lower the beam energy with 60 keV. The displacement of the beam at scanner *BC3* is sensitive on the setting of the quadrupoles *QC1*, *QC2* and *QC3*. The general relation between ray displacements and momentum resolution is :

$$x_2 = - M\, x_1 + D\, \frac{\Delta E}{E}\,, \tag{5.1}$$

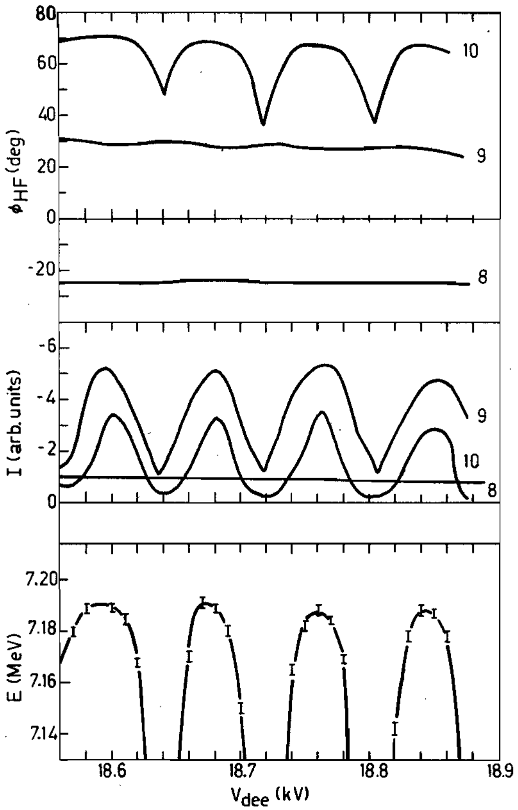

Figure 5.1 *Measured energy of the external beam as a function of the dee voltage employing the TOF method. The HF phase and intensity measured with phase probe 8 (outermost phase probe in the cyclotron), probe 9 (PB1) and probe 10 (PC1) are given. The phase and intensity in the cyclotron remain well constant while varying V_{dee}. On the external phase probes 100% current variations are observed ("single turn mode of operation"). The energy measurement with the TOF technique becomes inaccurate for very low currents. In the current peaks the same energy is measured.*

where x_1 and x_2 are the displacements of a ray at the entrance and the exit diaphragms (*SB1* and *SC2*) respectively, and where *M* and *D* are constants (*D* with the dimension of a length). Sandvik et al. found for a nearly optimal setting $M = 1.3$ and $D = 1.5\cdot10^3$ mm (Sandvik 73). The applied relative energy change with the degrader foil ($8.4\cdot10^{-3}$) gives thus according to eq. (5.1) a beam displacement of 12.6 mm. For a slightly different setting we measured a beam displacement at *BC3* of 11.0 mm, which has to be compared with the number 11.5 mm obtained from the beam transport program (BGS, Van Genderen 79). These data are in fair agreement with the one obtained with eq. (5.1).

The dispersion calibration was checked with the result obtained by relative changes of the current through both analysing magnets *MB4* and *MC1*. Assuming a linear behaviour of the magnetic induction versus current, and applying $\Delta p/p = \Delta B/B$, we found a 1 mm beam displacement for $\Delta E/E = 1.18 \cdot 10^{-3}$ for a slightly different experimental situation. The measured displacement using the foil was 1 mm per $\Delta E/E = 1.07 \cdot 10^{-3}$, which is again in fair agreement with the number given above.

The energy of the external beam was measured with the external phase probes *PB1* and *PC1* (cf. chapter 2). After correlation the phase probe signal provides a vector of which the length is a measure for the beam intensity and of which the angle gives the HF phase of the beam. However, a disturbance signal (measured at zero beam intensity) is always present, and the associated vector has to be subtracted from the probe signal vector. It is clear that for small intensities relatively important errors can be made. This occurs especially in our single turn experiments, where we varied the dee voltage to obtain external beam current variations of 100%. Figure 5.1 demonstrates the situation.

5.3 Aspects of single turn extraction

The process of single turn extraction can be conceived by regarding the energy of particles at the last turns in the cyclotron as a function of the initial HF phase. We extract the beam after about 180 revolutions. The maximum phase deviation from the optimum value must thus be less than $\arccos(180/181) = 6^o$. Figure 5.2 shows calculated energies at the last turn for the cyclotron setting mentioned in section 5.2.2. Asuming a radial oscillation amplitude equal to zero and taking the extraction radius at r = 52.40 cm, corresponding to an energy of 6.85 MeV, it is seen that when the initial HF phases lie between -14^o and -24^o all particles are extracted at the 183^{th} turn. In case the initial phase width is larger than 10^o more turns are extracted.

The extraction process is complicated, and, when radial oscillation amplitudes unequal to zero are present, is dependent on the

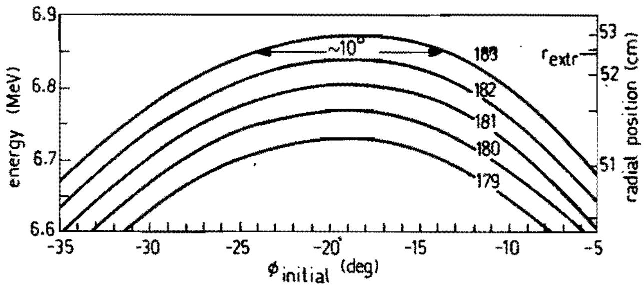

Figure 5.2 *Calculated energy and radial position at the extraction region as a function of the initial HF phase. The turn numbers are given. Nominal setting 7 MeV, frequency : 11.299 MHz, dee voltage : 18.95 kV. A radial oscillation amplitude equal to zero has been used. The particles with a HF phase lying between -24° and -14° are extracted at the 183th turn.*

setting of the inner and outer harmonic coils, on the magnetic field, and on the dee voltage. Using a simple model the effects of variations in these parameters and of initial phase changes are observed.
In the model the following equations are integrated :

$$\begin{aligned} dE &= 2\ eV \cos\phi\ dn \\ d\phi &= 2\pi\ \ \delta B/B\ \ dn \\ d\psi &= 2\pi(\nu_r - 1)\ \ dn \end{aligned} \tag{5.2}$$

Here, the turn number n is the independent variable, ϕ is the HF phase of the particle and ψ the radial oscillation phase, V is the dee voltage, E the energy, $\delta B/B$ is the deviation from the isochronous field, in which the fringing field is also contained. The orbit radius follows from

$$r = \{2.203\ m\ MHz\ (MeV)^{-\frac{1}{2}}\}\ f^{-1}\ E^{\frac{1}{2}}\ (1 - \delta B/B) \tag{5.3}$$

where f is the frequency.

At the first turn in the cyclotron initial values r_1, ϕ_1, A_1 and ψ_1 are given where A_1 and ψ_1 are the amplitude and the phase of the radial oscillation excited by the inner harmonic coils. At a radius of 0.485 m the vector (A_1, ψ_1) has been transformed to the vector $(A_1{}^*, \psi_1{}^*)$. At this radius the outer harmonic coils induce a radial oscillation with amplitude A_2 and phase ψ_2. The total effect of both actions is vectorially added. The radial position r_p of the particle is given by

$$r_p = r + A \cos\psi \tag{5.4}$$

With this model also the effect of field bumbs (more or fewer turns, hence a different oscillation phase at extraction) can be observed.

In figure 5.3 the radial position is given for several turn numbers as a function of the initial HF phase. Due to the radial oscillation there is no well defined relation between energy and radial position, however, the radial position is essential for the extraction. From this figure it is seen that a phase width smaller than 6^o is necessary to obtain single turn extraction, for a radial oscillation amplitude at extraction $A = 3.6$ mm resulting from $A_1 = A_2 = 2$ mm and $\psi_1 = 0^o$, $\psi_2 = 90^o$. The value of 6^o is considerably smaller than in the case where no radial oscillation has been assumed (see figure 5.2).

If the magnetic field is changed by $\delta B/B = 2 \cdot 10^{-4}$ (e.g. by varying B_{10}) the single turn effect completely disappears (dashed lines). Single turn extraction could be possible in this case ($\Delta\phi_{initial} < 3^o$); however, the allowed phases lie outside the originally selected area. Similar phenomena occur at a change of the harmonic coil settings, at ion source position changes, at variations in the bias voltage on the dee, etc.

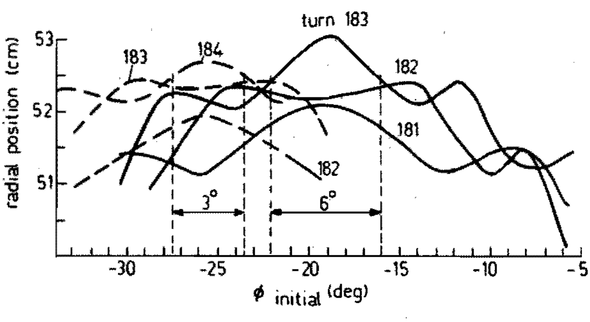

Figure 5.3 Calculated radial position at the extraction region. $A_1 = A_2 = 2$ mm, $\psi_1 = 0^o$, $\psi_2 = 90^o$. For the isochronous field (full lines) a HF phase width smaller than 6^o is required for single turn extraction. Single turn extraction is no longer present when the main magnetic field is changed by $\delta B/B = 2 \cdot 10^{-4}$ (dashed lines).

5.4 Experimental results

Experimental evidence of single turn extraction is found by observing 100% variation in the external current as a function of the dee voltage. Figure 5.4 shows the external beam current versus the dee voltage. Apparently the phase width is so small that it is possible to select the turn number at extraction radius with the dee voltage.

In this situation for the beam width at *BC3* 0.76 mm was found (see figure 5.5), corresponding to an energy spread $\Delta E/E$ = $0.85 \cdot 10^{-3} \pm 5\%$. In this experimental situation the dispersion was $\Delta E/E = 1.12 \cdot 10^{-3}$ per mm. The energy in the maxima has already been given in figure 5.1. In all maxima the energy is the same. The measured horizontal beam quality is better than 2.5 mm-mrad as has been determined with scanners *BB2* and *BB3* and with diaphragm *SB1*.

By increasing the beam current through the diaphragms in the cyclotron centre, the single turn effect slowly disappeared. Figure 5.6 shows this effect. It must be ascribed to the influence of space charge during the first dee gap transition, deteriorating the relation between energy and HF phase. An increase of the energy spread is measured.

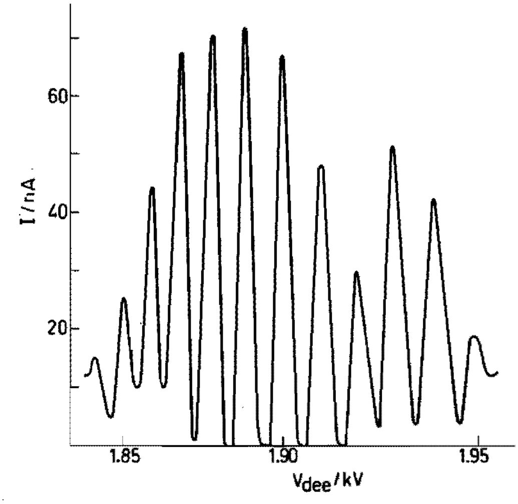

Figure 5.4 External beam current at measuring station aB3 as a function of the dee voltage in the case of single turn extraction. Nominal cyclotron setting : 7 MeV protons.

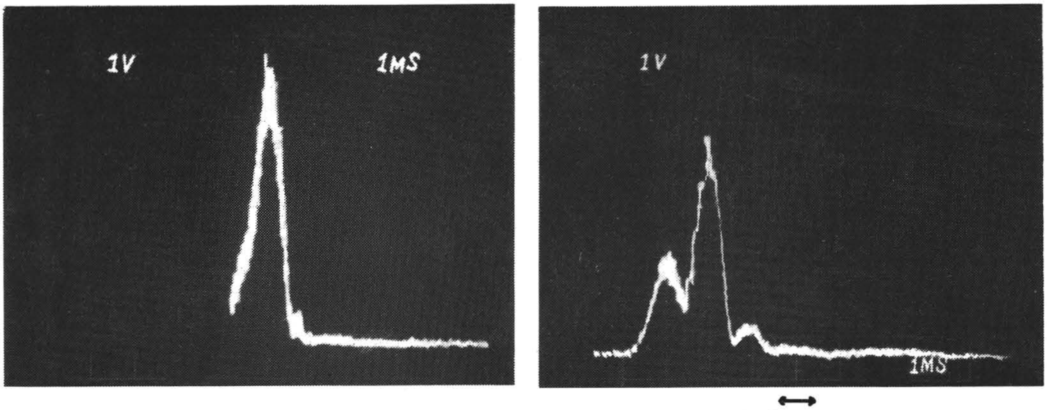

(a) (b)

Figure 5.5 a) *Scanner signal at BC3 in the case of single turn extraction. The scanner wire displacement in 1 ms is 1.28 mm. The dispersion is $\Delta E/E = 1.12 \cdot 10^{-3}$ per mm. The measured relative energy spread is $\Delta E/E = 0.85 \cdot 10^{-3}$*

b) *Scanner signal after a slight change of the setting of the harmonic coils. Several energy peaks are present, because the internal beam is extracted in several turns.*

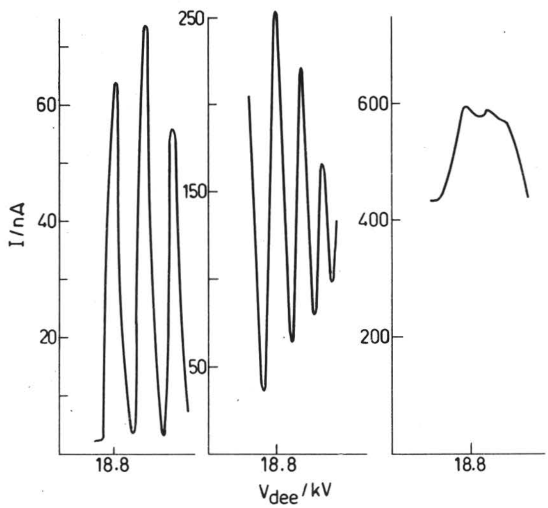

Figure 5.6 *The effect of space charge. External beam current at measuring station aB3 as a function of the dee voltage. I_{max} = 75 nA, 250 nA, 600 nA. The 100% current variations, typical for single turn extraction, disappear as the beam current is increased.*

A rough estimation of the influence of space charge is found by comparing the radial space charge force on the particles with the Lorentz force. The radial electric field strength due to space charge is approximated by

$$F = \frac{I}{\varepsilon_o \ \pi \ \Delta x \ L \ f} \tag{5.5}$$

assuming that the beam may be approximated by a cylinder of length L and diameter Δx ($L >> \Delta x$). Here f is the dee frequency. Due to the radial electric field a change in the revolution frequency of the particles will occur. The particles at the outside of the cylinder will show an increasing or decreasing HF phase with respect to the particles inside the cylinder. The HF phase change per revolution is now given as

$$\delta\phi = 2\pi \frac{e \ F_{sp\ charge}}{e \ v \ B} = \frac{I}{\varepsilon_o \ \pi \ \Delta x \ r^2 \ f^2 \ B \ \Delta\phi} \tag{5.6}$$

where B is the value of the magnetic induction, r is the radius of the turn, $\Delta\phi$ is the phase width, and where I is the current of the beam, which is equal to the time averaged beam current multiplied by $2\pi/\Delta\phi$

$$\delta\phi = \frac{I_{ext} \ 2\pi/\Delta\phi}{\varepsilon_o \ \pi \ \Delta x \ r^2 \ f^2 \ B \ \Delta\phi} \tag{5.7}$$

where I_{ext} is the external current.

If the space charge may be neglected, the HF phase almost uniquely determines the energy (chapter 4, Hagedoorn 69), and thus also the radius. Then, by using diaphragms in the cyclotron centre, phase selection may be expected and has been experimentally proved. Due to space charge the relation between energy and HF phase becomes uncoupled and thus also the relation between radial position and HF phase, so that the diaphragms in the cyclotron centre will become less phase selecting.

For I_{ext} = 50 μA we find at the first revolution phase changes of ± 3.15°, i.e. an extra phase spread of 6.3°. This number must be compared with the requirement for single turn operation : $\Delta\phi \leq 6^o$ (see figure 5.3). The current of 50 μA coincides with the current of

600 nA through the diaphragms. Higher energies yield an f^3 improvement.

This rough estimation corresponds with our observations regarding enhanced currents.

The single turn effect is sensitive on the cyclotron setting. In figure 5.7 we show the effect of a change in the main field realized by a variation of the correction coil B_{10}. The central peak has a FWHM value of about $0.2 \cdot 10^{-4}$. The origin of the satelite peaks has not yet fully been understood. The energies in the satelite peaks are not equal to the energy in the central peak. The single turn effect is largely lost applying a small relative field change of $1.5 \cdot 10^{-4}$. This is in correspondence with the model calculations shown in figure 5.4. The same phenomena occur for changes of the harmonic coil settings, bias voltage changes, etc.

It was observed, that a first harmonic field perturbation caused by the inner harmonic coils, could be corrected rather completely by a first harmonic of the outer harmonic coils, and vice versa. Also changes of V_{bias} could be corrected by a first harmonic field perturbation.

We mention that a first harmonic perturbation is always present in our cyclotron due to the effect of the bevelled dee (Corsten 80).

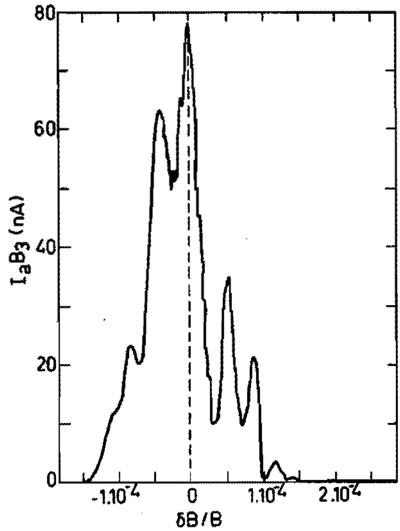

Figure 5.7 External beam current as a function of the main magnetic field. The field change $\delta B/B$ is realized by changing the outer circular correction coil B_{10}.

5.5 Dispersion in the external beam

We have measured the dispersion, i.e. correlation between energy and the density in the horizontal phase plane, in the external beam obtained with only one diaphragm in the cyclotron centre, or with no diaphragms.

Figure 5.8 shows this dispersion where one diaphragm was used in the cyclotron centre : with correction magnet *MB2* the external beam was swept over diaphragm *SB1* (1 mm aperture). In case no dispersion is present, the position of the beam after the analysing system is unaltered.

The dispersion in the external beam is also observed for the case without diaphragms in the cyclotron centre. Supposing dispersion is present in the beam, for instance due to the precession effect of the extraction system, then generally lines of equal energy in the radial phase plane at the entrance diaphragm of the analysing system are not upright. To observe the dispersion the phase plane has to be rotated i.e. we must realize an energy to position imaging. This can be done with the quadrupoles in the beam guiding system, but then the beam transport may be made worse. It is easier to obtain this situation by creating a field bumb, by which the radial phase plane at the extractor

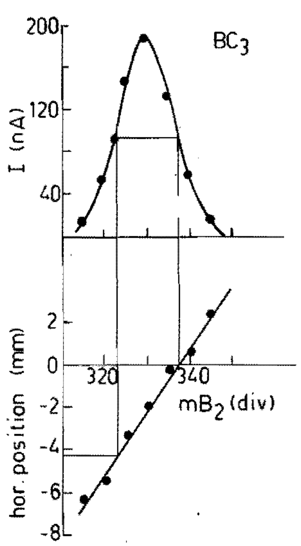

Figure 5.8
Current and horizontal position of the beam behind the analysing system (scanner BC3). Correction magnet mB2 was used to sweep the beam over the entrance diaphragm (SB1) of the analysing system. The position change of 4.4 mm for the resulting current distribution (FWHM) corresponds to an energy change of $\Delta E/E = 2.5 \cdot 10^{-3}$.

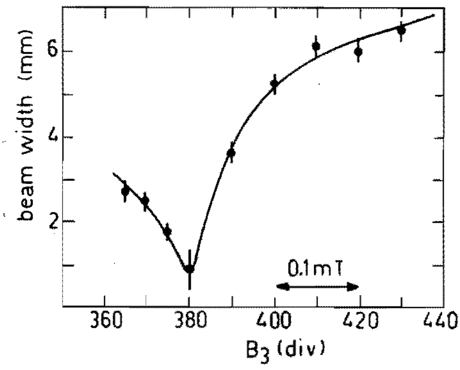

Figure 5.9 *Beam width at scanner station BC3 as a function of the setting of B_3. The external current remained constant. No diaphragms in the centre of the cyclotron were used. The dispersion is $\Delta E/E = 0.78 \cdot 10^{-3}$ per mm. The minimum relative energy spread is $\sim 0.7 \cdot 10^{-3}$.*

is rotated. Figure 5.9 shows the energy spread of the beam after the analysing system as a function of the third circular correction coil B_3. At a certain value of the field bumb an extremely small energy spread was observed.

5.6 Conclusion

Single turn extraction is evidenced by observing 100% current variations in the external beam as the dee voltage is changed by small amounts. This mode of operation is obtained with a beam transmitted through two radially selecting diaphragms on the first turns in the cyclotron centre. The phase width of the selected beam is smaller than 6^o. The central HF phase can be chosen by the position of the radially selecting diaphragms. The setting of correction coils and other parameters is rather critical, e.g. a magnetic field variation $\Delta B/B$ must be smaller than 10^{-4}, hence a stable cyclotron operation is required. A relative energy spread smaller than $0.8 \cdot 10^{-3}$ is obtained for currents up to several hundreds of nA. For larger currents space charge effects in the centre of the cyclotron destroy the radius-phase relation within the turns and enlarge the selected phase width.

CHAPTER 6

CONCLUDING REMARKS

1. The magnetic analogue method is a powerfull tool in the study of the ion beam behaviour in the centre of the cyclotron, since the enlarged three dimensional model of the electrode system allows a direct determination of the three electric field components and changes of the geometry of the electrode structure can be realized easily.

2. The electrical axial focusing strength depends strongly on the precise shape of the accelerating field in the centre of the cyclotron. We have increased ν_z^2 considerably by a small change of the geometry of the electrodes (adaptation of the puller). The induced change in the electric field shape has only a small influence on the radial particle motion. The axial cyclotron acceptance increased such that an increase in beam current by more than a factor three is obtained.

3. The median plane of the cyclotron magnetic field does in general not coincide with the midplane of the magnet. Then the axial acceptance is smaller than in the case of coincident planes. Due to oblique electric fields with respect to the magnet symmetry plane at the first few turns, or due to an axial mispositioning of the ion source the optical axis of the ion beam may be inclined with respect to this symmetry plane, causing again a loss of beam current due to limiting axial boundaries.
An asymmetric excitation of inner circular correction coils alters the position of the magnetic median plane and may yield an increased axial acceptance. A DC voltage on deflection plates in the centre of the cyclotron (e.g. on the first or on the second turn) can adapt the ion source emittance properly to the cyclotron acceptance.
In the Eindhoven cyclotron the application of the deflection plates alone have resulted in an increase of beam current of 50% to 100%,

depending on the specific cyclotron setting. This is of particular importance for the acceleration of polarized protons and for ^4He since the beam currents for these particles are relatively small. As an example with the new puller and with the use of deflection voltages the maximum alpha particle beam current has increased by a factor of 8 to 10.

4. The trochoidal median plane injector has a focusing effect on the axial motion of the accelerated ions; the effect on the radial particle motion can be neglected.

5. The new installed ion source facilitates emittance measurements in the cyclotron centre. Measured data are in agreement with those of DC test facilities and with the data of the externally measured emittance.

6. With a beam selected by diaphragms on the first few turns in the centre of the cyclotron having a HF phase width smaller than 6^o, single turn extraction is achieved, and may be inspected by observing 100% current variations in the external beam if the dee voltage is changed by small amounts.

7. The non-intercepting phase measuring equipment developed by Van Heusden has shown to be a reliable and accurate diagnostic device. Energy and beam position measurements with the phase probes in the beam guiding system are performed with a high accuracy within a tenth of a second.
   The beam scanner system has shown a stable and accurate performance. A check of the double achromaticity or of the dispersive setting of the beam guiding system is done by flipping a degrader foil in the beam line in front of the analysing magnets and observing the beam position behind the analysing magnets.

8. The on-line least squares parameter estimation method applied for the optimization of the extraction efficiency and described in the Addendum yields stable control matrices, by which deliberate changes in the cyclotron parameters are counteracted by the control system to attain the maximal external beam current.

ADDENDUM

EXTRACTION EFFICIENCY OPTIMIZATION [1)]

In this Addendum a method for computer controlled optimization of the extraction efficiency is described. An on-line least squares method is applied to determine the control matrix for the optimization system.

A.1 Introduction

The extraction of particles in the Eindhoven cyclotron is performed by means of an electrostatic channel (extractor) at the outer radius of the cyclotron, through which the beam is guided (see figure 1.2). Several parameters have an important influence on the extraction efficiency, which is defined as the ratio of the external and the internal beam current.

Some parameters, for instance the extractor voltage, remain well constant during one shift of cyclotron operation, and do not need to be altered, once set. However, the extraction efficiency will not remain constant after optimization at the beginning of a beam shift. Changes in the extraction efficiency are primarily caused by drift in the cyclotron magnetic field, e.g. through temperature effects. We have found that reoptimization is best carried out by readjusting the current through the harmonic coils (the inner harmonic coils A_{11}, A_{12} and the outer harmonic coils A_{31} and A_{32}) and the outer two concentric correction coils (B_8 and B_{10}).

A control system was designed for optimization of the extraction efficiency (Schutte 73, Van Heusden 76). Small block shaped pulses are induced on the aforementioned correction coils, and the response in the external beam current is correlated with the perturbating pulse.

---

1) To be published in the proceedings of the 9th International Cyclotron Conference, Caen, 1981.

The perturbation is limited by the requirement that the resulting changes in the external beam current remain below 1% of the total beam current, being the order of beam current variations due to ion source instability.

The described system consists of CAMAC modules with some external electronics. The timing of the measuring and perturbing equipment is controlled by a programmable CAMAC clock. An important part of the measuring equipment is a fast data logger that performs the measurements of the extracted beam current. The correlation is performed by a PDP 11 computer.

An on-line least squares parameter estimation method is applied which is used to determine the control matrix for extraction optimization (Kruis 80).

The extraction optimization system corrects slowly varying changes in cyclotron parameters, such as drift of the magnetic field, to preserve maximum external beam current.

Experiments performed with the system are presented.

A.2 Principle of the control system

Figure A.1 gives a general scheme of the control system. A pulse generator induces small perturbations on the parameters p_i (the currents through four harmonic and two concentric coils). The response of the external beam current I to these perturbations is proportional to the first derivatives $\partial I/\partial p_i$ around the optimum setting. From the derivatives $\partial I/\partial p_i$ the computer calculates the necessary changes in the parameter setting to optimize the extraction efficiency and carries them out via the control equipment. The beam current response is measured with a correlation method.

A schematic representation of the correlation method is given in figure A.2. The response in the external beam current (b), due to a perturbing pulse (a), is multiplied with a so-called second order correlation pulse (c) to give a product signal (d), which is integrated in time, yielding a correlation

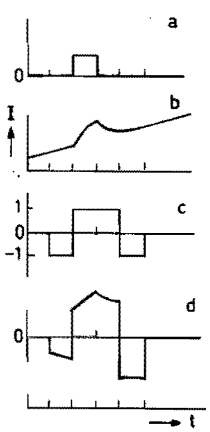

Figure A.2

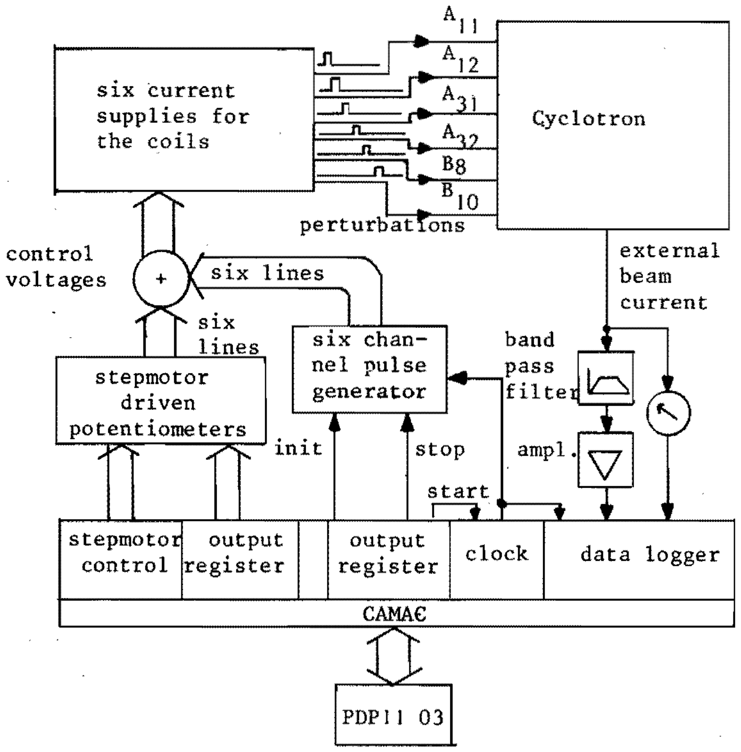

Figure A.1 Block diagram of the control system for extraction efficiency optimization.

product proportional to $\partial I/\partial p_i$. Due to the shape of the correlation pulse constant and linearly varying components in the beam signal will not contribute to the result.

Originally the correlation was performed with analogue correlators (Kooij 75, Van Heusden 76). Presently, the external beam current variations are sampled by a transient recorder (datalogger) in CAMAC, and the correlation is performed by the computer by multiplying the samples with plus or minus one and adding them. This makes the correlation fast and more versatile.

A.3 Measuring and control equipment

The heart of the system is a clock module (Le Croy 8501) in CAMAC, of which the number of pulses and the frequency of the pulse train can be software programmed. This module drives a six channel pulse generator, as well as the datalogger (transient recorder, Le Croy 8212), of which the sample rate is equal to the clock frequency.

The pulse generator delivers successively a perturbing pulse at each of the output channels. The pulses are added to the control voltage of the considered parameters. Pulse duration and rest time after each pulse may be varied; we used 80 msec for pulse duration, 896 msec rest time for a concentric coil and 96 msec rest time for a harmonic coil. Figure A.3 shows a complete measuring cycle. The difference in rest times arises from the fact that the time constant for the harmonic coils is ∿ 0.2 s, and ∿ 1.0 s for the concentric coils.

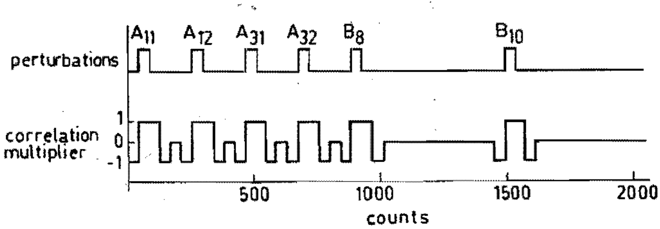

Figure A.3 Schematic presentation of the perturbation and correlation timing for one measuring cycle.

The external beam current can be measured either with a beam stop target behind an experiment station or with capacitive pick-up probes (see section 2.3). (For our measurements we always used a target). The DC level, slow variations and noise of the external beam current are filtered out for a major part by an 0.1 Hz to 20 Hz band pass filter. After that the signal due to parameter perturbations is amplified $5 \cdot 10^4$ times to bring it within the voltage range of the datalogger (± 5 V). A measure of the amplitude of the external beam current is logged separately to obtain information about the performance of the control system.

The sample rate of the datalogger was set to 500 Hz, while a pulse train of 2048 pulses was used for each measuring cycle. The samples are translated in 12 bit data and stored in a 32 K memory module (Le Croy 8800), organized as a circular shift register. The measurements stored in the memory module are read out by the computer via the datalogger after two complete measuring cycles. Then the aforementioned correlation can be performed. Necessary control actions are carried out via stepmotor driven potentiometers.

A.4 The on-line least squares method

We denote the control parameters by a vector $\underline{p}$ with components p_i (i = 1, ..., 6), for coils A_{11}, A_{12}, A_{31}, A_{32}, B_8 and B_{10}. The maximum $\hat{I}$ of external beam current occurs for the settings $\hat{p}_i$, i.e. : $\hat{I} = I(\hat{\underline{p}})$. Small deviations from the optimum parameter setting : $\Delta\underline{p} = \underline{p} - \hat{\underline{p}}$ will cause a change in the external beam current $\Delta I = I - \hat{I}$. This may be approximated by a quadratic function of the deviations :

$$I = \hat{I} + \sum_i \sum_j \alpha_{ij} \Delta p_i \Delta p_j \tag{A.1}$$

Differentiation with respect to p_i yields

$$r_i \underset{def}{=} \frac{\partial I}{\partial p_i} = 2 \sum_{j=1}^{6} \alpha_{ij} \Delta p_j \tag{A.2}$$

which is written in vector notation as

$$\underline{r} = \underline{\underline{V}} \Delta\underline{p} \tag{A.3}$$

where the 6 × 6 matrix $\underline{\underline{V}}$ is called the variation matrix. Under working conditions the variation matrix turns out to be non singular, therefore the inverted equation reads :

$$\underline{p} = \underline{\underline{C}}\,\underline{r} + \hat{\underline{p}} \tag{A.4}$$

where the matrix $\underline{\underline{C}} = \underline{\underline{V}}^{-1}$ is called the control matrix. We use this relation in two ways. In the learning phase we take many measurements of $\underline{r}$ as a function of $\underline{p}$ with the pulse apparatus. By a least squares method we determine the unknown quantities C_{ij} and $\hat{p}_i$. Then we enter the stabilizing phase where we compensate the slow drift of the cyclotron : a measurement of $\underline{r}$ together with the known matrix $\underline{\underline{C}}$ gives the optimum as

$$\hat{\underline{p}} = \underline{p} - \underline{\underline{C}}\,\underline{r}\ . \tag{A.5}$$

Both phases overlap as the new measurements of $\underline{r}(\underline{p})$ can be used for a further improvement of the estimation of $\underline{\underline{C}}$.

The unknown quantities in the least squares problem are the 36 elements of $\underline{\underline{C}}$ and the 6 elements of $\hat{\underline{p}}$, adding up to 42 unknowns. This is inconveniently large as the numerical effort increases at least as the square of the number of unknowns. The matrix $\underline{\underline{C}}$ is symmetric, this reduces this number to 27. We cannot use this symmetry, however, as time constant effects in our pulse method give unknown scaling factors for the various derivatives r_i. These factors are moreover dependent on the value of the main field. Therefore we decided to ignore the symmetry of $\underline{\underline{C}}$. The equation (A.4) can be written as six independent equations, each with 7 unknowns, for each component p_i. From now on we drop the subscript i for this component, and have thus :

$$p = \underline{C}^T \underline{r} + \hat{p} \,, \tag{A.6}$$

where $\underline{C}^T$ is the i^{th} row of matric $\underline{\underline{C}}$. So we have in fact six different equations of this type for the six values of i.

Equation (A.6) has 7 unknowns. We perform a much larger number N of measurements than seven for different values of the parameter setting p, and determine the unknowns employing a least squares method. The measurements have to be sufficiently independent. We take the unknowns together in the system vector $\underline{s}$:

$$\underline{s} = \begin{pmatrix} \underline{C}^T \\ - \\ \hat{p} \end{pmatrix}. \tag{A.7}$$

We define the measurement vector $\underline{m}_n$ for measurement number n by

$$\underline{m}_n^T = (\underline{r}^T, 1) \,, \tag{A.8}$$

and define the deviation from eq. (A.6) as the error E_n :

$$E_n = p - \underline{m}_n^T \underline{s} \,. \tag{A.9}$$

The least squares criterion reads

$$\sum_{n=1}^{N} E_n^2 \text{ is minimal} \,, \tag{A.10}$$

with all measurements weighted equally.

The N vectors $\underline{m}_n^T$ are the rows of the so-called design matrix $\underline{\underline{M}}$ (Eadie 71); the N parameter settings p_n form the observation vector $\underline{P}$. The least squares problem reads :

$$|\underline{P} - \underline{\underline{M}}\,\underline{s}|^2 \textit{ is minimal for } \underline{s} = \underline{\hat{s}} \,. \tag{A.11}$$

This can be interpreted in $\mathbb{R}_N$ with the base vectors $\underline{e}_n$: $\underline{P}$ is a point, $\underline{\underline{M}}\,\underline{s}$ is a seven-dimensional surface. This surface is described by seven base vectors $\underline{M}_k$, the columns of $\underline{\underline{M}}$. The best value is the projection of $\underline{P}$ on $\underline{\underline{M}}\,\underline{s}$.

It should be remarked that the design matrix is the same for all the six values of i, which gives a drastic reduction of the numerical work involved.

Although the solution $\underline{\hat{s}}$ of the criterion (A.11) can be given directly in terms of a matrix form of the matrix $\underline{\underline{M}}$ and the vector $\underline{P}$ (Eadie 71), the required memory space may become prohibitive if the number of measurements increases continuously, which happens in our case. We have chosen a solution method proposed by Peterka and Smuk (Peterka 69) to satisfy criterion (A.11), which has turned out suitable for the use of on-line computers. In this method the amount of memory space is independent of the number of measurements, and the calculation time is limited. After the addition of a measurement (increasing the dimension by one) a rotation of the axes $\underline{e}_n$ is carried out such that the seven dimensional surface supported by the vectors $\underline{M}_k$ lies in $[\underline{e}_1, \ldots, \underline{e}_7]$, while $\underline{P}$ lies in $[\underline{e}_1, \ldots, \underline{e}_8]$. In this new basis the number of rows of $\underline{\underline{M}}$ remains limited to 7 and the number of coefficients of $\underline{P}$ remains limited to 8.

A comparison of the amounts of memory space, and of calculation times for comparible least squares estimation methods is given by Schreurer (Schreurer 75).

A.5 The performance of the control system

We present here some measurements which were done for a 7 MeV proton beam cyclotron setting.

Figure A.4 shows the response in the beam current to the perturbation in the four harmonic coils A_{11}, A_{12}, A_{31} and A_{32} and in the two concentric coils B_8 and B_{10}. The picture represents the read out of the data logger. Two complete measuring cycles are displayed. The parameters were deliberately set beside the optimum beam current to show a response to each perturbation.

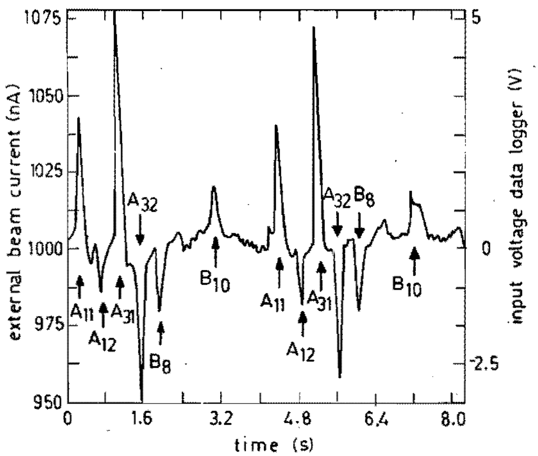

Figure A.4 *Example of the response of the external beam current to perturbations of the coil currents. The coil currents are adjusted to obtain a response to each perturbed current. With an arrow the coil perturbed causing the response is indicated.*

The amplitude for the current perturbation was generally set to 0.2 A for the concentric coils and 0.15 A for the harmonic coils, which means a change in the magnetic induction of $19.2\cdot10^{-6}$ T and $18.75\cdot10^{-6}$ T respectively. The main magnetic induction for 7 MeV protons is 0.7 T.

The noise amplitude in the beam signal differs from day to day. The mean amplitude of the noise in the correlation products, expressed in the data logger voltage units, was found to vary between 150 mV and 400 mV corresponding to 2.3 nA and 6 nA variations, for an external beam current of 1 μA. The contribution to the noise on the correlation products due to the measuring system itself was found to be low : 10 mV or less.

During the experiments we took the average over four measurements. Thus the error in the correlation products is less than 200 mV. This means that variations of about 3 nA can still be detected for an 1 μA beam. Figure A.5 shows a parameter perturbation response picture for one measuring cycle in which the noise in the beam current is clearly seen. In this picture the responses to pulses in coil A_{12} and A_{31} are not present, indicating that in this situation coils A_{12} and A_{31} have an optimal setting.

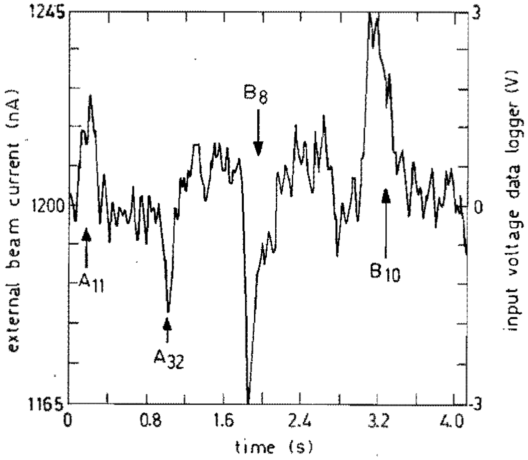

Figure A.5 *Example of the response of the external beam current to perturbation of the coil currents. With arrows the response to the perturbation of the coil specified is indicated.*

In a previous optimization system the control matrix $\underline{\underline{C}}$ was found by inversion of the variation matrix $\underline{\underline{V}}$. The elements of the variation matrix were obtained experimentally by a graphical determination. The matrix elements depend strongly on several parameters, such as dee voltage, ion source position, bias voltage on the dee, etc.
As an example figure A.6 shows the correlation products $\partial I/\partial A_{31}$ and $\partial I/\partial B_{10}$ and the external beam current both as a function of A_{31} for three slightly different settings of the acceleration voltage.

The graphical method employing these plots to determine the matrix elements of the variation matrix costs a lot of labour; the on-line determination of the control matrix is more handy and faster.

Figure A.7 gives an example of the performance of the control system as a function of time. A control action is done every 40 seconds, but only when the correlation products are larger than a small threshold value.

A first estimate for the control matrix was obtained from the learning procedure, by which successively the setting of a parameter p_i was changed a little, and by then measuring the correlation products $\partial I/\partial p_j$. Sometimes the control actions may not be quite perfect as is seen in the figure : the first 440 seconds the system based the control actions on the start matrix, which resulted in an oscillatory behaviour of $\partial I/\partial A_{31}$ and of A_{31}.

In this figure a new estimate for the control matrix at the time *1* was taken, in which all the previous measurements, including the oscillations, were incorporated. It is seen that the new control matrix gave more stable control actions.

After 920 seconds (time *2*) the setting of parameter A_{11} was deliberately changed. The control system counteracts this change making the correlation products small again. At the same time other parameters are slightly varied, indicating that there are non-zero off-diagonal matrix elements in the control matrix.

The control system can correct parameter changes within several minutes.

Other examples of the behaviour of the control system in various situations are given in a report written by R. Kruis (Kruis 80).

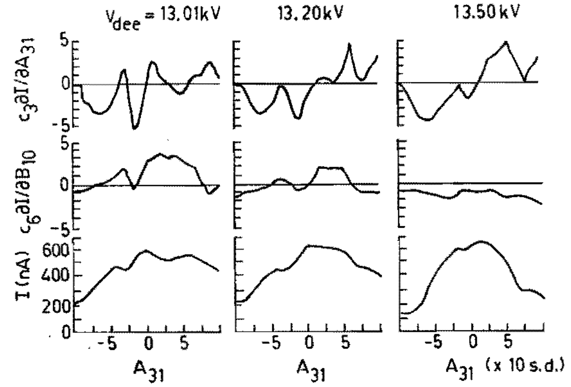

Figure A.6 *Correlation products $\partial I/\partial p_i$ and the external beam current I as a function of the potentiometer position A_{31} for three different dee voltages. c_i is a proportionality constant.*

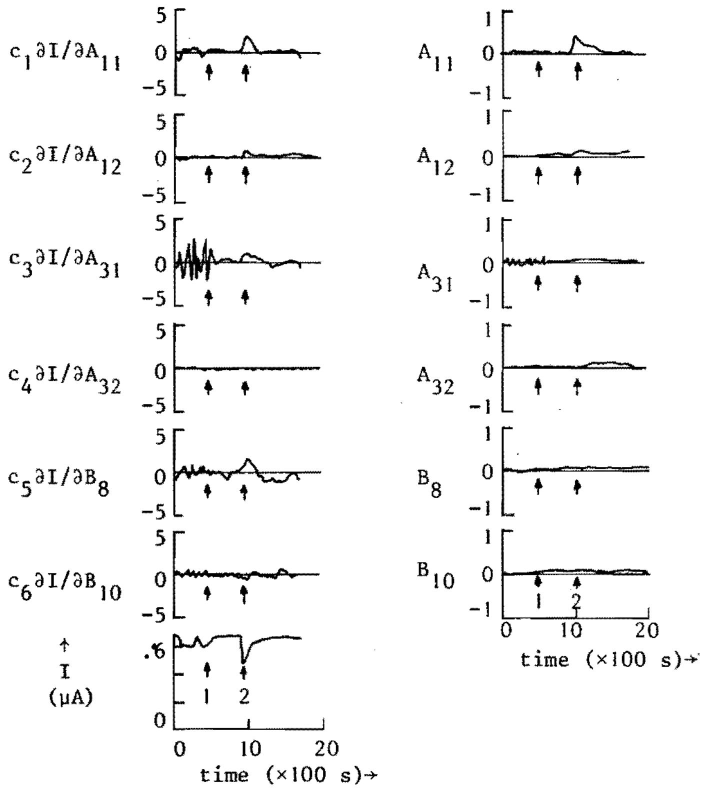

Figure A.7 *Correlation products $\partial I/\partial p_i$, external beam current I and potentiometer positions p_i as a function of time. The control system uses a first matrix c_1 until time 1 and after that a second matrix c_2. At time 2 A_{11} was changed from 8 div. to 50 div. The factors c_i are proportionality constants. The full range (-1, 1) of the potentiometer positions p_i in the figures at the right hand side corresponds to (-100, +100) potentiometer divisions.*

A.6 Discussion

1. The control matrix for optimizing the extraction efficiency, on-line determined with the described least squares method, yields stable control actions. Deliberate changes in cyclotron parameters are counteracted by the control system to attain the maximum external beam current. However, large changes in the parameters may be optimized in the direction of an unwanted extremum.
2. The calculated control matrix is strongly dependent on several cyclotron parameters, e.g. the energy of the external beam, the dee voltage, bias voltage, ion source position, etc.
3. Due to point 2 we believe that this method is a meaningful improvement of the original graphical method (Van Heusden 76).
4. The described control system and method can also be applied to optimize the transport of the ion beam in the beam guiding system, using as control parameters the settings of quadrupoles and bending magnets.
5. Possible improvements of the system can be made : A DC-free rectangular modulation pulse could be used as perturbing pulse. This can lead to a slight improvement in control time.
   The correlation may be performed with a sine function, which gives a slightly better signal to noise ratio.
   The sampling frequency and the ADC resolution are determined on account of the available hardware, in particular of the datalogger. The same performance could be expected from a system with substantially lower sampling frequency and lower ADC resolution.

REFERENCES

International Cyclotron Conferences :

1ICC — Proceedings of the Conference on Sector-Focused Cyclotrons, Sea Island, Georgia, 1959, Nuclear Science Series Report No. 26, NAS-NRC, Washington D.C. (1959).

2ICC — Proceedings of the International Conference on Sector-Focused Cyclotrons, Los Angeles, California, 1962, Nucl. Instr. and Meth. 18,19 (1962).

3ICC — Proceedings of the International Conference on Sector-Focused Cyclotrons and Meson Factories, Geneva, 1963, CERN Report 63-19 (1963).

4ICC — Proceedings of the International Conference on Isochronous Cyclotrons, Gatlinburg, Tennessee, 1966, IEEE Trans. on Nucl. Sci. NS 13-4 (1966).

5ICC — Proceedings of the Fifth International Cyclotron Conference, Oxford, 1969, Butterworths, London (1971).

6ICC — Proceedings of the Sixth International Cyclotron Conference, Vancouver, 1972, AIP Conference Proceedings No. 9, New York (1927).

7ICC — Proceedings of the Seventh International Conference on Cyclotrons and their Applications, Zürich, 1975, Birkhäuser Verlag, Basel (1975).

8ICC — Proceedings of the Eighth International Conference on Cyclotrons and their Applications, Bloomington, 1978, IEEE Trans. on Nucl. Sci. NS 26-2 (1979).

9ICC — Proceedings of the Ninth International Conference on Cyclotrons and their Applications, Caen, 1981, to be published.

ECPM — European Cyclotron Progress Meeting, held every year, no proceedings.

PAC — Particle Accelerator Conference, held every two years, published in IEEE Transaction on Nuclear Science.

Aerssens 80 — P. AERSSENS, Rectifier and oscillator circuits of the E.U.T. AVF cyclotron (in Dutch), E.U.T. internal report (1980).

van Asselt 79 — W. VAN ASSELT and J.I.M. BOTMAN, Design studies for the cyclotron central region, KVI annual report (1979) 135.

Baghuis 74 — L.C.J. BAGHUIS, On the use of ^{20}Na tracers to study mean gas discharges, thesis, Eindhoven University of Technology (1974).

Banford 66 — A.P. BANFORD, The transport of charged particle beams, Spon, London (1966).

Bardin 67 B.M. BARDIN and M.E. RICKEY, Kinematic method for determination of accelerator beam energies, Rev. Sci. Instr. 35 (1964) 902.

Beurtey 67 R. BEURTEY et al., Trochoidal median plane injection in the Saclay cyclotron, Nucl. Instr. and Meth. 57 (1967) 313.

Blosser 63 H.B. BLOSSER et al., Central region studies for the MSU cyclotron, 3ICC (1963) 193.

Blosser 69 H.G. BLOSSER, Optimisation of the cyclotron central region for the nuclear physics user, 5ICC (1969) 257.

Borneman 77 H. BORNEMAN, Determination of electrical fieldstrengths using the magnetic analogue method (in Dutch), E.U.T. internal report NK 240.

van den Bosch 79 R.L.P. VAN DEN BOSCH, Production of ^{123}I, ^{77}Br and ^{87}Y with the Eindhoven AVF cyclotron, thesis, Eindhoven University of Technology (1979).

Botman 80a J.I.M. BOTMAN, H.L. HAGEDOORN and W.M. VAN DER LIGT, Improvements of the central region of the Eindhoven AVF cyclotron, Nucl. Instr. and Meth. 171 (1980) 203.

Botman 80b J.I.M. BOTMAN, M.P.A. QUEENS, Contributions of the E.U.T. Cyclotron Laboratory to the 17th ECPM, Karlsruhe (1980); E.U.T. internal report VDF/NK 80-36.

Botman 81a J.I.M. BOTMAN and H.L. HAGEDOORN, Median plane effects in the Eindhoven AVF cyclotron, 1981 PAC, IEEE Trans. Nucl. Sci. NS 28-3 (1981) 2128.

Botman 81b J.I.M. BOTMAN, R.F. KRUIS and H.L. HAGEDOORN, Extraction efficiency optimization for the Eindhoven AVF cyclotron, to be published in 9ICC, Caen, 1981.

Brautigam 79 W. BRAUTIGAM et al., Beam phase detection with a fixed intermediate frequency system at JULIC, 8ICC (1979) 2375.

Cohen 59 B.L. COHEN, Handbuch der Physik XLIV (1959) 105.

Coolen 76 F.C.M. COOLEN, Fluorescence studies on ^{20}Na and excited neon atoms in proton-induced plasmas, thesis, Eindhoven University of Technology (1976).

Corsten 80 C.J.A. CORSTEN et al., The effect of a bevelled dee on the beam centering process in an AVF cyclotron, Nucl. Instr. and Meth. 171 (1980) 1.

Dutto 75 G. DUTTO and M.K. GRADDOCK, Focusing in RF accelerating gaps with asymmetrically curved electric equipotentials, 7ICC (1975) 271.

Feldmann 66 H.H. FELDMANN, Non-intercepting ion phase measuring equipment of the isochronous cyclotrons at Karlsruhe and Jülich, 4ICC (1966) 30.

van Genderen 79 — W. VAN GENDEREN, Manual for the program beam transport, E.U.T. internal report (1979) VDF/NK 79-47.

Gordon 80 — M.M. GORDON and FELIX MARTI, Electric focusing in cyclotrons with unusual dees, M.S.U. report MSUCL-336 (1980).

Hagedoorn 62 — H.L. HAGEDOORN and N.F. VERSTER, Orbits in an AVF cyclotron, 2ICC (1962) 201.

Hagedoorn 69 — H.L. HAGEDOORN et al., Some factors determining the beam quality of AVF cyclotrons, 5ICC (1969) 274.

Hazewindus 67 — N. HAZEWINDUS, J.M. VAN NIEUWLAND, Some formulas describing the electric focusing in the cyclotron centre, Philips Nat. Lab. Report nr. 4280 (1967).

Hazewindus 74 — N. HAZEWINDUS et al., The magnetic analogue method as used in the study of a cyclotron central region, Nucl. Instr. and Meth. 118 (1974) 125.

Hazewindus 75 — N. HAZEWINDUS, The axial injection system of the SIN injector cyclotron, Nucl. Instr. and Meth. 129 (1975) 325.

van der Heide 72 — J.A. VAN DER HEIDE, On the construction and use of a polarized ion source, thesis, Eindhoven University of Technology (1972).

van Heusden 76 — G.C.L. VAN HEUSDEN, On the computer control of the Eindhoven AVF cyclotron, thesis, Eindhoven University of Technology (1976).

van Heusden 79 — G.C.L. VAN HEUSDEN et al., A multi-input phase measuring system, 8ICC (1979) 2209.

Johnson 69 — W.P. JOHNSON et al., Cyclotron beam pulser for particle time of flight experiments, 5ICC (1969) 325.

Kerst 41 — D.W. KERST and R. SERBER, Electronic orbits in the induction accelerator, Phys. Rev. 60 (1941) 53.

Kivits 80 — H.P.M. KIVITS, Particle induced X-ray emission for quantitative trace-element analysis using the Eindhoven cyclotron, thesis, Eindhoven University of Technology (1980).

Kooij 75 — P. KOOIJ, Optimization of the extraction efficiency of the Eindhoven AVF cyclotron (in Dutch), E.U.T. internal report (1975) NK 199.

Kost 80 — C.J. KOST and H. HOUTMAN, Relax 3D, A fortran program to solve the 3 dimensional Helmholtz-Laplace equation, internal report Triumf UBC.

Kramer 63 — P. KRAMER et al., The central region of the Philips AVF cyclotron, 3ICC (1963) 214.

Kruip 80 — M.J.M. KRUIP, The effect of the trochoidal median plane injector on the accelerated particles in the Eindhoven AVF cyclotron, E.U.T. internal report (1980) VDF/NK 80-47.

Kruis 80 — R.F. KRUIS, Experiments with extraction optimization equipment, E.U.T. internal report (1980) VDF/NK 80-48.

Linz 75 — J. LINZ et al., Modification of the center region for better beam quality at JULIC, 7ICC (1975) 279.

Liukkonen 79 — E. LIUKKONEN et al., Design of the central regions for the MSU 500 MeV superconducting cyclotron, 8ICC (1979) 2107.

Livingston 54 — L.R.S. LIVINGSTON and R.J. JONES, High intensity ion source for cyclotrons, Rev. Sci. Instr. 25 (1954) 552.

Mallory 66 — M.L. MALLORY and H.G. BLOSSER, Phase space density studies on cyclotron ion sources, 4ICC (1966) 163.

Melssen 78 — J.P.M.G. MELSSEN, Scattering of polarized protons by yttrium, iron and nickel nuclei, thesis, Eindhoven University of Technology (1978).

van Nieuwland 68 — J.M. VAN NIEUWLAND et al., Magnetic analogue of electric field configurations applied to the central region of an AVF cyclotron, Rev. Sci. Instr. 39-7 (1968) 1054.

van Nieuwland 72 — J.M. VAN NIEUWLAND, Extraction of particles from a compact isochronous cyclotron, thesis, Eindhoven University of Technology (1972).

van Nieuwland 77 — J.M. VAN NIEUWLAND et al., The central region of the SIN injector cyclotron, Nucl. Instr. and Meth. 142 (1977) 393.

van Nijmweegen 80 — F.C. VAN NIJMWEEGEN, The Eurobussystem (in Dutch), E.U.T. internal report VDF/CO 79-10.

Peterka 69 — V. PETERKA and K. SMUK, On-line estimation of dynamic model parameters from input-output data, Proc. 4th IFAC Congr. Warsaw (1969) 26-1.

Polane 81 — J.H. POLANE, Transfer reactions on ^{58}Ni and ^{56}Fe induced by polarized protons of 25 MeV, thesis, Eindhoven University of Technology (1981).

Prins 80 — M. PRINS and L.J.J. HOFFMAN, The Eindhoven proton microbeam, Nucl. Instr. and Meth. 181 (1981) 125.

Reiser 68 — M. REISER and J. MULLENDORE, A fully automated electrolytic tank system and its use in cyclotron injection studies, Nucl. Instr. and Meth. 59 (1968) 93.

Rethmeier 69 — J. RETHMEIER et al., Sub-nano second bursts from an AVF cyclotron, Nucl. Instr. and Meth. 68 (1969) 135.

Rose 38 M.E. ROSE, Focusing and maximum energy of ions in the cyclotron, Phys. Rev. 53 (1938) 392.

Sandvik 73 G.E. SANDVIK et al., Measurements and second-order calculations of the Eindhoven beam transport system, Nucl. Instr. and Meth. 106 (1973) 245.

Schneider 80 S. SCHNEIDER et al., Beam phase measurement using the mixing technique, NAC Annual Report 1980, NAC/AR/80-01.

Schreurer 75 H.G. SCHREURER, Ein aditives, explizites Parameter Schätzverfahren mit geringem Speicher Platz- und Rechenzeit Bedarf, Reglungstechnik 12 (1975) 427.

Schutte 73 F. SCHUTTE, On the beam control of an isochronous cyclotron, thesis Eindhoven University of Technology (1973).

Schulte 78 W.M. SCHULTE, The theory of accelerated particles in AVF cyclotrons, thesis, Eindhoven University of Technology (1978).

Smith 60 W.I.B. SMITH, Improved focussing near the cyclotron source, Nucl. Instr. and Meth. 9 (1960) 49.

Smythe 64 R. SMYTHE, Relativistic equations and tables for ion energy determination by the crossover technique, Rev. Sci. Instr. 35 (1964) 1197.

van Steenbergen 67 A. VAN STEENBERGEN, Evaluation of particle beam phase space measurement techniques, Nucl. Instr. and Meth. 51 (1967) 2145.

Vader 79 R.J. VADER and H.W. SCHREUDER, New methods for stabilizing dee voltage and beam RF phase, 8ICC (1979) 2205.

Vader 81 R.J. VADER, private communication.

Verster 62a N.F. VERSTER et al., Some design features of the Philips AVF prototype, 2ICC (1962) 88.

Verster 62b N.F. VERSTER and H.L. HAGEDOORN, Computer programs for an AVF cyclotron, 2ICC (1962) 327.

Wassenaar 81 S.D. WASSENAAR, thesis (to be published) Eindhoven University of Technology (1981).

Wilson 38 R.R. WILSON, Magnetic and electrostatic focusing in the cyclotron, Phys. Rev. 53 (1938) 408.

Zaidens 74 C.S. ZAIDENS, A method for energy loss and range calculations based on empirical approximations, Nucl. Instr. and Meth. 120 (1974) 125.

SUMMARY

In this thesis a study of the ion beam behaviour in the central region is described for the AVF cyclotron of the Eindhoven University of Technology. This study has been carried out in the Cyclotron Applications Group of the Applied Physics Department.

A good cyclotron acceptance is required to obtain a large beam current. The shape of the electric and the magnetic field fixes the properties of the accelerated beam such as the emittance and acceptance and the HF phase structure. For the determination of the electric field strengths in the cyclotron centre the magnetic analogue method is employed. With the obtained fields numerical calculations of the particle trajectories have been carried out.

Experimentally, the axial and radial phase space areas of the beam have been determined on the first revolutions in the cyclotron. Furthermore a HF phase-radial position relation was found. Thus phase selection with two diaphragms on the first turns is possible. With a beam having a small phase width, obtained by the use of two radial selecting diaphragms in the centre, single turn extraction is achieved in the cyclotron that is designed as a multi turn machine.

Diagnostic equipment is required for the measurement of the properties of the ion beam. A large stability of the cyclotron parameters is necessary, especially for the single turn experiment.

Without using diaphragms in the cyclotron centre dispersion in the beam due to the precession extraction system was observed, i.e. a relation between the energy and the position in radial phase space. By creating a field bumb in the cyclotron energy selection can be obtained using only one diaphragm in the beam guiding system and without employing analysing magnets.

In the Addendum an extension of a special part of the diagnostic equipment is described, viz. an extension of the extraction

optimization system. An on-line least squares parameter estimation method is used to keep the external beam current at the maximal value. The control system corrects small disturbances in relevant cyclotron parameters.

A short survey of experimental results and methods is given below. Measurements with the beam diagnostic equipment are described together with extensions of this equipment : with the HF phase measuring system the HF phase of the beam can be measured with an accuracy of 0.5° at a current of 50 nA, with the external HF phase probes the beam position can be determined with an accuracy of 0.5 mm for a current of 10 nA, and the energy can be determined with a time of flight measurement with a relative accuracy of 10^{-4}. With the time structure system the time resolution can be measured with an accuracy better than 1°. With the beam scanners a beam position measurement with an accuracy of 0.1 mm for a minimal current of 1 nA is achieved.

Electric field measurements were derived from a magnetic analogue model. Numerical calculations have been carried out with the obtained fields. Field measurements for different shapes of the puller geometry show that axial focusing occurs when $\partial E_x/\partial x \geq 0$, where the x-axis lies along the acceleration gap and where E_x is the field component along this x-axis. Axial defocusing occurs when $\partial E_x/\partial x < 0$. The use of a new puller with which the above mentioned focusing has been realized at the third dee gap crossing, has resulted in an increase of beam current of at least a factor 3 with respect to an old puller geometry where axial defocusing occurs.

The causes of the deviation of the optical axis of the ion beam with respect to the symmetry plane of the cyclotron magnet are mentioned. This deviation can be corrected by an asymmetric excitation of the inner circular correction coils. For example, with a current of 90 A through the upper coils and a current of 50 A through the lower coils, both coils with 8 turns, the median plane position can be lowered with about 20 mm. Another correction method is the application of a voltage (300 to 600 V over 8 mm distance) on deflection electrodes placed on the second revolution, and at an azimuth of 270°.

This may increase the beam current with 50% to 100%.

As an application of the central region investigations the lense action exerted on accelerated particles by the electrodes of the trochoidal beam injection system for polarized protons has been computed numerically. The calculations are based on the fields determined with the magnetic analogue method. The radial particle motion is hardly affected; the axial focusing is increased, for instance for the third turn ν_z^2 is increased with 60%.

Measurements of the axial and radial phase space area are presented. An axial ion source emittance is found of 100 mm-mrad for a particle energy of about 11 keV. For a 45 keV beam an axial phase space area has been measured of 120 mm-mrad, where the phenomenon of HF phase mixing increased the ion source emittance. For the radial phase space area at 100 keV a value of 150 mm-mrad has been measured.

Finally "single turn extraction" experiments are discussed. They have been performed for a 7 MeV proton cyclotron setting with a beam that has been selected with two diaphragms on the fourth revolution. The HF phase width of the selected beam is smaller than 6^o. The beam current can amount to about 100 nA. The external horizontal beam emittance is smaller than 2.5 mm-mrad; this is about 8 times smaller than for the normal situation. The relative energy spread is smaller than $0.8\cdot10^{-3}$. When the selected beam current is increased (for instance to 600 nA) the "single turn" effect disappears due to space charge.

SAMENVATTING

In dit proefschrift wordt een studie van het bundelgedrag in het cyclotroncentrum beschreven ten behoeve van het AVF-cyclotron van de Technische Hogeschool Eindhoven. Deze studie is uitgevoerd binnen de groep Cyclotron Toepassingen van de afdeling der Technische Natuurkunde.

Om veel bundelstroom te verkrijgen is een goede cyclotronacceptantie vereist. De vorm van het elektrische en het magnetische veld in het centrum van het cyclotron bepaalt de bundeleigenschappen, zoals de emittantie en acceptantie en de HF-fasestruktuur. Voor de bepaling van de elektrische veldsterkten in het cyclotroncentrum is gebruik gemaakt van de magnetisch-analogonmethode. Met de verkregen velden zijn numerieke berekeningen van de banen uitgevoerd.

Experimenteel zijn de axiale en radiale faseruimte-oppervlakten van de bundel op de eerste omwentelingen in het cyclotron bepaald. Verder is een relatie tussen de radiale positie en de HF-fase gevonden. Hierdoor is faseselectie met twee diafragma's op de eerste omwentelingen mogelijk. Met een in fase begrensde bundel, verkregen door van twee radiaal selecterende diafragma's in het centrum gebruik te maken, is "single turn" extractie bereikt in het cyclotron dat van oorsprong een "multi turn" extractiemachine is.

Voor de meting van de bundeleigenschappen is diagnostische apparatuur vereist. Een grote stabiliteit van de cyclotronparameters is noodzakelijk, met name bij de "single turn" experimenten.

Zonder gebruik te maken van diafragma's in het cyclotroncentrum is dispersie in de bundel ten gevolge van het precessie-extractiesysteem aangetoond, dat wil zeggen een relatie tussen energie en positie in de faseruimte. Door het aanbrengen van een veldbobbel in het cyclotron kan men energieselectie verkrijgen met behulp van één diafragma in het bundelgeleidingssysteem, en zonder van analysemagneten gebruik te maken.

In het Addendum is apart een uitbreiding aan een speciaal onderdeel van de diagnostische apparatuur beschreven, namelijk aan het extractie-optimaliseringssysteem. Er is een on-line parameterschattingsmethode toegepast waarmee voldaan wordt aan het kleinste-kwadratencriterium. De externe bundelstroom wordt hiermee op maximale waarde gehouden. Het regelsysteem corrigeert kleine verstoringen die in relevante cyclotronparameters kunnen ontstaan.

Metingen met en uitbreidingen aan het bundeldiagnostische systeem worden beschreven : met het HF-fasemeetsysteem kan de HF-fase van de bundel met een nauwkeurigheid van 0.5° gemeten worden bij een stroom van 50 nA, met de externe HF-fasesondes kan eveneens de bundelpositie bepaald worden met een nauwkeurigheid van 0.5 mm bij een stroom van 10 nA en kan de energie bepaald worden met behulp van een vluchttijdmeting met een relatieve nauwkeurigheid van 10^{-4}. Met de tijdstruktuuropstelling kan de tijdresolutie gemeten worden met een nauwkeurigheid beter dan 1°. Met de bundelscanners is het mogelijk de bundelpositie te bepalen met een nauwkeurigheid van 0.1 mm bij een minimale stroom van 1 nA.

Elektrische veldmetingen zijn uitgevoerd met behulp van een magnetisch-analogonmodel. Numerieke berekeningen zijn gebaseerd op de verkregen velden. Veldmetingen bij verschillende vormen van de puller laten zien dat axiale focusering optreedt indien $\partial E_x/\partial x \geq 0$, en defocusering indien $\partial E_x/\partial x < 0$. Daarbij ligt de x-as langs de versnelspleet en is E_x de veldcomponent langs deze x-as. Een nieuwe puller waarbij bovengenoemde focusering is gerealiseerd bij de derde oversteek van de versnelspleet heeft geresulteerd in een stroomwinst van minimaal een faktor 3 ten opzichte van de oude pullergeometrie waarbij defocusering optrad.

De invloed van de afwijking van de optische as van de ionenbundel ten opzichte van het symmetrievlak van de cyclotronmagneet wordt vermeld. Deze afwijking kan gecorrigeerd worden door een asymmetrische bekrachtiging van de binnenste concentrische correctiespoelen. De genoemde spoelen, beide met 8 wikkelingen, kunnen dan bekrachtigd worden met een stroom van b.v. 90 A door de bovenste spoel en een stroom van 50 A door de onderste spoel. Als gevolg daarvan kan het mediaanvlak ongeveer 20 mm lager geplaatst worden. Een andere correctiemogelijkheid is het toepassen van een spanning (300 tot 600 V over een afstand van 8 mm) op afbuigelektroden ter plaatse van de tweede omwenteling op aan azimuth van 270°. Dit laatste kan een stroomwinst van 50% à 100% opleveren.

Als voorbeeld van een toepassing van de cyclotroncentrumstudie is de lenswerking die de elektroden van het trochoidale injectiesysteem voor gepolariseerde protonen uitoefenen op de versnelde deeltjes, numeriek nagegaan (met velden verkregen met behulp van de magnetisch-analogonmethode). De radiale deeltjesbeweging wordt nauwelijks aangetast; de verticale focusering wordt vergroot : b.v. voor de derde omloop is ν_z^2 vergroot met ca. 60%.

Metingen van de axiale en de radiale faseruimte-oppervlakte van de bundel worden gegeven. Een axiale bronemittantie wordt gevonden van 100 mm-mrad voor deeltjes van ca. 11 keV. Voor een 45 keV bundel werd een axiale faseruimte-oppervlakte gemeten van 120 mm-mrad, waarbij het verschijnsel van "HF-fase mixing" de emittantie van de ionenbron heeft vergroot. Voor de radiale faseruimte-oppervlakte bij 100 keV is een waarde van 150 mm-mrad gemeten.

Tenslotte worden "single turn extractie" experimenten besproken, uitgevoerd voor een 7 MeV protoneninstelling met een bundel die geselecteerd is met behulp van twee diafragma's op de vierde omloop. De HF-fasebreedte van de geselecteerde bundel is hierbij kleiner dan 6°. De bundelstroom kan ca. 100 nA bedragen. De externe horizontale bundelemittantie is kleiner dan 2.5 mm-mrad, terwijl deze normaal ca. 8 keer groter is. De relatieve energiespreiding is kleiner dan $0.8 \cdot 10^{-3}$. Bij een verhoging van de geselecteerde bundelstroom (tot b.v. 600 nA) verdwijnt het "single turn effect" ten gevolge van ruimteladingsinvloeden.

NAWOORD

Het in dit proefschrift beschreven onderzoek is uitgevoerd in de groep Cyclotron Toepassingen van de afdeling der Technische Natuurkunde van de Technische Hogeschool Eindhoven.

Tijdens de onderzoekperiode zijn A.A.S. Sluijterman en R.F. Kruis afgestudeerd op onderdelen van de beschreven studie; A.A.S. Sluijterman, W.M. van der Ligt, R.F. Kruis, W.J.F. Dries, M.J.M. Kruip en P.J.M. Renders zijn tijdens deze periode als stagiair werkzaam geweest; W.J.F. Dries verricht momenteel afstudeerwerk.

Dr.ir. G.C.L. van Heusden en dr.ir. W.M. Schulte, met wie ik gedurende een belangrijke periode uiterst plezierig heb samengewerkt, dank ik voor de experimentele en theoretische kennis omtrent cyclotron-onderzoek, die zij mij hebben aangereikt.

De discussies over versneller-technologie met ir. C.J.A. Corsten wil ik speciaal vermelden.

Een aantal mensen die bij de verwezenlijking van de in dit proefschrift vermelde werkzaamheden een essentiële betekenis hebben gehad, noem ik met name :

- de leden van de cyclotron bedrijfsgroep : M.P.A. Queens, J. van de Berg, G.J.S.M. van Hirtum en W. Verseijden, die naast een goede werking van het cyclotron altijd een collegiale steun bij het onderzoek verleenden.
- A.H. Kemper voor de vele adviezen op elektronisch gebied, en tevens zijn broer W. Kemper. Apart zij vermeld hun werk aan het beam scanner systeem.
- H.J. Schouten voor het werk aan de elektronika van de fasemeet-apparatuur.
- ir. W. van Genderen voor de berekeningen van het bundeltransport.
- P. Magendans en A. Platje voor de constructie en planning van de "nieuwe" ionenbron, die onmisbaar was bij de uitvoering van de emittantie- en single turn experimenten.
- F.C. van Nijmweegen voor de inbreng van het Eurobussysteem.

De leden van de afdelingswerkplaats en van de afdelingsadministratie komt mijn dank toe.

De uiteindelijke weergave van het onderzoek beschreven in dit proefschrift is tot stand gekomen met de medewerking van Ruth Gruijters die de tekeningen heeft verzorgd, van dra. S.F. van Hurck, die adviezen heeft gegeven betreffende de Engelse taal en van drs. A.J. Vervoorn, die geadviseerd heeft over de Nederlandse taal. Speciaal noem ik Thérèse-Anne die het typewerk heeft verricht en de lay-out heeft verzorgd.

Tot slot spreek ik mijn erkentelijkheid uit tot alle personen in het Cyclotrongebouw voor de plezierige werkomgeving, en dank ik allen die op enigerlei wijze hebben bijgedragen aan de totstandkoming van dit proefschrift.

LEVENSLOOP

9 oktober 1948	Geboren te Haarlemmerliede en Spaarnwoude c.a.
26 mei 1966	Eindexamen H.B.S.-b aan het "Thomas More College" te Oudenbosch.
september 1972 - augustus 1973	Leraar Natuurkunde aan de "Nijmeegse Scholen Gemeenschap" te Nijmegen.
13 maart 1975	Doctoraal examen Theoretische Natuurkunde (Hoge Energie Fysica) aan de Katholieke Universiteit te Nijmegen.
5 maart 1975 - 27 augustus 1976	Militaire Dienst, artillerie.
vanaf 1 januari 1977	Wetenschappelijk ambtenaar, Afdeling der Technische Natuurkunde, Technische Hogeschool te Eindhoven.

STELLINGEN

behorend bij het proefschrift van

J.I.M. Botman

Eindhoven, 15 september 1981

1

Radiale elektrische veldkomponenten in het centrum van het cyclotron beïnvloeden de oscillatiefrequenties van de deeltjes. Indien $\partial E_r/\partial r > 0$, waarbij r de straal en E_r de radiale veldcomponent is, treedt verticale focusering op. Verbeteringen in de centrumgeometrie van een cyclotron waarbij bovenstaand criterium gerealizeerd wordt, veroorzaken een verbetering van de transmissie van de bundel door het cyclotroncentrum.

Dit proefschrift, hoofdstuk 3.

2

Afwijkingen van de optische as van de ionenbundel in een cyclotron ten opzichte van het symmetrievlak van de magneet, kunnen voldoende gecompenseerd worden door een combinatie van een asymmetrische bekrachtiging van binnenste cirkelvormige correctiespoelen, en door het aanbrengen van een afbuigspanning op afbuigelektroden die gesitueerd zijn op een van de eerste omwentelingen.

Dit proefschrift, hoofdstuk 3.

3

Indien 100% variaties in de externe bundelintensiteit worden verkregen met variaties van de versnelspanning van een cyclotron kleiner dan 1%, is op afdoende wijze "single turn extractie" aangetoond.

Dit proefschrift, hoofdstuk 5.

4

Een controle op de dubbel-achromatische instelling van een bundel-transportsysteem van een deeltjesversneller, kan op eenvoudige wijze geschieden door de energie van de uit de versneller tredende deeltjes sprongsgewijs met behulp van een folie te verkleinen.
Indien ook de afremmende werking van het folie bekend is, kan deze methode eveneens gebruikt worden voor de ijking van een dispersieve instelling van een bundel-transportsysteem.

Dit proefschrift, hoofdstuk 2.

5

De door Guignard gegeven formule voor stopbandbreedtes in versnellers bij somresonanties kan eenvoudiger en doorzichtelijker worden afgeleid door een geschikte transformatie toe te passen waarbij het tweedimensionale probleem van de gekoppelde oscillatoren tot een ééndimensionaal probleem herleid wordt.

C.J.A. Corsten en H.L. Hagedoorn, IEEE Trans. Nucl. Sci. NS-28-3 (1981) 2624.

6

Het vaak gebruikte criterium in de literatuur voor versnellertheorie voor het vaststellen van stopbandbreedtes waarbij de maximale bundelafmeting gelijk genomen wordt aan de afstand in de faseruimte van het centrale stabiele vaste punt tot de dichtstbijzijnde instabiele vaste punten, geeft een te optimistische schatting.

G. Guignard, CERN 70-24 (1970).

M. Month, Brookhaven National Laboratory, AGSCD-17 (1967).

7

Het verplaatsen van een spiegel van een interferometer met behulp van een piezo-elektrisch kristal, gestuurd door de ongefilterde spanning van een digitaal-analoog-omzetter, is in strijd met de gebruikelijke voorzichtigheid die bij optische precisie-apparatuur in acht wordt genomen.

8

Bij vaste-stofdetectoren voor kernfysisch onderzoek dient, behalve de gebruikelijke specificaties zoals energie-resolutie en depletielaagdiepte, ook een maat opgegeven te worden voor de continue achtergrond die ontstaat bij detectie van een mono-energetische ionenbundel.

S.S. Klein en M. Knapen, Nucl. Instr. & Meth. 69 (1969) 194.

9

Isotopen voor medische toepassingen aangekocht door Nederlandse ziekenhuizen worden vaak indirect betrokken van buitenlandse researchinstituten. Het betrekken van die isotopen van Nederlandse versnellerinstituten die goed zijn ingericht voor een dergelijke productie, levert in ons land een bijdrage tot de instandhouding van technologische kennis.

Chemisch Weekblad, 22 mei 1980, pagina 233.

10

Ten onrechte wordt de wettelijk vastgestelde dosislimiet voor stralingsbelasting bij toepassing van ionizerende straling vaak als enige norm gehanteerd.
In een opleidingsinstituut waar met ionizerende stralen wordt gewerkt vervult een beleid waarbij er naar gestreeft wordt dat de opgelopen stralingsdosis zo ver mogelijk onder de norm voor de maximale dosis blijft, een belangrijke didaktische functie.

Chr.J. Huyskens, Grondbeginselen en normen in de stralings hygiëne, uit Straling in de Samenleving, Stafleu's Wetensch. Uitg. Mij. Alphen aan den Rijn (1981).

11

De in de vakgroep Deeltjesfysica van de THE aanwezige kennis in verschillende onderzoeksdisciplines is zeer geschikt om een onderzoek uit te voeren naar nieuwe principes voor en naar verbetering van het functioneren van ionenbronnen in versnelmachines.

12

Met mono-energetische protonen met een energie tussen 1,5 en 7 MeV in een bundel van ongeveer 20 μm diameter kunnen in betrekkelijk korte tijd spore-element-concentraties van de orde van 10 ppm gemeten worden in een gebiedje ter grootte van de bundeldoorsnede.
Voor veel biologische structuren is het met een dergelijke bundel aftasten van een gebied van 1 mm^2 interessant. Dit kan bijvoorbeeld door in zo'n gebiedje 50 × 50 meetpunten te bestralen gedurende 5 seconden per meetpunt. Verkleining van de bundeldiameter verhoogt weliswaar het ruimtelijk scheidend vermogen, maar verhoogt tevens de onderste detectiegrens of maakt de meettijd onaanvaardbaar laag.

M. Prins en L.J.B. Hoffman, Nucl. Instr. & Meth. 181 (1981) 125.

13

Een industrieland dat zich geen synchrotronstralingsbron kan permitteren, is een arm land.

H.L. Hagedoorn en J.C.B. Missel, NTvN A43 (1977) 86.
Y. Farge en P.J. Duke, The scientific case, Supplement I of European Synchrotron Radiation Facility, ESF, Strasbourg (1979).